PHYSICAL OCEANOGRAPHIC AND METEOROLOGICAL CONDITIONS IN THE NORTHWEST GULF OF ALASKA

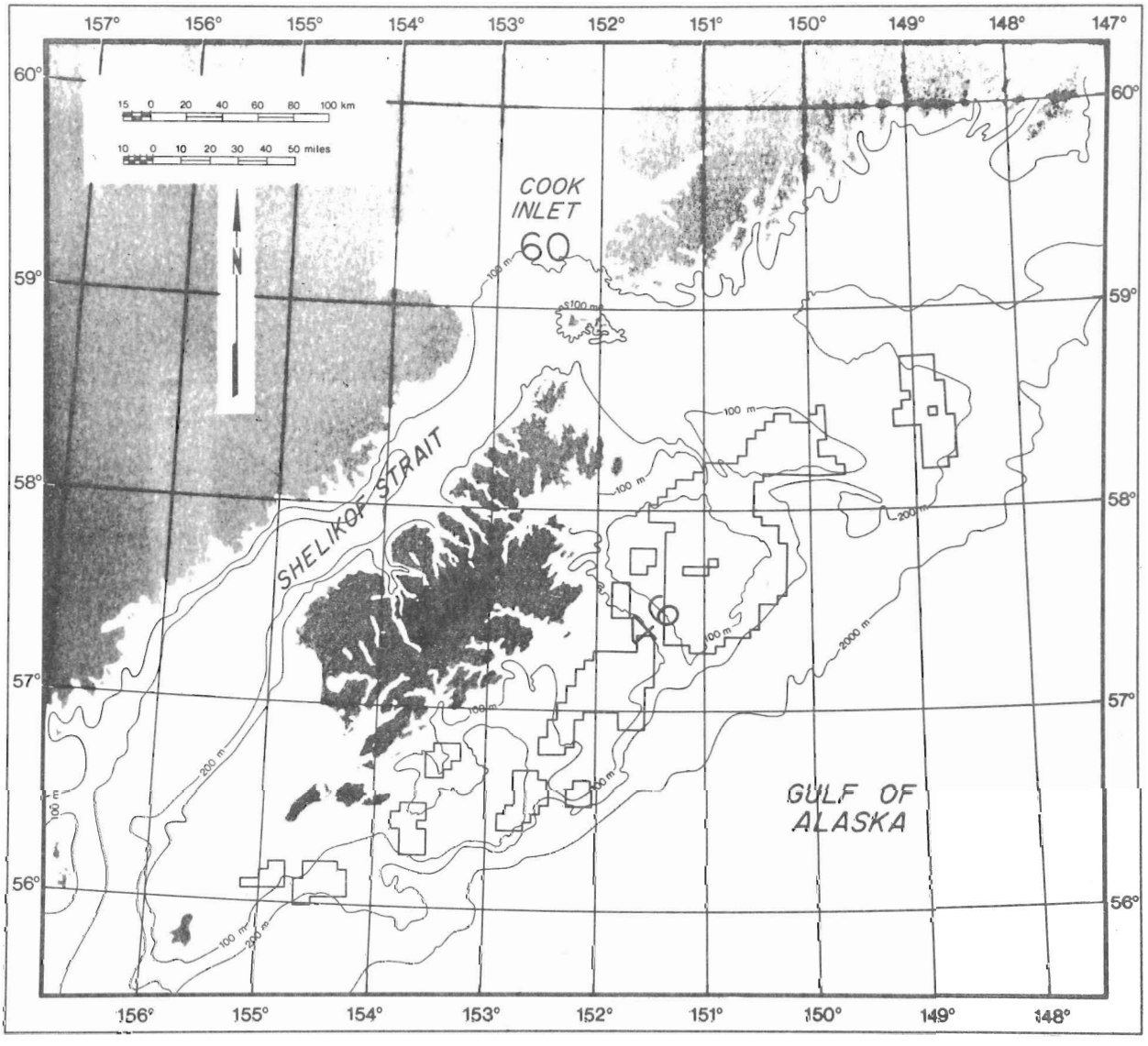

Frontispiece. Geographical locations in the northwest Gulf of Alaska, showing specific locations of present Outer Continental Shelf lease areas south of Kodiak Island (Sale 46) and general location of present lease area in lower Cook Inlet (Sale 60).

NOAA Technical Memorandum ERL PMEL-22

PHYSICAL OCEANOGRAPHIC AND METEOROLOGICAL CONDITIONS IN THE NORTHWEST GULF OF ALASKA

Robin D. Muench
James D. Schumacher

Contributors:
C. A. Pearson
R. M. Reynolds
R. Overstreet

Pacific Marine Environmental Laboratory
Seattle, Washington
October 1980

UNITED STATES DEPARTMENT OF COMMERCE
Philip M. Klutznick, Secretary

NATIONAL OCEANIC AND ATMOSPHERIC ADMINISTRATION
Richard A. Frank, Administrator

Environmental Research Laboratories
Joseph O. Fletcher, Acting Director

DISCLAIMER

The NOAA Environmental Research Laboratories does not approve, recommend, or endorse any proprietary product or proprietary material mentioned in this publication. No reference shall be made to the NOAA Environmental Research Laboratories, or to this publication furnished by the NOAA Environmental Research Laboratories, in any advertising or sales promotion which would indicate or imply that the NOAA Environmental Research Laboratories approves, recommends, or endorses any proprietary product or proprietary material mentioned herein, or which has as its purpose an intent to cause directly or indirectly the advertised product to be used or purchased because of this NOAA Environmental Research Laboratories publication.

TABLE OF CONTENTS

EXECUTIVE SUMMARY

This report presents a summary of the major findings of Outer Continental Shelf Environmental Assessment Program research into physical oceanographic conditions in the northwest Gulf of Alaska. The stress is on circulation features, since water circulation plays a major role in the path and dispersal of surface contaminants, a problem of major impetus for the OCSEAP program. Reference is made throughout this summary section to Figure i, which summarizes the net circulation regime as deduced from this study. On the figure, arrows depict sense of net flow while the numbers represent a typical range of current speeds, in centimeters per second, which might be encountered in that region. In general, the smaller numbers represent spring-summer conditions while the larger numbers represent autumn-winter conditions. It is stressed here that instantaneous flow observed at a given time need not agree with our simplified graphical depiction. The patterns shown are, rather, indicative of mean conditions and of a normal response to the dynamics which we feel exert dominant control over the system.

The results can be summarized as follows:

1. The Alaskan Stream is a major regional oceanic circulation feature. It flows southwesterly, roughly coincident with the shelf break and slope, with mean speeds of 50-100 cm sec^{-1}. Its width is about 50 km, and its computed annual mean baroclinic volume transport is about 12 x 10^6 m^3 sec^{-1}. There was no significant annual variability detected either in baroclinic current speed or volume transport. There were eddy-like perturbations observed in the current, at times, which appeared to be related to bottom

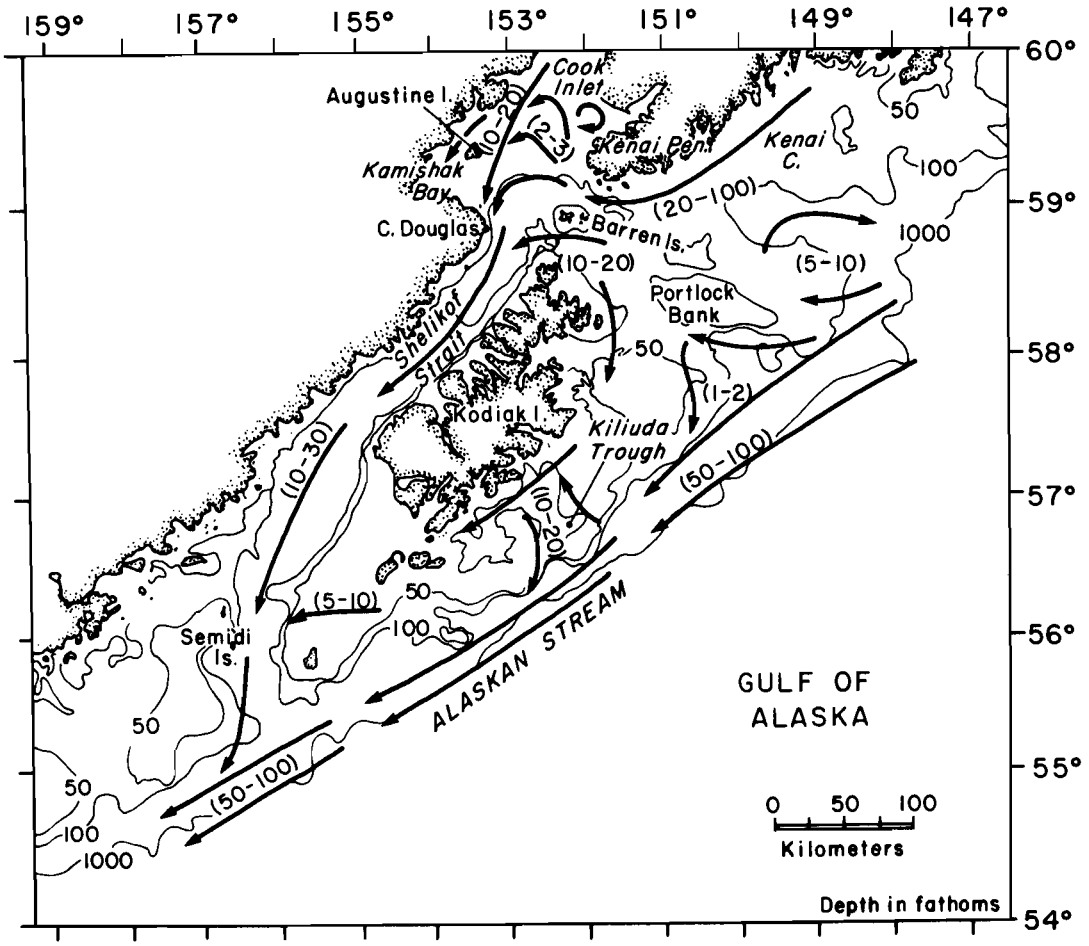

Figure i. Schematic diagram of net circulation in the northwest Gulf of Alaska. Arrows indicate direction of mean surface flow, and numbers in parentheses indicate approximate range of speeds in cm sec^{-1}.

topography. A principal driving force for the Alaskan Stream is the wind stress curl over the Gulf of Alaska, which forces the North Pacific subarctic gyre. The Alaskan Stream is the intensified, northwestern leg of this gyre.

2. Dominant circulation on the banks south and southeast of Kodiak Island is predominantly driven by the Alaskan Stream. This includes a poorly defined, weak (5-10 cm sec^{-1}) anticyclonic circulation over Portlock Bank, and a complex flow regime connected with the bank-trough region to the southwest. This bank-trough flow, which apparently represents a bathymetric effect upon the inshore edge of the Alaskan Stream, consists of shoreward flow along the upstream (northeastern) sides of the troughs and a compensatory seaward flow along the downstream (southwestern) sides. The coastal southwesterly flow at the head of Kiliuda Trough reflects this residual circulation, but is probably also due in part to a baroclinic coastal wedge consequent to freshwater input along the south coast of Kodiak Island.

3. A nearshore southwesterly flow along the Kenai Peninsula, the Kenai Current, is a baroclinic coastal current driven by the density field created by freshwater input along the Alaskan coast. This flow is 20-30 km in width and attains maximum current speeds in autumn following the annual period of maximum coastal precipitation and freshwater input. This flow is at its annual minimum during spring and early summer.

4. Flow through Shelikof Strait is southwesterly, with observed speeds during winter ($\sim$20 cm sec^{-1}) twice those in summer ($\sim$10 cm sec^{-1}). No flow reversals were observed during winter; during summer, the weaker mean flow was accompanied by occasional reversals. This flow is driven in part by the Kenai current upstream and in part by a large-scale alongshore pressure gradient established by the Alaskan Stream. The flow through Shelikof Strait continues to the southwest in a well-defined channel bounded by

relatively shallow banks, merging with the Alaskan Stream some 200 km southwest of Kodiak Island.

5. Circulation in lower Cook Inlet is dominated by the southwesterly flow into Shelikof Strait, which is constrained by bottom topography to traverse an arcuate east-west path across the lower Inlet. Off Cape Douglas, this flow merges with a weaker southward current generated by the freshwater input to upper Cook Inlet, creating a particularly intense southward flow in the region off Cape Douglas. Flow in the central lower inlet out of these two well-defined currents is weak and highly variable.

6. Currents throughout the study region are characterized by speed and direction fluctuations having time scales between about 2 days and a week. These fluctuations are probably related either to meteorological factors or to propagation of ocean eddies across the shelf, though the exact mechanisms are uncertain. In regions such as Shelikof Strait, with a strong mean flow, these fluctuations are of lesser significance relative to the mean flow, leading to speed fluctuations but only minor perturbations to direction. In regions of weak mean flow, such as in central lower Cook Inlet and on Portlock Bank, the fluctuations both in speed and direction are the dominant flow characteristics.

7. Tidal currents vary widely in magnitude throughout the study region. Tidal current effects in Shelikof Strait are minimal because of the standing wave nature of the tidal wave there, and tidal currents become small as the coast is approached south of Kodiak Island. Lower Cook Inlet is characterized, conversely, by large tidal currents particularly in the passages north and south of the Barren Islands due to the near-resonant conditions which lead to extremely large tides in upper Cook Inlet. Tidal currents are also significant in comparison with mean flow on the banks south of Kodiak Island.

8. Winds are controlled by the interaction between large-scale northeastward migrating cyclonic low pressure systems and regional topography. Over the banks south of Kodiak Island, observed winds appear to agree reasonably well with geostrophic winds computed from the atmospheric surface pressure distributions. In lower Cook Inlet, winds are orographically channelled into two orthogonal paths whose axes are aligned with upper Cook Inlet-Shelikof Strait and Barren Islands-Kamishak Bay. This leads to a complex wind pattern there which results from the interaction between these orthogonal flows. Katabatic (drainage) winds may be important locally, particularly in lower Cook Inlet and Shelikof Strait, and wake effects perturb the wind field downstream from such features as Augustine Island.

The picture presented here of major circulation features in the northwest Gulf of Alaska is one of extreme complexity. The various possible combinations of mean, low frequency fluctuating and tidally fluctuating flow lead to a regime wherein prediction of instantaneous flow is impossible. We believe, however, that the flow field has been sufficiently well defined to allow a good prediction of seasonal mean flow. Combined with knowledge of the local and regional wind field, this allows at least an approximate predictability of contaminant dispersion and trajectory.

PHYSICAL OCEANOGRAPHIC AND METEOROLOGICAL CONDITIONS IN THE NORTHWEST GULF OF ALASKA[1]

Robin D. Muench[2] and James D. Schumacher

1. INTRODUCTION

1.1 Statement of Purpose

1.1.1. Objectives

The primary objective of the Alaska OCS Environmental Studies Program is to provide background information for management decisions that may be necessary to protect the OCS marine environment from damage during oil and gas exploration and development. Meaningful data must be readily available in useable form so that informed management decisions can be made before serious or irreversible damage occurs. Protection of the marine and coastal environment is a direct outgrowth of the National Environmental Policy Act of 1969.

In an assessment of the potential impact of OCS development on the marine environment, transport and transformation of petroleum-related contaminants is of key significance. Petroleum or other contaminants introduced into the environment can be transported in the atmosphere, water column and sea ice. During transport, oil and other contaminants undergo continual physical and chemical change brought about by such processes as evaporation, flocculation, emulsification, weathering, biodegradation, and chemical decomposition.

Transport studies are specifically designed to provide data that will enable the Department of the Interior and other agencies to:

. Plan stages and siting of offshore petroleum development so as to minimize potential risk to environmentally sensitive areas.

[1]Contribution No. 482 from the NOAA Pacific Marine Environmental Laboratory
[2]Now at SAI/Northwest, 13400B Northrup Way #36, Bellevue, WA 98005

- Provide trajectory, coastal landfall, and impact predictions required for cleanup operations in the event of an oil spill or the introduction of other contaminants.
- Assist in planning the locations of long-term environmental monitoring stations in the study area.

The programmatic objectives described above have resulted in several disciplinary studies of which one element, coastal oceanography and meteorology, directly addresses the problem of movement of contaminants in continental shelf waters.

The primary objective of the OCSEAP oceanography/meteorology studies in the western Gulf of Alaska is to provide, through experimental and theoretical studies, a capability to predict movement and distribution of contaminants introduced into the marine environment through OCS oil and gas development activities. Specific program elements have required the development of methodologies and implementation of studies designed to supply information on:

- Energetics and temporal and spatial variability of coastal ocean circulation in the northwestern Gulf of Alaska;
- Energetics and spatial variability of tidal currents;
- Local wind fields and their influence on coastal circulation;
- Influence of the seasonal heat budget, runoff and precipitation on coastal and estuarine circulation and water mass structure;
- Bathymetric influence on tidal and nontidal circulation and turbulent mixing; and
- Ways to apply data to the prediction of pathways and impact areas of potential pollutants (especially oil) that will aid the assessment of vulnerability of biotic resources and the design of more effective cleanup strategies.

This presents an integrated description of the oceanography and meteorology of the western Gulf of Alaska continental shelf. This description

includes the rationale for the various elements of the study program and a presentation of results, analysis techniques and interpretive procedures by which these program elements have been combined to provide an improved understanding of coastal circulation and winds and their likely influence on pollutant transport.

1.1.2 Rationale

Development of an information base that permits prediction, in a probabilistic sense, of the spatial and temporal distribution of petroleum-related contaminants following hypothetical release in coastal waters is a primary function of the OCSEAP transport studies. Such information, in conjunction with seasonal and spatial description of potentially vulnerable marine resources, provides a critical input to the Bureau of Land Management's (BLM's) environmental assessment process. Insofar as this assessment concerns the potential impacts of OCS-related pollutants, BLM's major effort is focused on spilled oil and its subsequent movement on the water surface.

In the Draft Environmental Impact Statement (DEIS), which is to be prepared by the Bureau of Land Management, the most readily apparent use of the oceanographic and meteorological study results is the oil spill risk analysis performed by the U.S. Geological Survey. However, problems of oil incorporation into the water column and sediments and potential impacts of drilling muds, toxic metals, formation waters and other potential pollutants are also of concern. Hence the oceanographic and meteorological studies provide information on both surface and subsurface phenomena that have bearing on the overall problem of contaminant distributions on the continental shelf. Similarly the modeling activities, aside from producing information for the calculation of spilled oil trajectories, also perform important roles in data synthesis, hypothesis formulation and field study design.

Prior to OCSEAP, no systematic studies had addressed mesoscale oceanographic features on the Gulf of Alaska continental shelf. Oceanographic knowledge was limited to a description of large-scale circulation obtained almost exclusively from water mass analyses based on irregular, widely spaced hydrographic data. While knowledge of large-scale flow features such as the Alaska Current and Alaskan Stream was useful in providing a gross picture of Gulf of Alaska circulation, it furnished little insight into smaller scale features present on the continental shelf and responsible for near-coastal transport of contaminants. A need for such information has required the development, through OCSEAP, of a systematic program of mesoscale physical oceanographic and meteorological studies on the continental shelf.

Oceanographic studies in the western Gulf of Alaska cover the geographic region comprising the present Kodiak (Sale 46) and lower Cook Inlet-Shelikof Strait (Sale 60) OCS lease areas shown on the frontispiece. The region consists of the Alaska continental shelf area between Seward and Mitrofania Island on the Alaska Peninsula, including Shelikof Strait and that portion of Cook Inlet south of Kalgin Island.

Oceanographic field studies have employed a variety of techniques including seasonal hydrographic surveys, time series observations of currents, pressure and water properties, Lagrangian current observations, HF Doppler radar current observations, and drift cards. The primary purpose of these studies is to provide the information necessary to develop a picture of continental shelf circulation and mixing processes, including significant temporal and spatial variability scales, relevant to the transport of pollutants.

The importance of local wind forcing to the dynamics of continental shelf waters and to the subsequent movements of potential contaminants was recognized from the program's beginning. It was also recognized that local winds along the Gulf of Alaska coast can differ significantly, because of the effects of coastal orography and land-sea boundaries, from those determined from synoptic weather charts or land-based stations. These differences can lead to substantial errors in pollutant transport predictions based on traditional synoptic geostrophic wind calculations or inappropriately located (for OCSEAP's requirements) weather stations. Consequently, the oceanographic program has been accompanied by concurrent coastal meteorological investigations that include an expanded network of shore stations, over-the-water wind and pressure measurements from meteorological data buoys and ships of opportunity, and computer simulations of coastal winds. These studies have resulted in the development of a technique for determination of mesoscale wind fields that consists of (1) derivation of a synoptic weather pattern climatology in the form of a limited number of surface pressure distributions, based on historical data and judged adequate in number to characterize the region; (2) development of appropriate synoptic climatology statistics, including pattern durations and transition probabilities; (3) calculation, via a combination of direct observations and modeling, of the mesoscale wind field most likely to be associated with and driven in part by each synoptic pattern; and (4) use of (1) - (3) above to derive a statistical description of the local wind climatology. This technique attempts to correlate local wind patterns with regional synoptic distributions which have a statistically meaningful data base and are routinely observable.

Oceanographic and meteorological field studies in the western Gulf of Alaska have been accompanied by computer simulation models of coastal

circulation patterns and likely pollutant trajectories. Models employed to date have been of three general types: (1) a diagnostic circulation model utilizing observed winds and hydrography as input and observed currents as calibration data; (2) a tidal model; and (3) an empirical model based on observed currents and winds. Specific model application has depended on the study area in question and the driving forces and physical mechanisms believed to be dominant in that region. These models have been used both in a predictive sense and as vehicles for the synthesis and interpretation of observed data.

Collectively, the modeling activities and oceanographic field studies have been employed in an interactive fashion to provide an improved understanding of coastal circulation patterns and dynamical processes.

1.2 Geographical Setting

In discussing physical oceanographic processes in the northwestern Gulf of Alaska, we focus primarily upon coastal and continental shelf regimes. Physical factors which are known to exert primary controls over circulation in such regions include bottom depth and slope, continental shelf width, and orientation of the coastline relative to north. On a smaller scale, coastline and bottom topographic irregularities can exert significant influence over local circulation features. Since we address a broad range of both temporal and spatial scales of oceanographic processes, it is necessary to discuss in some detail those geographical and bottom features which we expect a priori to significantly affect oceanographic conditions.

The northern Gulf of Alaska is an arcuate, east-west trending bight which forms the northern boundary of the northeastern Pacific Ocean (Fig. 1). We are concerned here with the portion of the Gulf extending from the shoreline seaward to the continental shelf break, as defined approximately

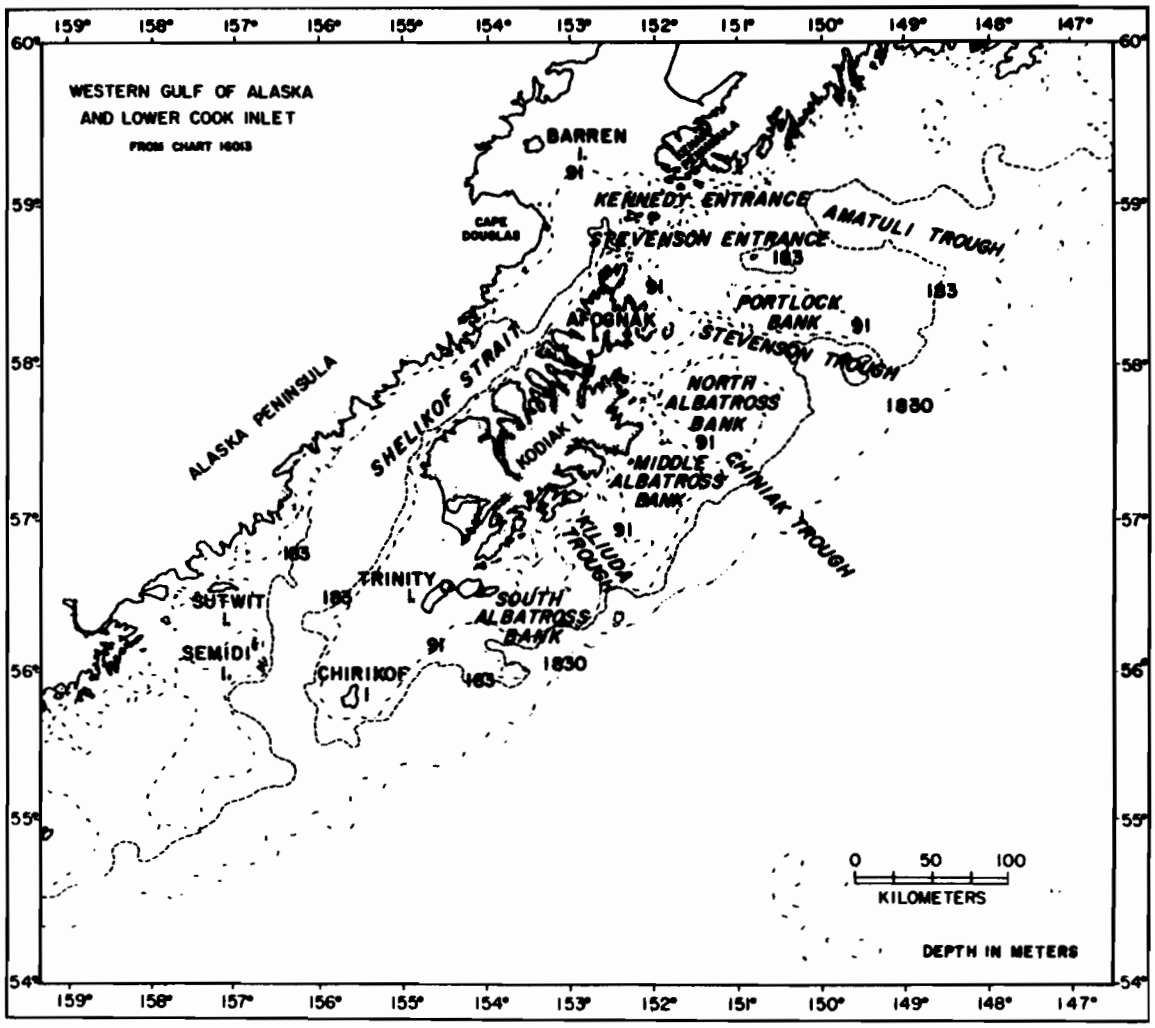

Figure 1. Northwest Gulf of Alaska regional bathymetry and geographical locations.

by the 200-m isobath, and westward from 148°W to about 160°W. This area encompasses a segment of continental shelf characterized by complex shoreline and bottom topography which includes numerous embayments and channels, banks and troughs. The shelf is about 175 km wide throughout our study region. Kodiak Island, along with its smaller adjacent islands, may be viewed as a barrier to flow which is centrally located on the shelf and surrounded by a system of relatively shallow banks. Alternately, the shelf may be considered to occupy the region southeast and east of Kodiak Island, with Shelikof Strait being a major channel separate from the shelf proper. (Both viewpoints will be used, depending upon the context.) Cook Inlet extends northeasterly from the shelf directly north of Kodiak Island; the lower Cook Inlet-Shelikof Strait system comprises a complex system of deep channels. Overall alongshore orientation of this continental shelf system is northeast-southwest. Seaward of the 200-m deep shelf break, the bottom drops abruptly to attain maximum depths of 5000-6000 m in the Aleutian Trench.

The continental shelf area southeast of Kodiak Island is about 60 km wide. Bottom topography there and to the northeast is dominated by four relatively shoal (∿90 m) areas separated from one another by deeper channels which transect the shelf in a direction roughly normal to the coastline (Fig. 1). The shoals are, from northeast to southwest, Portlock and North, Middle and South Albatross Banks. At the northeastern extremity of this system of banks, Amatuli Trough trends east-west with depths exceeding 200 m. At its western end, this trough bifurcates to form the deeper portions of the channels entering Cook Inlet via Kennedy and Stevenson Entrances and, in so doing, provides a relatively deep access (∿100 m) from the shelf break to the waters of lower Cook Inlet. To the south of Amatuli Trough lies Portlock Bank, which has depths of less than 50 m and is separated from

North Albatross Bank to the southwest by Stevenson Trough. At its shallowest point, in the narrow channel west of Portlock Bank, Stevenson Trough is about 110 m deep. Depths on North Albatross Bank are 70-90 m. North and Middle Albatross Banks are separated by Chiniak Trough, which has maximum depths of about 145 m. Minimum depths on both Middle and South Albatross banks are about 30 m and are found at the seaward boundary of the banks. Kiliuda Trough separates Middle and South Albatross Banks, has maximum depths of about 150 m, and near the coastline turns and trends southwest to form an inverted L-shaped depression with generally complex topography. Maximum vertical relief in this system of banks and troughs is found surrounding Kiliuda Trough.

Shelikof Strait lies between Kodiak and Afognak Islands and the Alaska Peninsula and is uniformly about 45 km wide, forming a major channel for alongshore flow. At its northern end it is connected to the open shelf via Kennedy Entrance north of the Barren Islands, and via Stevenson Entrance between the Barren Islands and Afognak Island. Kennedy Entrance is the narrower of the two but has greater depths (~200 m). Maximum depths in Stevenson Entrance are about 120 m. The northeastern half of Shelikof Strait is somewhat shallower than the southwestern half, or about 180 m as compared to 200 m. The extension of the Strait across the shelf southwest of Kodiak Island is bounded on both sides by banks and has maximum depths of about 200 m. The adjacent banks are 30-40 m deep to the southeast and 100 m deep to the northwest where they shoal to form Sutwik and the Semidi Islands.

Cook Inlet is a broad (70-90 km), shallow (mean depth about 60 m), elongate embayment extending northeastward from the confluence between Shelikof Strait and Kennedy and Stevenson Entrances (Fig. 2). This study deals only with the lower portion of the Inlet defined as that region

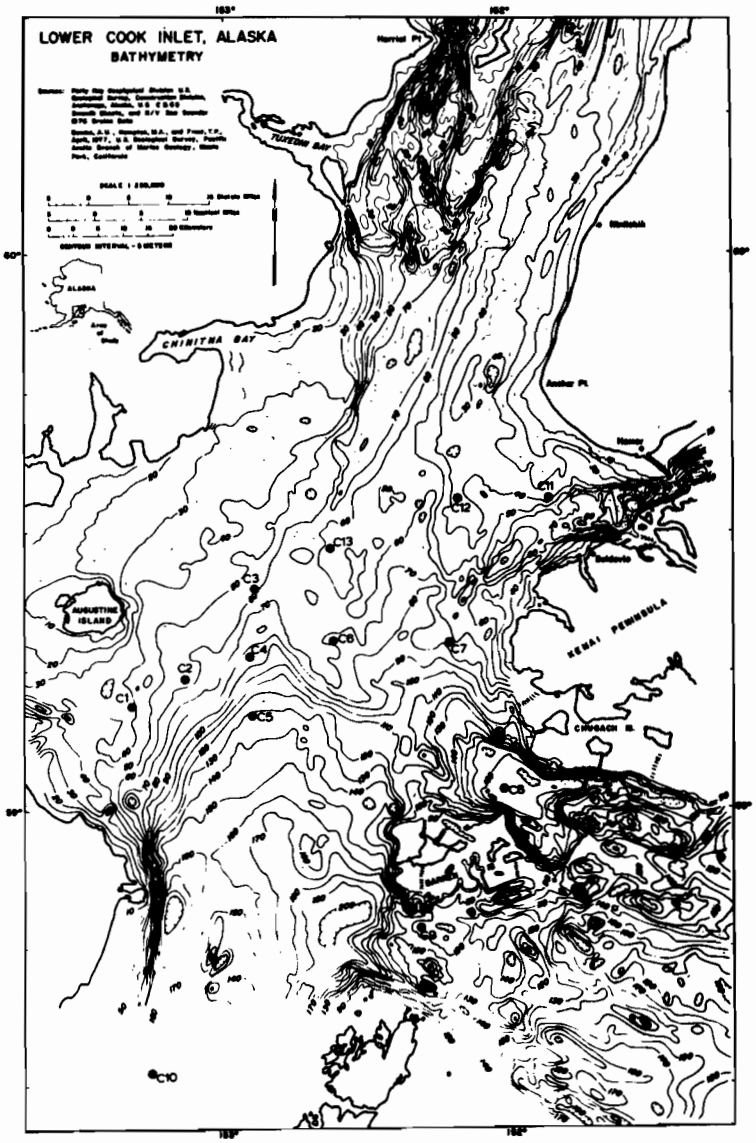

Figure 2. Detail of lower Cook Inlet bathymetry.

bounded on the north by the Forelands and on the south by Kennedy and Stevenson Entrances and Shelikof Strait. At the northern end of lower Cook Inlet, Kalgin Island and its associated shoals reduce water flow in the western half of the Inlet. In the central portion of the lower Inlet, bottom depths are 60-80 m. Depth increases to the south in regular fashion except for a prominent ramp-like feature which traverses the inlet from east to west in arcuate fashion along the 100-m isobath. Maximum depths in the inlet occur in a depression just west of Stevenson Entrance. Several embayments extend laterally from the Inlet.

Land areas surrounding the northwestern Gulf of Alaska are extremely mountainous. On Kodiak Island, these mountains rise to elevations of 1000-2000 m, while along the northern shores of Cook Inlet and Shelikof Strait elevations are 2000-3000 m. The mountains are transected by valleys, many containing glaciers or snowfields at their heads. This rugged topography surrounding the study region is of interest because it exerts a marked effect upon local winds, which in turn can affect water circulation.

1.3 History of Past Research

Prior to commencement of the OCSEAP studies, little information was available concerning physical oceanographic conditions on the northern Gulf of Alaska shelf. Few field data were available from the shelf region, since early investigations were confined primarily to the Alaskan Stream or the Gulf of Alaska subarctic gyre. The Alaskan Stream is an offshore boundary current which flows southwestward along the shelf break, forming the northwestern branch of the subarctic gyre. The single exception to this was the early work of McEwen, et al. (1930), who used temperature and salinity data obtained along sections normal to the coastline in the northeast Gulf of Alaska to describe and analyze temperature, salinity and current structures over the shelf and shelf break.

Some three decades following the work of McEwen, et al. (1930), acquisition of substantial sets of new field data allowed investigators to concentrate on the northwestern Gulf. Resulting manuscripts used temperature and salinity data to address circulation processes in the Alaskan Stream southwest of Kodiak Island and westward along the Aleutian Islands (Dodimead et al., 1963; Favorite, 1967; Roden, 1969; Favorite et al., 1976). These analyses led to definition of the Alaskan Stream as a western boundary current which acts as a return flow for the wind-driven circulation in the northern Gulf of Alaska (Favorite et al., 1976), an observation which was subsequently supported by the theoretical work of Thomson (1972). Reed and Taylor (1965) computed peak baroclinic surface speeds in the Alaskan Stream of order 100 cm sec^{-1}, and presented evidence that the flow was predominantly baroclinic and in geostrophic balance. Ingraham et al. (1976) computed Sverdrup transports in the Gulf of Alaska using calculated geostrophic winds, and concluded that transports in the Alaskan Stream can vary from about 20 x 10^6 m^3 sec^{-1} in winter to less than 5 x 10^6 m^3 sec^{-1} during summer. Reed et al. (1980) have used OCSEAP temperature and salinity data to show, however, that a mean baroclinic transport of about 12 x 10^6 m^3 sec^{-1} in the Alaskan Stream does not reflect the large annual variation of wind stress curl over the Gulf of Alaska.

Direct observations of circulation in the Gulf of Alaska are sparse, consisting primarily of the drift-card studies carried out by Favorite (1964) and Favorite and Fisk (1971) which provided qualitative support for cyclonic circulation in the Gulf of Alaska and a westerly flow south of the Aleutians. An excellent summary of subarctic Pacific oceanography was prepared by Favorite et al. (1976). Most recently Reed (1980) used satellite-tracked drogued buoys to document the closed gyre circulation in the Gulf of Alaska.

Prior to inception of the OCSEAP research program, acquisition of new temperature and salinity data from the Gulf of Alaska continental shelves allowed characterization of seasonal variations in the water column (Royer, 1975). Royer and Muench (1977) discussed some large-scale features in the surface temperature distribution and related these to the regional circulation and to vertical mixing regimes on the shelf. Hayes and Schumacher (1976) and Hayes (1979) described and discussed the interrelations between winds, currents and bottom pressures on the continental shelf in the northeastern Gulf. Their work suggests that oceanic forcing is dominant at the shelf break, but that inner shelf or coastal circulation is primarily dependent upon other factors. This was substantiated by Royer et al. (1979), who provided evidence for a coastal flow extending some 500 km east from Prince William Sound in a 15- to 20-km wide coastal band. Royer (1979) discussed the impact that extensive precipitation and runoff can have on the near-coastal circulation. In related work Schumacher et al. (1978; 1979) indicated that for the northwest Gulf of Alaska shelf the Alaskan Stream acts as an offshore feature whose typically high speeds (50-100 cm sec^{-1}) do not extend appreciably onto the shelf. However, they indicate that the hydrographic data show a shoreward flux of heat and salt over the shelf.

Previous work in Cook Inlet, which forms a major embayment on the northwest Gulf of Alaska shelf and is especially subject to pollution problems because of active petroleum activities and other industrial development, has been limited primarily to unpublished manuscripts from various sources (e.g. Kinney et al. 1970a, 1970b; Knull and Williamson, 1969; Wright et al., 1973; Gatto, 1976; Burbank, 1977). Previous field activities focused primarily upon the upper portion of the Inlet (e.g. Kinney et al., 1970a, 1970b). Studies using surface drifters have attempted to define the circula-

tion in Kachemak Bay (Knull and Williamson, 1969) and in the lower Inlet (Burbank, 1977). Landsat data, which qualitatively indicate suspended sediment distributions in near-surface waters, have led to several qualitative expositions on Cook Inlet surface circulation (Wright et al., 1973; Gatto, 1976). In the most recent work on lower Cook Inlet, Muench et al. (1978) used summer 1973 oceanographic data obtained by the National Ocean Survey of NOAA to qualitatively discuss circulation and hydrography in the lower Inlet.

At the time of preparation of this report, then, much is known of the general, large-scale circulation on the northwest Gulf of Alaska continental shelf and in lower Cook Inlet, a major appended embayment. Our goal has been to synthesize this general information while at the same time incorporating the data from our experimental and theoretical studies.

1.4 Oceanographic and Meteorological Setting

In order to clarify the rationale used for field sampling, it is necessary to discuss in general fashion the main physical features which control regional oceanographic processes. The major oceanographic feature in the northwest Gulf of Alaska is the Alaskan Stream, an intense, southwestward-flowing current lying along the continental shelf break and slope to the southeast of Kodiak Island (Fig. 3). This current is the northwestern branch of the closed subarctic Pacific gyre which occupies the Gulf of Alaska and is driven primarily by the wind-stress curl over the North Pacific (Reed et al., 1980). The current is generally most intense near the shelf break, where it can attain daily mean surface speeds of order 100 cm sec^{-1} or more. Speeds taper off to seaward, and the current width from the shelf break to the point where speeds approach zero is of order 50 km. Baroclinic

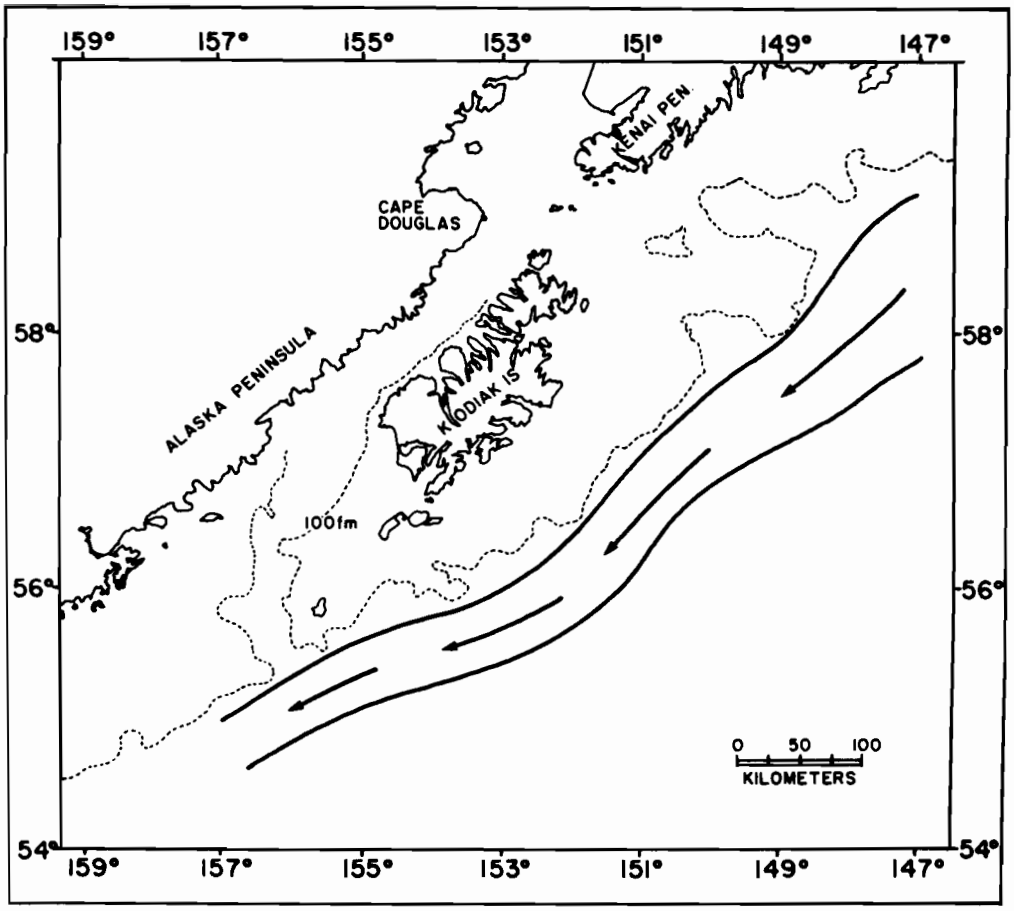

Figure 3. Approximate location of the Alaskan Stream along the shelf edge in the northwest Gulf of Alaska.

volume transport in the Alaskan Stream averages about 12 x 10^6 m^3 sec^{-1}, as computed using available temperature and salinity data; there does not appear to be a significant seasonal signal in this transport, contrary to what we would expect considering the large annual variation in wind-stress curl over the Gulf of Alaska (Reed et al., 1980). Since there are few direct observations of current in the Alaskan Stream, magnitude of the total volume transport remains uncertain.

Flow on the continental shelf and in Shelikof Strait is toward the southwest throughout the year. This flow is driven primarily by a combination of alongshore sea-level slope, consequent to the presence along the shelf break of the westward-flowing Alaskan Stream, and the baroclinic field established by freshwater input along the Alaskan coast (Muench et al., 1978; Schumacher and Reed, 1980).

Annual variability of shelf water properties in the northern Gulf of Alaska has been characterized by Royer (1975) (Figure 4). During winter, intensification of cyclonic atmospheric circulation over the Gulf of Alaska leads to easterly coastal winds and a downwelling tendency. At the same time, wind and thermohaline processes contribute to vertical mixing. Consequently, the water is characterized during winter by vertical near-homogeneity, elevated salinities and low temperatures. During summer, coastal winds diminish to allow relaxation of downwelling and create a weak upwelling tendency, and freshwater input and solar insolation act to increase stratification. As a result, the coastal waters are stratified in temperature, salinity and density during summer and fall, during which time temperature and salinity attain their maximum and minimum values, respectively, with respect to the annual cycle.

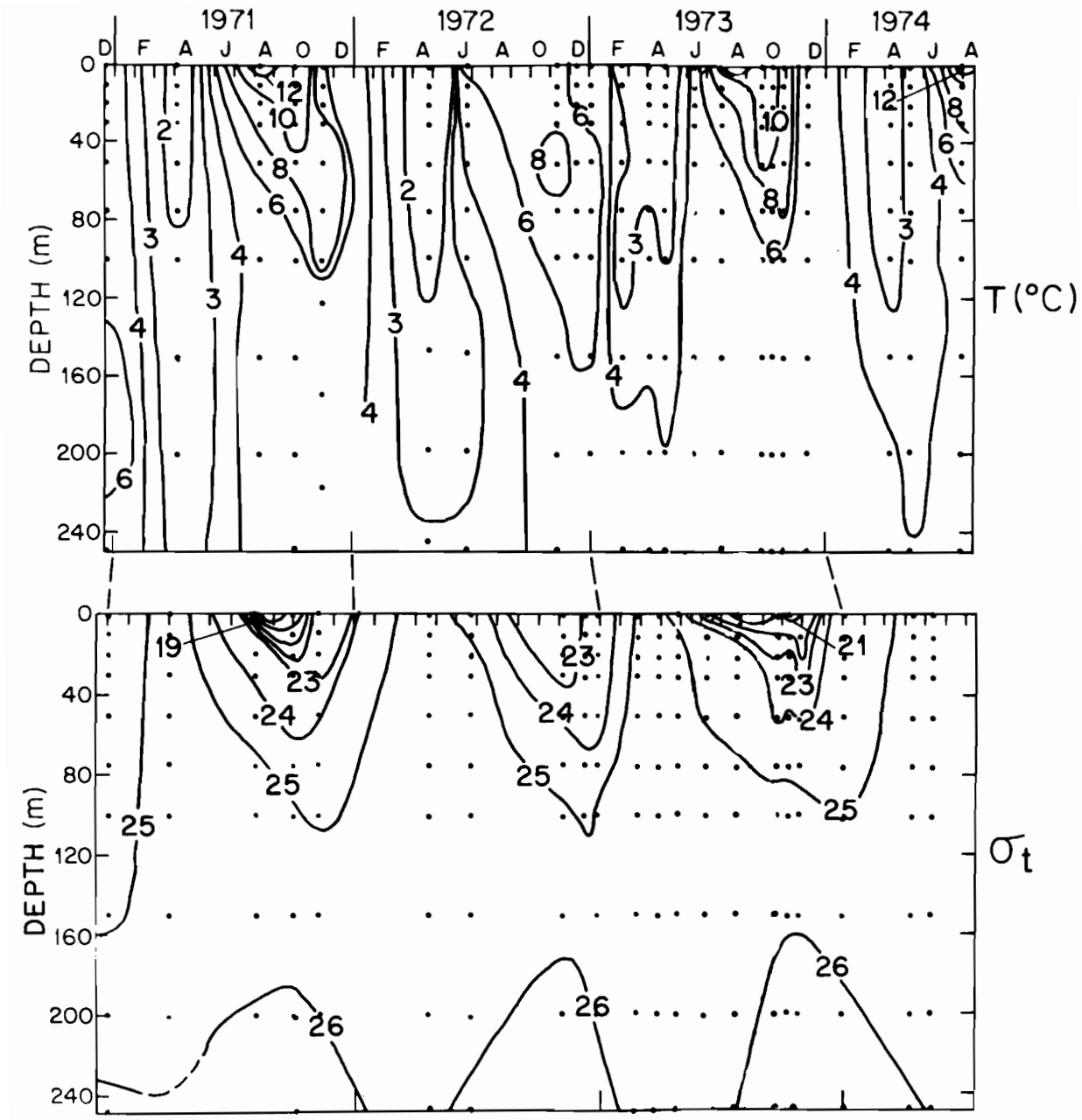

Figure 4. Variation of temperature and density (as sigma-t) at a location on the northern central Gulf of Alaska shelf (after Royer, 1975).

Regional meteorology is dominated by the Aleutian atmospheric low pressure system. During winter this system intensifies and intense, cyclonic low pressure systems migrate northeasterly off Kodiak Island. During summer, the North Pacific atmospheric high pressure region dominates, and the intensity and frequency of cyclonic storms decreases, leading to weak and variable winds. Air temperatures are occasionally below 0°C. during winter, but rise to well above freezing during summer. A useful summary of such regional climatological data has been prepared by Brower et al. (1977).

A final factor which can be significantly effective upon continental shelf circulation is freshwater input from continental sources. This input is not generally well known along the northwestern Gulf of Alaska coast, due to the scarcity of gaging stations. It is known, however, that there are generally two annual peaks in runoff. The first, or spring peak, results from melting of the previous winter's snow cover. The second, or autumn, peak occurs with the onset of severe storms which bring large quantities of rain to coastal regions. This second peak drops off once air temperatures have become low enough so that the precipitation occurs as snow rather than rain. In some areas, one of the peaks may be negligible, or the low-flow period between peaks may disappear. The latter is true of major river input into upper Cook Inlet because of the long duration of the spring snow-melt peak, which actually continues well into summer, coupled with low summer rainfall (cf. Muench et al., 1978).

Sea ice is not generally encountered in the northern Gulf of Alaska. The exception is in Cook Inlet, where low air temperatures and a high freshwater content due to river input lead to local ice formation in the upper Inlet. Some landfast and floe ice also occurs in Kachemak Bay during extreme winters. In Kamishak Bay, a combination of landfast ice in the embayments

and floes from the upper Inlet can result in heavy winter ice accumulation. Much of this ice is advected southward along the western shore of the Inlet by wind and water circulation, and is occasionally found as far south as Cape Douglas.

The factors summarized in this section, in conjunction with bathymetric features discussed in Section 1.2, ultimately determine the physical oceanographic characteristics of the northwestern Gulf of Alaska shelf.

2. OBSERVATIONAL PROGRAM

2.1 Program Rationale

The OCSEAP field observation program in the Gulf of Alaska was designed to define and explain the fields of wind and water motion as they affect contaminant trajectories and dispersion. At the outset of the study, little was known either of local winds or of water motion on the Gulf of Alaska continental shelf. Therefore, the initial phases of the program attempted a large-scale definition of motion and the associated temperature-salinity-density (for water) and pressure (for winds) fields needed to address the regional oceanographic and meteorological dynamics. Early phases of the program involved field work extending from east of Kodiak Island westward to Unimak Pass in the Aleutians, but were of too coarse a resolution to define specific local features. Once large-scale winds and water flow on the shelf had been defined, specific process-oriented experiments such as the meteorological-oceanographic study of lower Cook Inlet and the intensive oceanographic study of the bank and trough region off Kodiak Island were undertaken. In this way the field program evolved continually, with new phases of the field work being determined by the outcome of previous phases. The emphases were always on more localized, process-oriented studies as time progressed. Thus, the general survey of oceanic circulation on the shelf between Kodiak Island and Unimak Pass evolved into separate process studies in Cook Inlet, in Shelikof Strait and in the Kiliuda Trough area south of Kodiak Island. Results from the general scientific literature, obtained from experiments in other parts of the world ocean, were also used in planning the process studies and in attempting to foresee results. Results of the studies were integrated with related results from other regions to comprise contributions to basic science, as well as further knowledge of

the northern Gulf of Alaska. Aspects of this development will be further clarified in the following discussion.

2.2 The Current Observation Program

Currents were observed in the northwest Gulf of Alaska using moored current meters deployed on subsurface arrays, surface drift cards, satellite-tracked, drogued drifters and HF radar. The first method yielded time series of currents at fixed locations, or Eulerian measurements. The second method provided us with points of release and recovery which, in turn, allowed crude estimation of Lagrangian drift trajectories. The third method provided us with Lagrangian drift trajectories which approximate those followed by a water parcel. The final method yielded actual observations of surface water motions.

2.2.1 Taut-Wire Moorings

Moored current meters were deployed using taut-wire moorings and acoustic releases (Fig. 5). Aanderaa RCM-4 recording current meters were used for all moorings. These use Savonius rotors to measure current speed and vane/compass assemblies for determining current direction relative to magnetic north.

The pattern for deployment of the moorings can be divided into subsets. The first set of moorings was designed to investigate large-scale (~500 km) alongshelf flow seaward of Kodiak Island and as far southwest as Unimak Pass (Fig. 6). Durations of these observations, broken down according to individual instruments on each mooring, are indicated in Appendix A. These moorings carried the prefix designation "WGC".

The second set of moorings was designed to investigate circulation around Kodiak Island, and included deployments in Shelikof Strait and on the banks southeast of the island (Fig. 7).

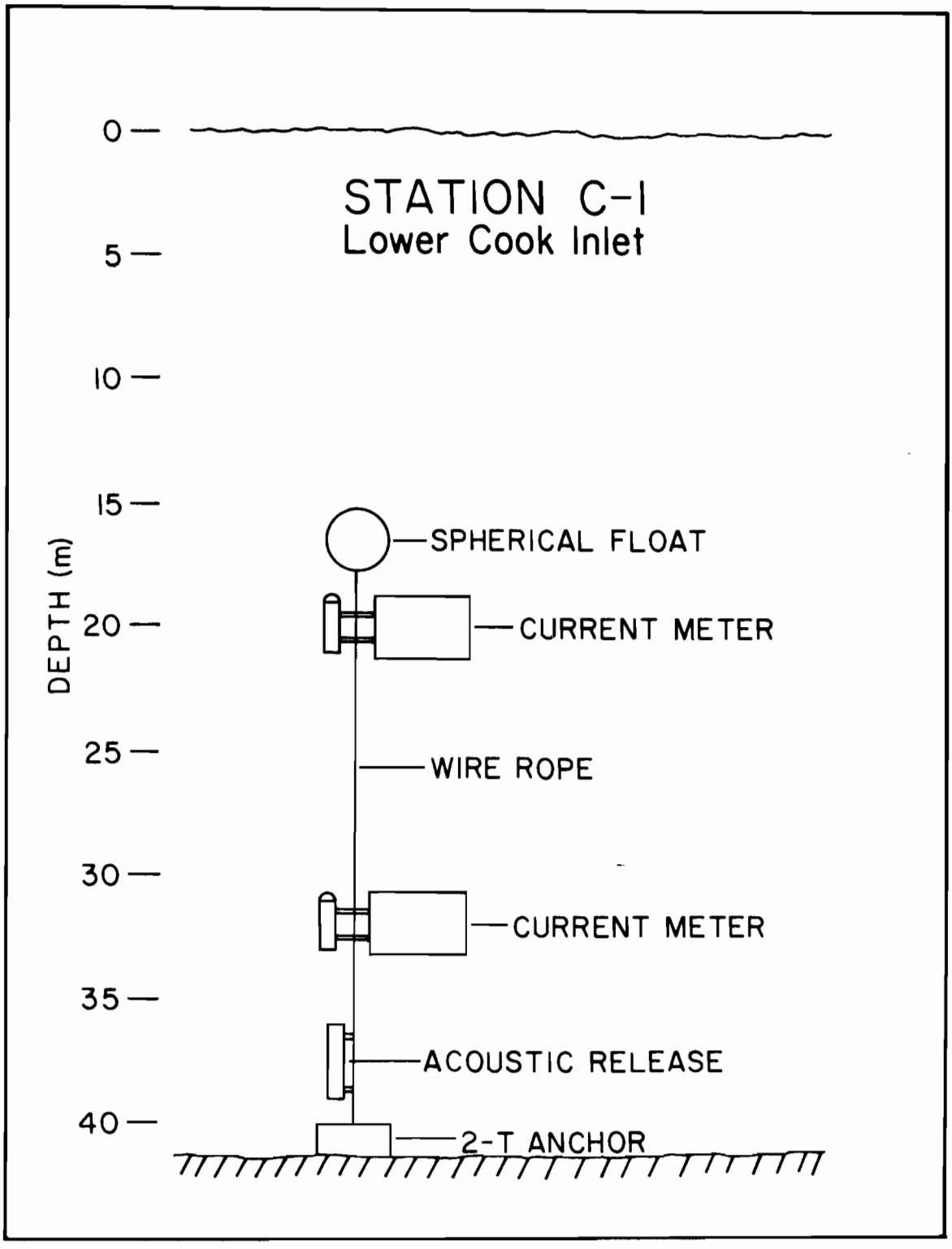

Figure 5. Example of configuration of taut-wire current meter mooring used in the northwest Gulf of Alaska. Number of meters and their vertical spacing varied with different stations and depended upon such factors as water depth and stratification.

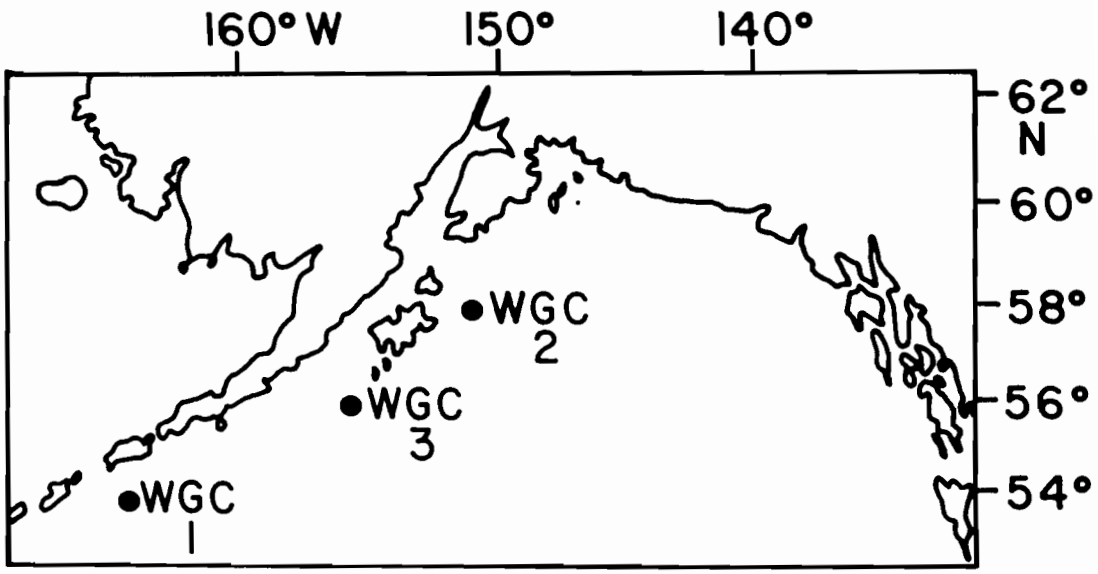

Figure 6. Current meter mooring locations for preliminary, large-scale investigations of shelf flow in the northwest Gulf of Alaska. Mooring statistics are given in Appendix A.

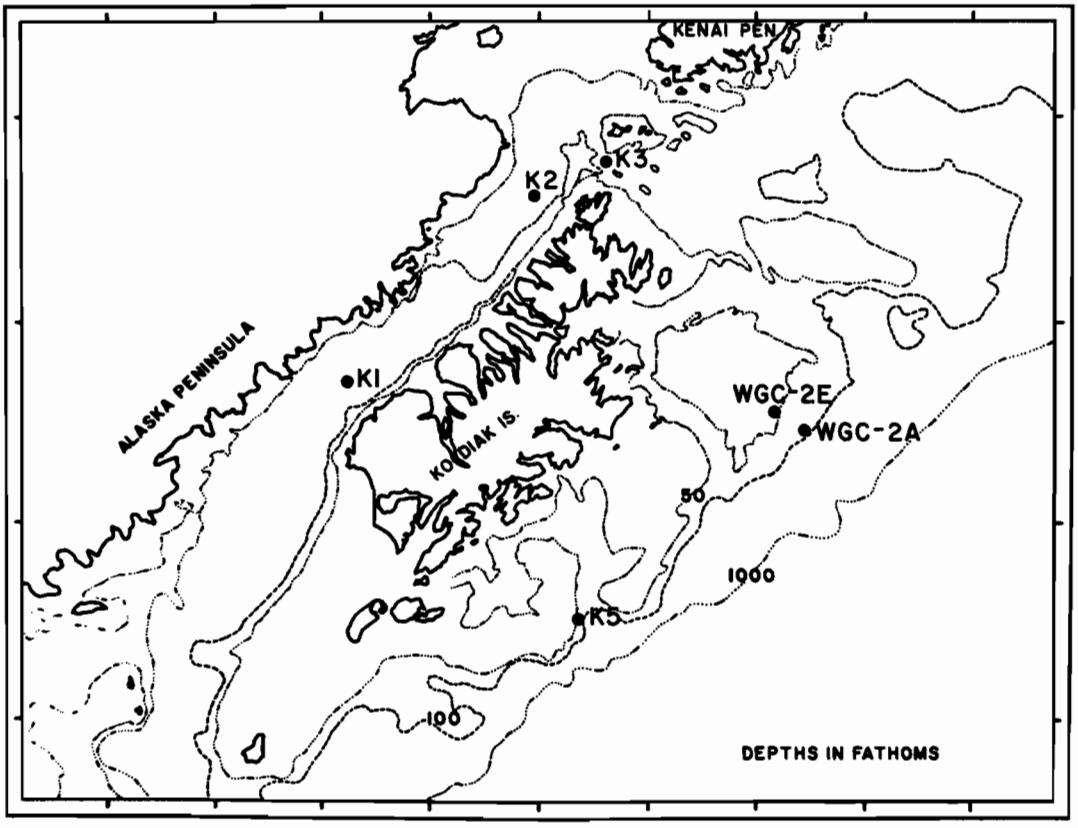

Figure 7. Locations of current meter moorings deployed during winter 1976-77 in the region surrounding Kodiak Island. Mooring statistics are given in Appendix A.

A third set of moorings was deployed on two separate occasions, approximately 5-mo periods in winter 1977-78 and again in summer 1978. These moorings encompassed three separate process-oriented studies. Moorings C1-C13 were deployed in lower Cook Inlet in an attempt to better understand circulation connected with the bathymetry and in the region of convergence defined by Muench et al. (1978) (cf. Section 3.2)(Fig. 8). Moorings K6-K13 were deployed in the region surrounding Kodiak Island as an extension of the experiment initiated with K1-K5 to investigate circulation around the island (Fig. 9). A particularly important aim of this experiment was investigation of circulation in the region south of Kodiak Island where the shelf is transected by banks and troughs. Finally, moorings M1-M4 were deployed, during winter 1977-78 only, in the coastal region off Mitrofania Island southwest of Kodiak Island to attempt a comparison between the coastal dynamics there and in the northeast Gulf of Alaska where a similar experiment had been carried out (cf. Hayes, 1979) (Fig. 10). Failure to recover the shelf break mooring M3 severely limited the usefulness of this data set, however.

The current meters sampled at 15- or 20-min intervals. Raw data were low-pass filtered to remove high-frequency noise; this filter passed more than 99% of the amplitude at periods greater than 5 h, 50% at 2.86 h and less than 0.5% at 2 h. This series was then further filtered to remove most of the tidal energy; the second filter passed more than 99% of the amplitude at periods of more than 55 h, 50% at 35 h and less than 0.5% at 25 h. This second, low-pass filtered series was then resampled at 6-hr intervals and was used for examining nontidal circulation. Details of this processing are discussed in Charnell and Krancus (1976).

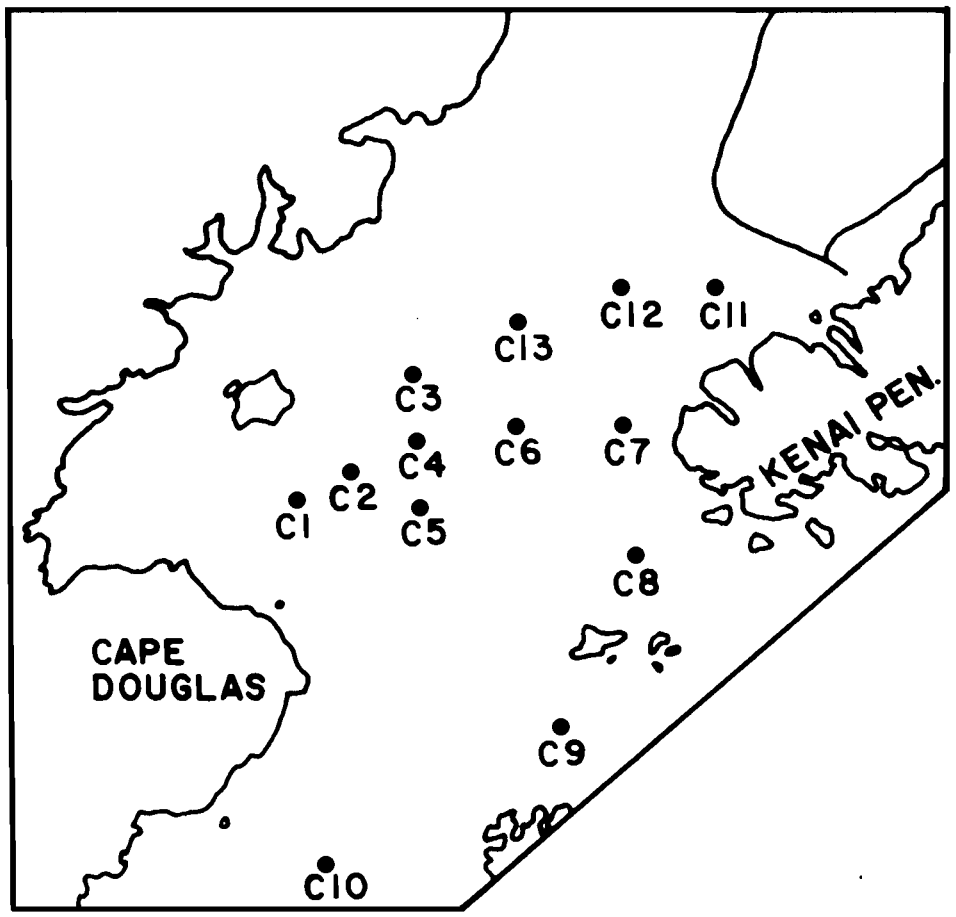

Figure 8. Locations of current meter moorings in lower Cook Inlet in 1977-78. Mooring statistics are given in Appendix A.

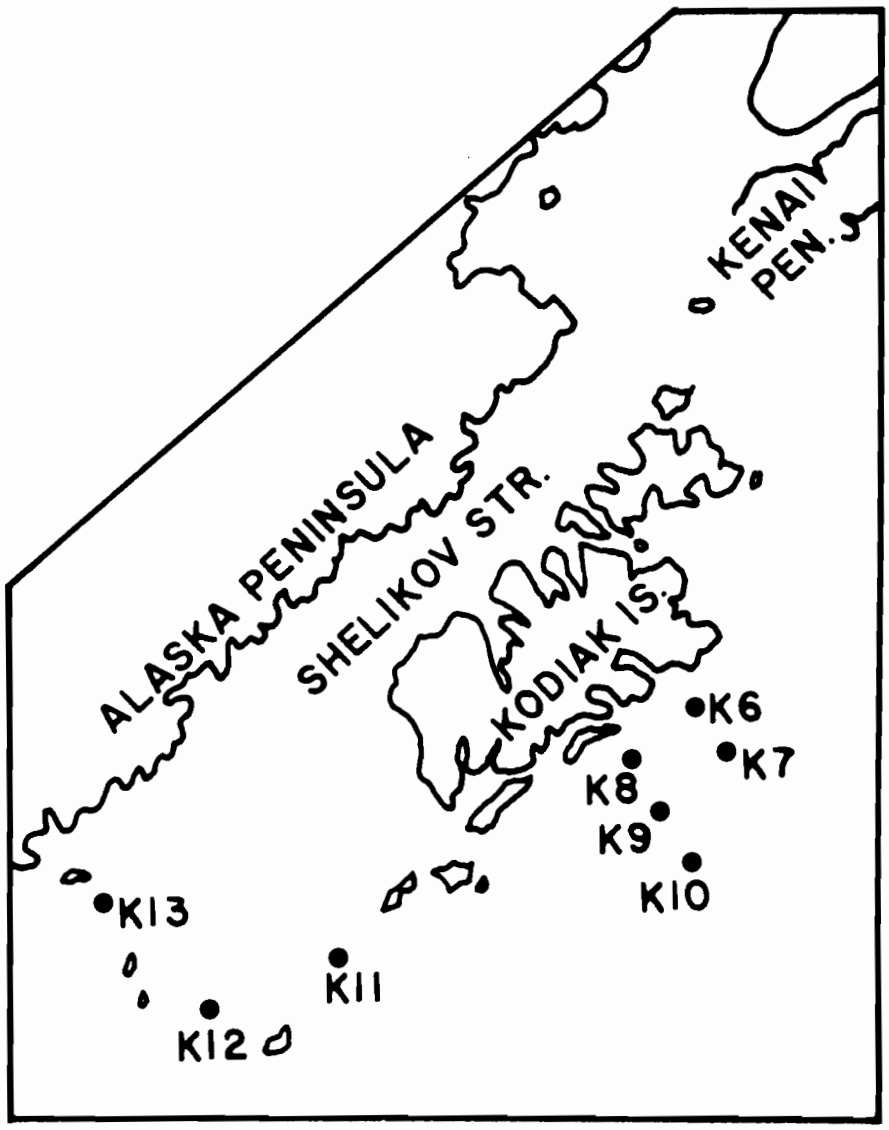

Figure 9. Current meter mooring locations south and west of Kdiak Island in 1977-78. Mooring statistics are given in Appendix A.

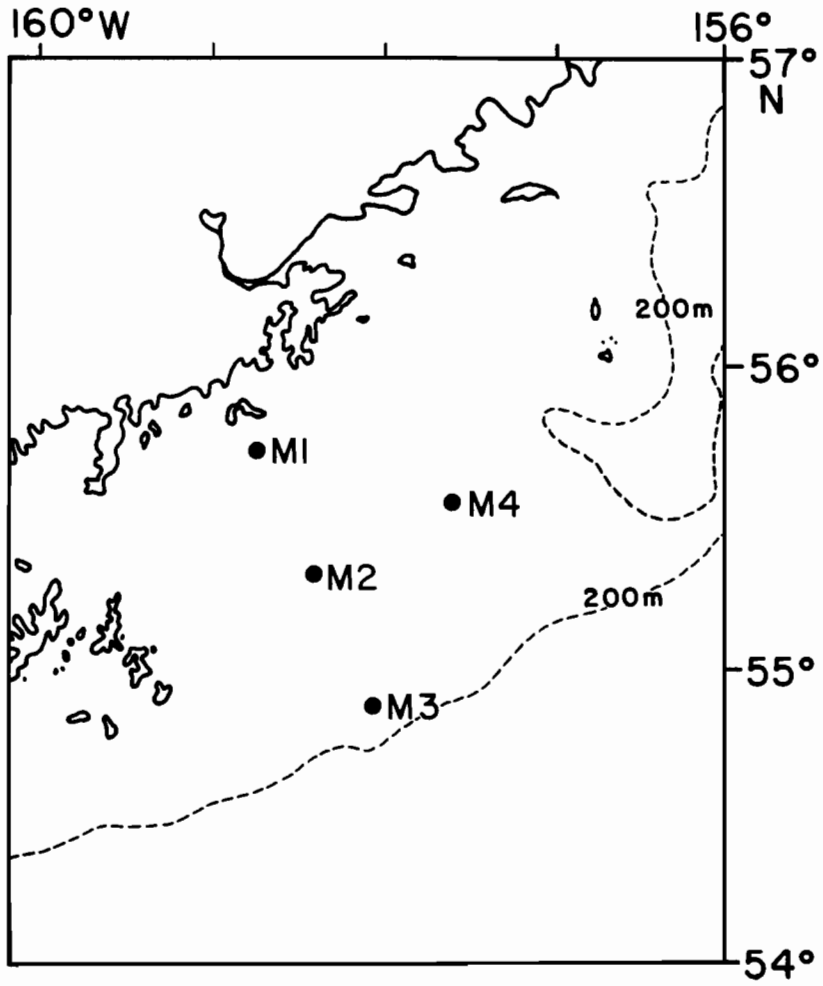

Figure 10. Locations of current meter moorings used for the winter 1977-78 Mitrofania Island experiment.

2.2.2 Drift-Card and Seabed Drifter Studies

Since a major objective of the program in the northwest Gulf of Alaska was to provide information that would aid in prediction of the ultimate fate of an oil spill, it was decided to deploy drift cards which float at the surface and which should behave similarly to an oil spill and indicate where beaching might occur. Cards used for this purpose were made of plastic, were 3" x 5" in size and had a specific gravity of about 0.9 which caused them to float nearly submerged at the water surface. The resultant low above-water profile minimizes wind effect upon the cards, consequently movements should be representative of surface water motions. It should be stressed that the cards were not intended to yield actual trajectories, rather to provide, by distribution of their recoveries, a description of possible areas for grounding of an oil spill occurring at a given location. No attempts were made to compute transit times, since there was no way of knowing how long the cards had lain upon the beaches from which they were recovered. This was particularly true in our study region, where the beaches are relatively uninhabited.

Three sets of cards were released: 1400 cards in early March 1978, 1000 cards in late May 1978 and 2000 cards in early October 1978. The release locations were situated to sample flow in three localities: (1) along the Kenai Peninsula; (2) through the entrances to lower Cook Inlet; and (3) along the Kodiak Island shelf. By the end of 1978 the number of responses to the request for recovery information had reached 137 or 3% of the total number of cards released. This was a surprisingly high recovery rate in view of the remote nature of the sampled area. Overall drift-card returns as of the end of 1978 are listed in Appendix B.

In an attempt to define near-bottom water motion on the bank and trough region south of Kodiak Island, sea-bed drifters were deployed by NMFS/NOAA during winter 1977-78 (Dr. Gene Dunn, NMFS/NOAA, personal communication).* These drifters follow water motions within about 1 m of the seabed. Release and recovery data are tabulated in Appendix C.

2.2.3 Satellite-Tracked Drift Buoys

Surface buoys having subsurface window-shade drogues were deployed at various locations in the eastern (i.e. upstream) part of the study region. The buoys, designed and constructed at Nova University on contract to the NOAA Data Buoy Office, were fiberglass spars about 5 m long attached to a 2-m x 10-m window-shade drogue by a 30-m long nylon tether. The designed center of drogue resistance was therefore near a depth of 35 m. Location of the buoys was determined by means of the Random Access Measurements System (RAMS) of the NIMBUS-6 satellite (Levanon, 1975). At the latitude of the northern Gulf of Alaska, the system provided up to five locations per day for each buoy, but at irregular times.

The rms location error was about 4 km. Each satellite overpass provided data for an ambiguous pair of locations. Between sequential orbits it was usually, but not always, possible to identify the proper location. Hence in addition to the location error arising from uncertainties in the satellite orbit, Doppler measurement, etc., individual errors of tens or even hundreds of kilometers were present in the data. These erroneous locations were removed by an objective routine that checked each location for displacement from preceding and succeeding locations, then rejected all locations that implied velocities in excess of an assignable criterion. For this Gulf of Alaska data set we used 150 cm sec^{-1} as the criterion, which retained 70 to 80% of the original data. To facilitate automated computation of

*NMFS/NOAA, Seattle, WA 98105.

velocity time series and plotting of results, the position component data were smoothed and interpolated to 6-hr intervals by piecewise least-square fit to a low-order (usually cubic) polynomial. Velocity series were additionally smoothed by a simple three-point triangular filter. The result of this procedure was a set of trajectories and associated velocity time series comparable to what would be done by a skilled subjective analyst, and in which features having a time scale of about 2 days were retained. Tidal flows and inertial currents, where important, were suppressed along with other rapid accelerations.

2.2.4 Wave Radar (CODAR) Observations

Investigations of surface currents were carried out in lower Cook Inlet using a Doppler-shift radar method which is fully described by Barrick et al. (1977). This method utilizes the Doppler shift of surface waves under the effect of a current to measure the current field, and has the advantage of providing an instantaneous picture of actual surface currents, an observation virtually impossible by other means. These observations covered the region just off Kachemak Bay and the area between Cape Douglas and Augustine Island (Fig. 11). The observation periods were short in duration compared to the moored current meter measurements, of order 1 week or less, and provided both instantaneous and daily mean values of surface currents in the indicated regions.

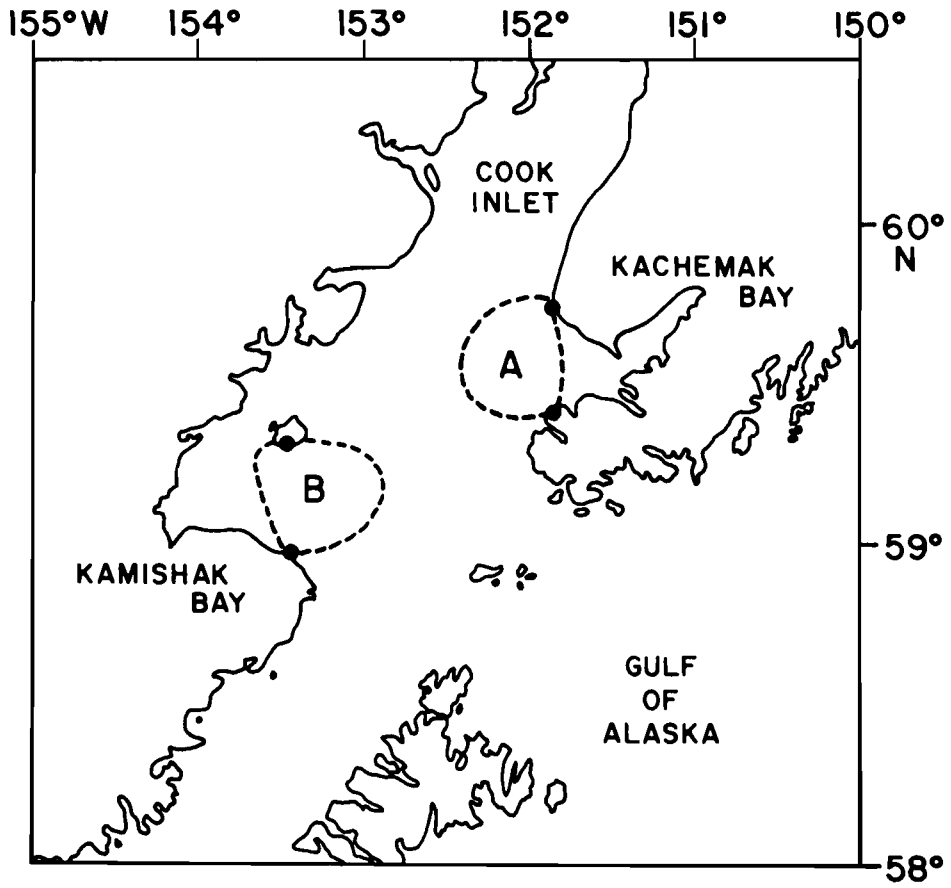

Figure 11. Areas, designated A and B, where surface current observations were carried out using the Doppler-shift wave radar (CODAR) unit. Solid circles indicate locations at which radar units were deployed.

2.3 Temperature and Salinity Observations

Temperature and salinity data were obtained from shipboard using Plessey Model 9040 conductivity/temperature/depth (CTD) profiling systems. These data were recorded during the downcast, and descent rate was held to about 1 m sec^{-1} or less to minimize error in the recorded data due to thermal lag in the sensors in regions where large vertical temperature gradients were present. In some areas, the descent rate during the upper 200 m of the cast was limited to 0.5 m sec^{-1} due to extreme vertical gradients.

Since the Plessey systems are subject to drift and other possible problems, it was necessary to provide data calibration at frequent intervals. To this end, water samples were obtained and analyzed for conductivity and temperature at roughly half of the CTD stations. These samples were obtained using a rosette sampler equipped with calibrated reversing thermometers. Conductivity was measured aboard ship using a portable salinometer calibrated with standard seawater. These calibration data confirmed an overall accuracy for the CTD temperature and salinity values of ±0.02°C and ±0.02°/oo, respectively.

Temperature and salinity data were used for water mass analyses and for computing geostrophic current speeds and transports, therefore, it is of interest to consider the accuracy of the derived parameters used in these analyses. Given temperature and salinity accuracies of ±0.02°C and ±0.02°/oo, density may be computed to an accuracy of ±0.02 kg m^{-3}. Use of these density values in calculating dynamic heights led to an accuracy of within 1.0 dyn cm referred to the 1500 db level. Using these values to compute surface current speed between two stations spaced 40 km apart, the results were accurate to ±4 cm sec^{-1}.

Temperature and salinity data obtained during the OCSEAP program in the northwest Gulf of Alaska bracket all seasons for the 1976-78 period. Appendix D lists stations occupied according to cruise number and date. All data are archived at, and available on request from, the National Oceanographic Data Center.

2.4 Meteorological Observation Program

This program was designed to define the dominant meteorological features in three specific coastal subregions in the northwest Gulf of Alaska: lower Cook Inlet, Kiliuda Bay and Albatross Bank (Fig. 12). Data sources for this study include land based weather stations, moored data buoys, oil drilling platforms, NOAA research vessels, ships of opportunity, ferries, AMOS stations and remote weather recording installations which were deployed as part of this study (Table 1). The data base also includes information in the form of synoptic data from the U. S. Navy's Fleet Numerical Weather Central (FNWC) analyses. The data collection effort occurred primarily during early 1978 (Table 2), a period which coincided with intensive current observation programs in the lower Cook Inlet and Kodiak Island areas.

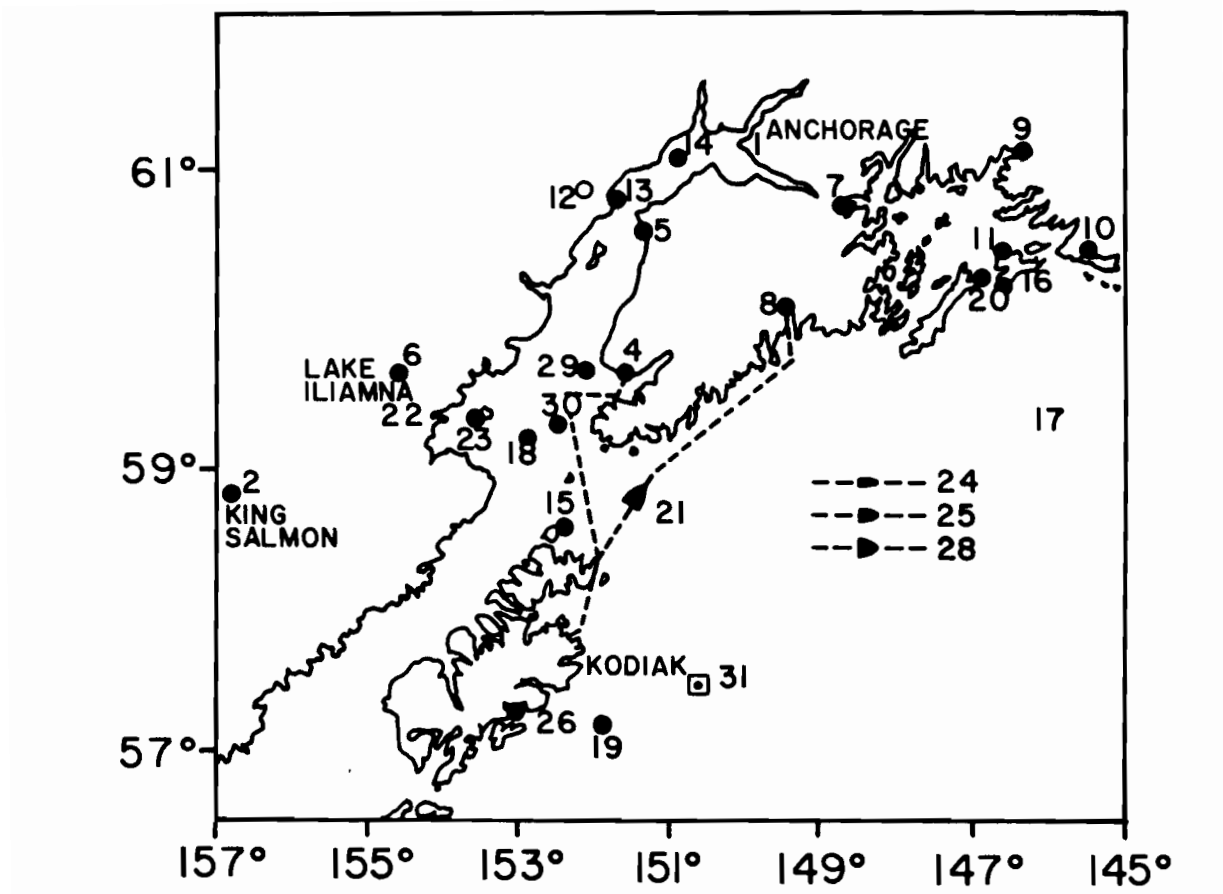

Figure 12. Map of the study area showing sources of data which are included in this study. Names of numbered stations, sources of data and time periods of data collection are given in Tables 1 and 2.

TABLE 1

Listing of meteorological data collection stations shown on Figure 12.

1.	Anchorage	NWS[1]
2.	King Salmon	NWS
3.	Kodiak	NWS
4.	Homer	NWS
5.	Kenai	NWS
6.	Iliamna	NWS (part-time AMOS[2])
7.	Whittier	NWS
8.	Seward	NWS
9.	Valdez	NWS
10.	Cordova	NWS
11.	Johnston Point	NWS (Air Force)
12.	Big River Lake	NWS (contract)
13.	"Dolly Varden"	Oil Platform
14.	"Phillips"	Oil Platform
15.	Shuyak	NWS (remote wind)
16.	Cape Hinchinbrook	NWS (AMOS)
17.	Middleton Island	NWS (AMOS)
18.	EB-346007	NDBO[3]
19.	EB-46008	NDBO
20.	EB-46009	NDBO
21.	*TUSTUMENA*	Alaska State Ferry
22.	Contact Point	NOAA/PMEL remote[4]
23.	Augustine Island	NOAA/PMEL remote
24.	*SURVEYOR*	NOAA vessel
25.	*DISCOVERER*	NOAA vessel
26.	Kiliuda Bay	NOAA/PMEL remote
27.	Copper River	NOAA/PMEL remote
28.	Ships of opportunity	Miscellaneous
29.	"Diamond M. Dragon"	Oil Platform
30.	"Ocean Bounty"	Oil Platform
31.	FNWC[5]	Computer

[1]National Weather Service, NOAA.
[2]Automatic weather station.
[3]National Data Buoy Office, NOAA.
[4]Remote recording weather station.
[5]Fleet Numerical Weather Central.

TABLE 2

Summary of status of meteorological data base listed according to station location shown on Figure 12. Data indicated by heavy solid lines are available in the automated data base system, While dashes indicate data which are available at PMEL/NOAA.

No.	Name	1977 J F M A M J J A S O N D	1978 J F M A M J J A S O N D	1979 J F M A M J J A S O N D
1	Anchorage			
2	K. Salmon			
3	Kodiak			
4	Homer			
5	Kenai			
6	Iliamna			
7	Whittier			
8	Seward			
9	Valdez			
10	Cordova			
11	Johnston Pt			
12	Big River Lks			
13	Dolly Vorden			
14	Phillips			
15	Shuyak			
16				
17	Middleton I			
18	EB-46007			
19	EB-46008			
20	EB-46009			
21	Tustumena			
22	Contact Pt.			
23	Augustine I.			
24	SURVEYOR			
25	DISCOVERER			
26	Kiliuda Bay			
27				
28	Ship of Oppy.			
29	D. M. Dragon			
30	D. Bounty			
31	FNWC-Alb.			
32	EB-43			
33	EB-70			
34	FNWC-NEGOA			
35	Pt. Rice			
50	Test Data			

3. RESULTS AND DISCUSSION

3.1 Mean Currents, Seasonal Variations and the Temperature, Salinity and Density Fields

3.1.1 Introduction

The internal density structure of an oceanic system reflects the baroclinic portion of the total time-averaged mean flow. Because of the time interval required for readjustment of this density field following any change in current patterns, the density field reflects time-averaged circulation and can be used to detect seasonal variability. It does not generally reflect, however, the 2- to 10-day period events or tidal fluctuations which are prominent in the northwest Gulf (cf. Section 3.2).

Mean flow can be obtained only by computing a time average of measured current, where the observation and averaging time must extend over a long enough period to allow averaging out of prominent low-frequency fluctuations such as those to be discussed in Section 3.2. In the present study this generally required a record at least 1 mo in length. Since the time scale for seasonal events is of order 3 mo, records longer than 3 mo but shorter than several years record conditions spanning more than one season but still not representing a true annual mean. As our current moorings generally were deployed for periods of 4-5 mo, this limitation must be borne in mind. Lengths of the individual current records are listed in Appendix A.

3.1.2 The General Northwestern Gulf Region

Winter net flow is well represented by the observed mean current vectors depicted on Figure 13. The southwesterly flow at the shelf break at 20 m was about 35 cm sec^{-1} (Station WGC2A). This agreed with a later drogue trajectory (cf. drogue 1220, Fig. 14), which indicated net summer speeds

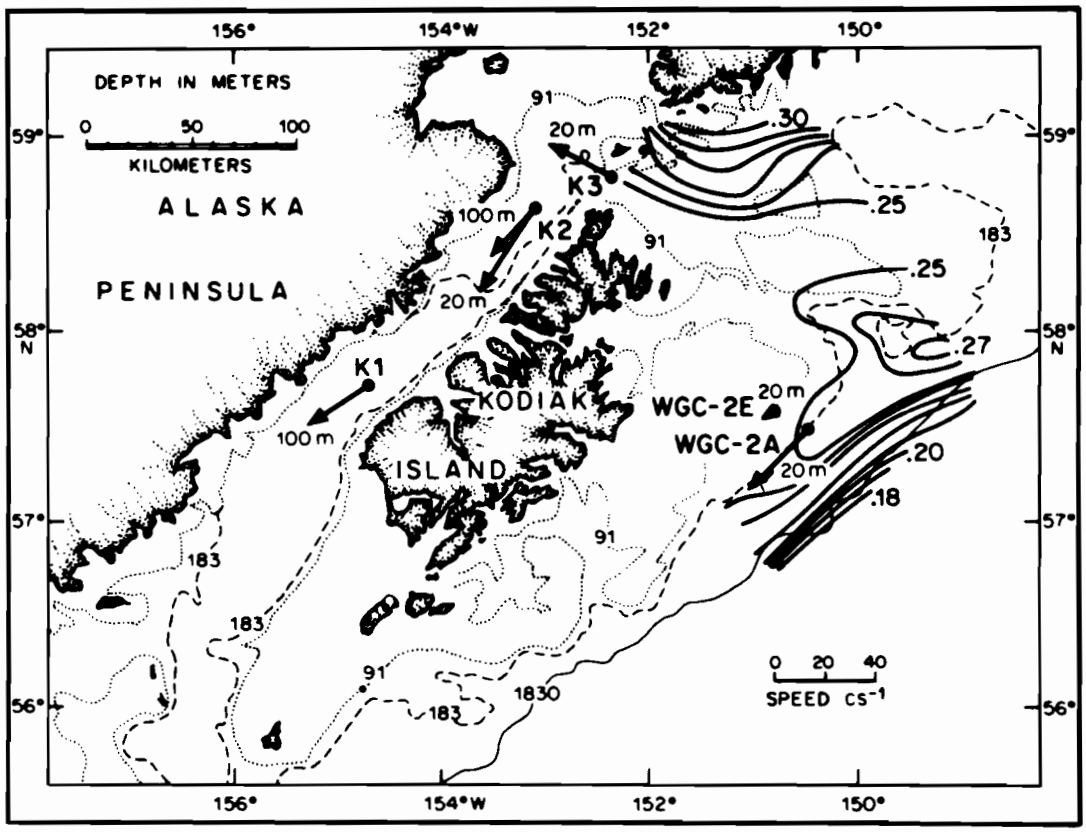

Figure 13. Mean winter 1976-77 current speed vectors at five locations on the northwest Gulf of Alaska shelf. Actual mooring periods are given in Appendix A. The dynamic topography has a contour interval of 0.01 dyn m and was constructed using March 1977 data.

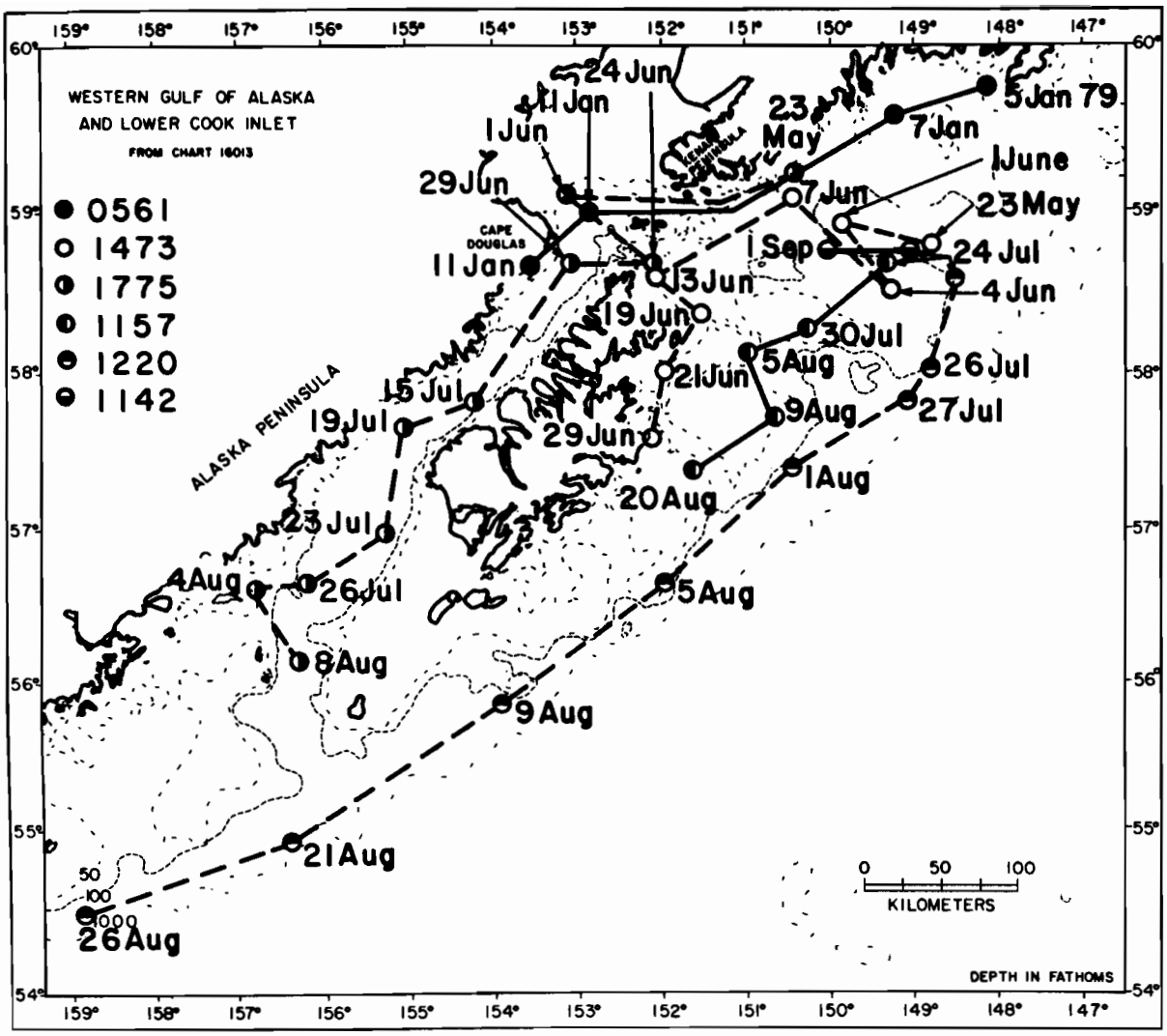

Figure 14. Satellite-tracked drogue trajectories in the northwest Gulf of Alaska. Drogued buoys were deployed in 1978, and were drogued to track at a water depth of about 25 m.

in the Alaskan Stream of about 40 cm sec^{-1} off Kodiak Island. At a later period the mooring had been moved about 20 km farther inshore (to WGC2E), due to repeated damage from fishing activity at the original location. At the new location, mean speed had dropped to about 5 cm sec^{-1}, still in a southwesterly direction. These two moorings bracketed the zone of large horizontal shear at the inshore edge of the Alaskan Stream.

Moorings K1-K3 were deployed in Shelikof Strait as shown (Fig. 7) during the same period as WGC2E. These indicated a mean 100-m deep flow through Shelikof Strait of about 25 cm sec^{-1} to the southwest. At 20-m depth mean flow was somewhat higher, about 35 cm sec^{-1}, and also southwesterly. These observations were the first current measurements obtained in the region and indicated a general southwesterly flow with its most intense region manifested as the Alaskan Stream along the shelf break. This southwesterly flow, both through Shelikof Strait and south of Kodiak Island, was qualitatively demonstrated by the results of the satellite-tracked buoy and drift card programs (Figs. 14-18).

3.1.3 The Kenai Current

During March, September and October-November 1977 (Fig. 19, 20 and 21), two baroclinic flow regimes were evident on these dynamic topographies: (1) the southwestward-flowing Alaskan Stream over the continental slope south and east of Kodiak Island, accompanied by apparent inshore counterflows east of Portlock Bank; and (2) a well-defined westerly coastal flow along the Kenai Peninsula, designated by Schumacher and Reed (1980) as the Kenai Current. Generally weak and variable circulation occurred between these two relatively well-organized flows. This was supported by summer drogue data, which

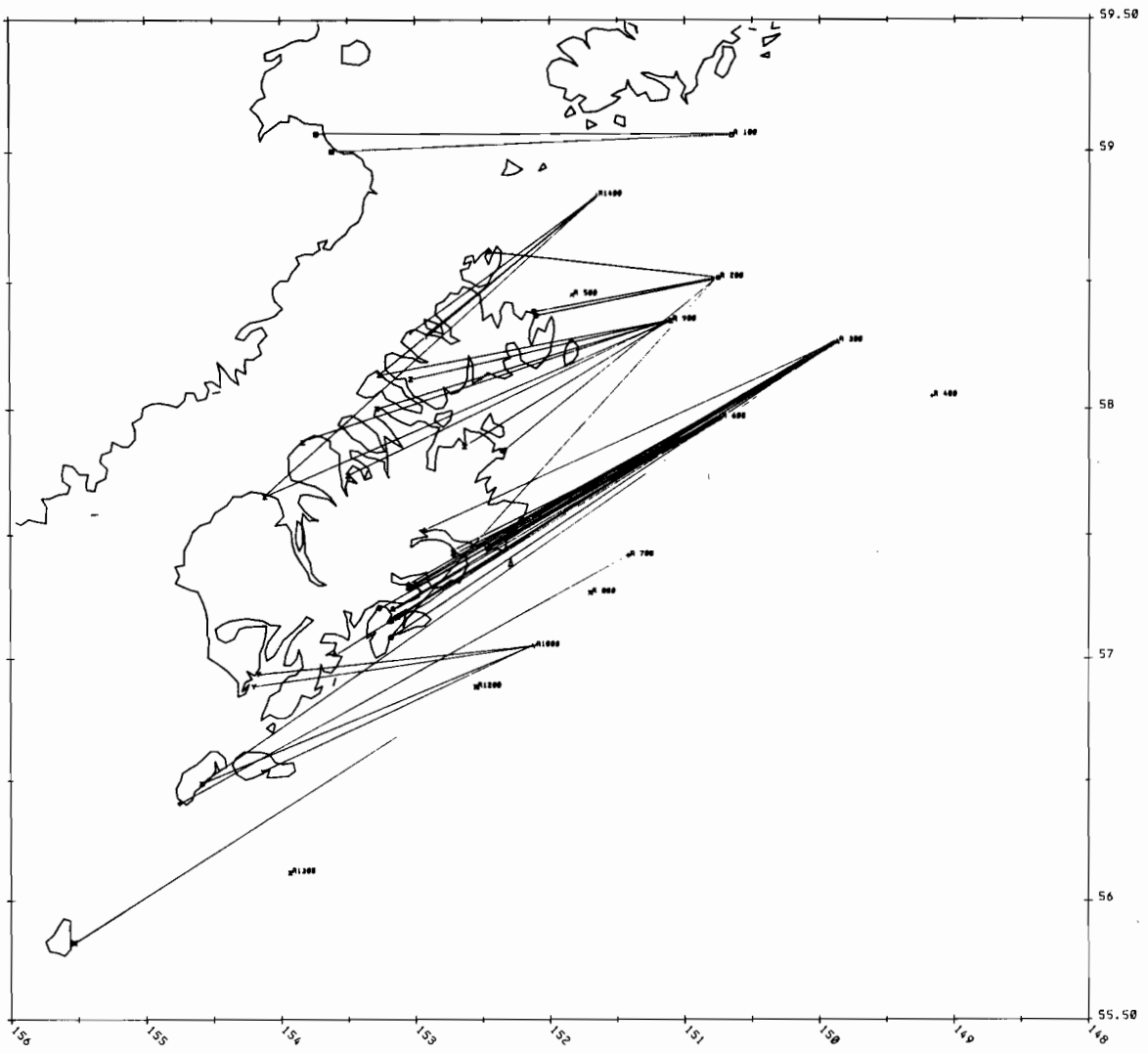

Figure 15. Summary of recovery and release points for drift cards released in March 1978.

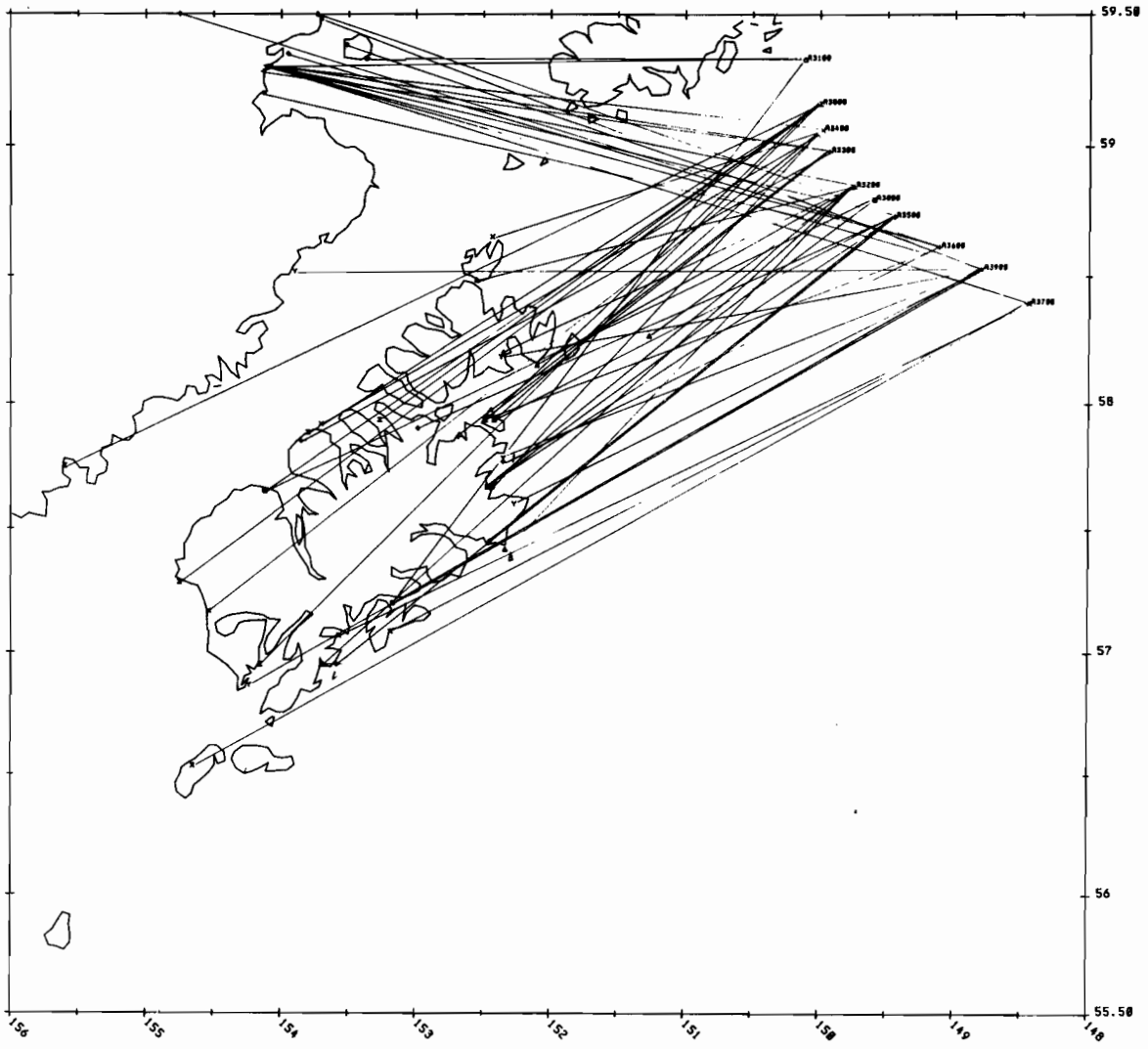

Figure 16. Summary of recovery and release points for drift cards released in May 1978.

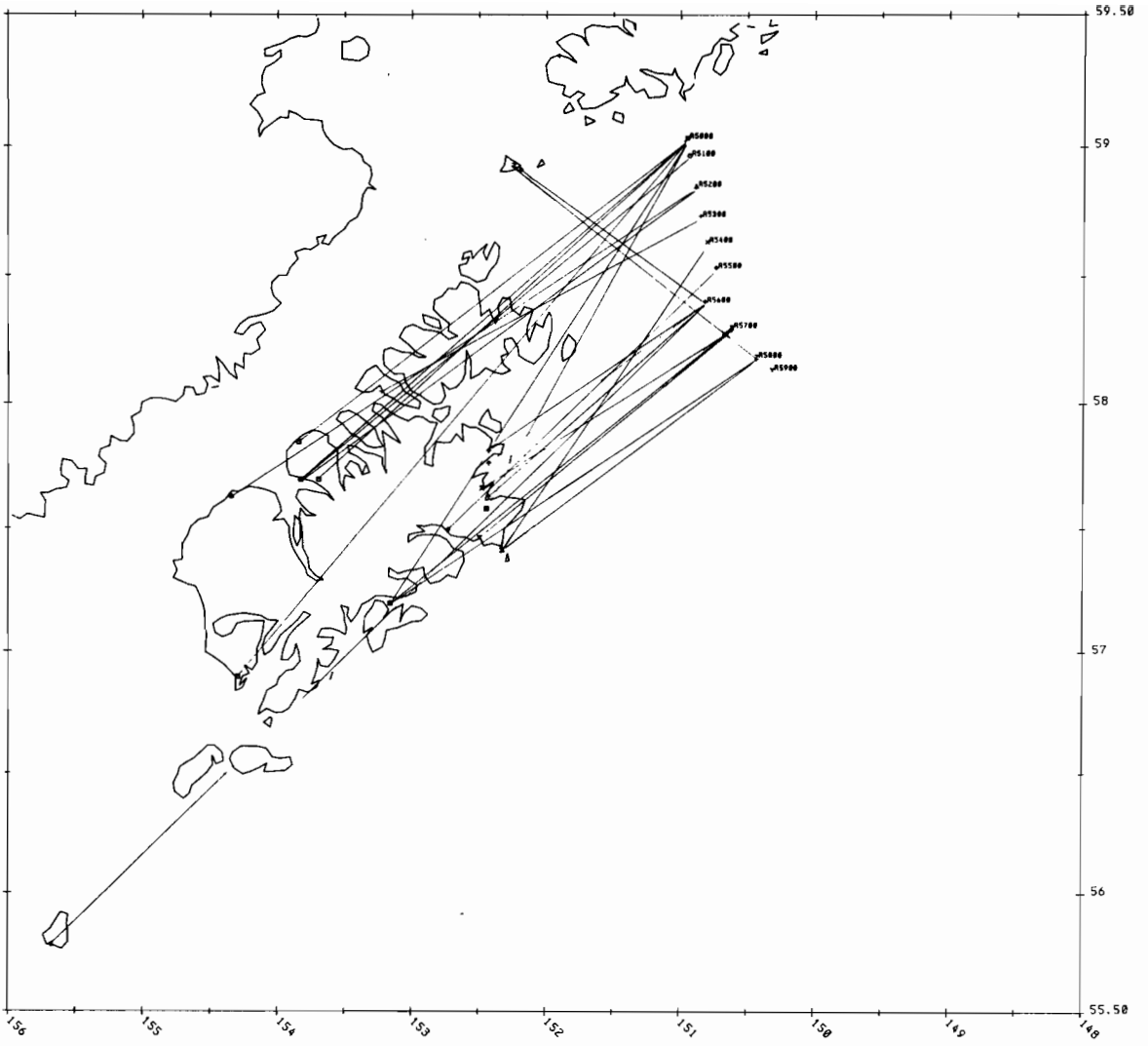

Figure 17. Summary of recovery and release points for drift cards released in October 1978.

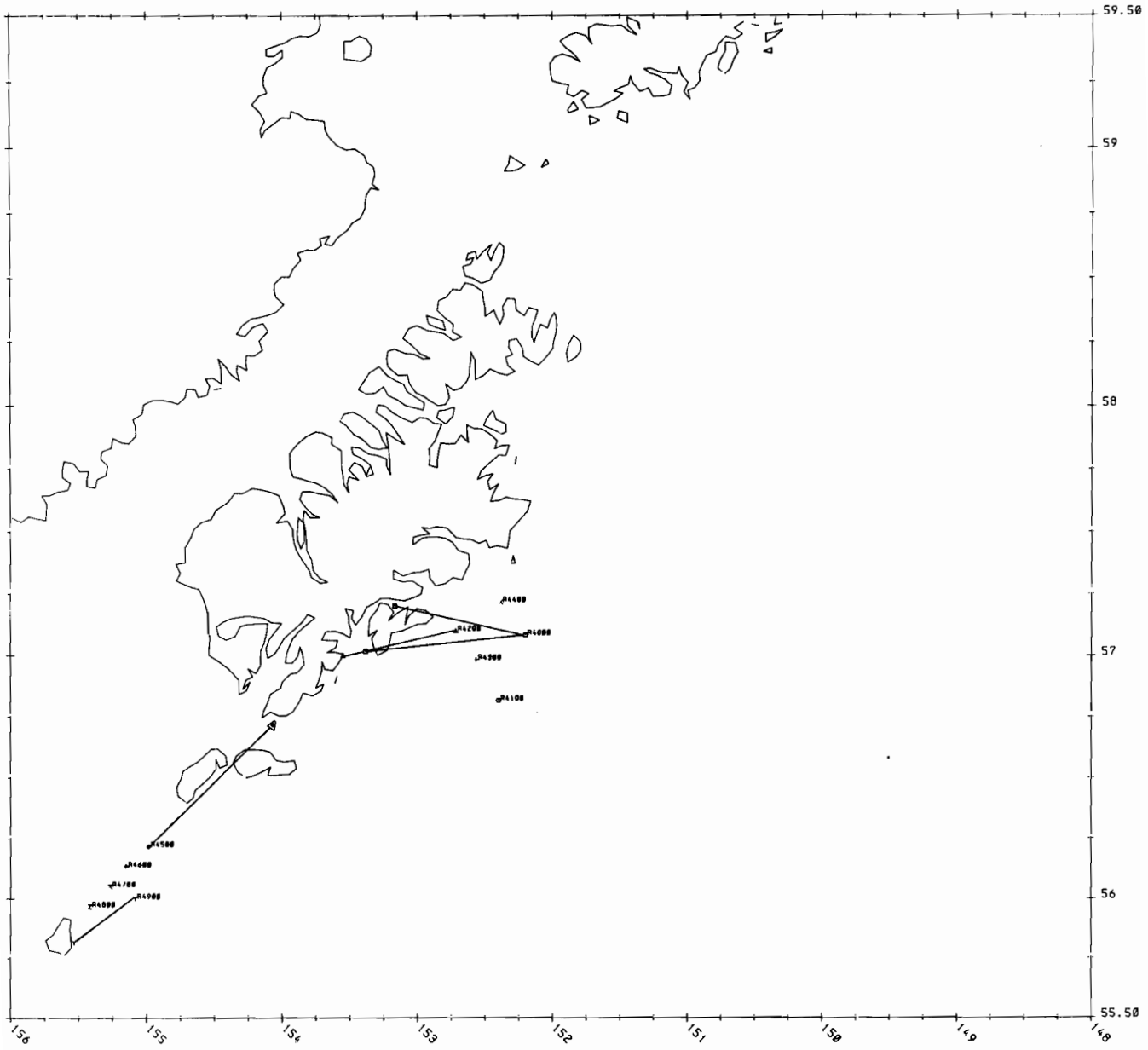

Figure 18. Summary of recovery and release points for drift cards released in October 1978.

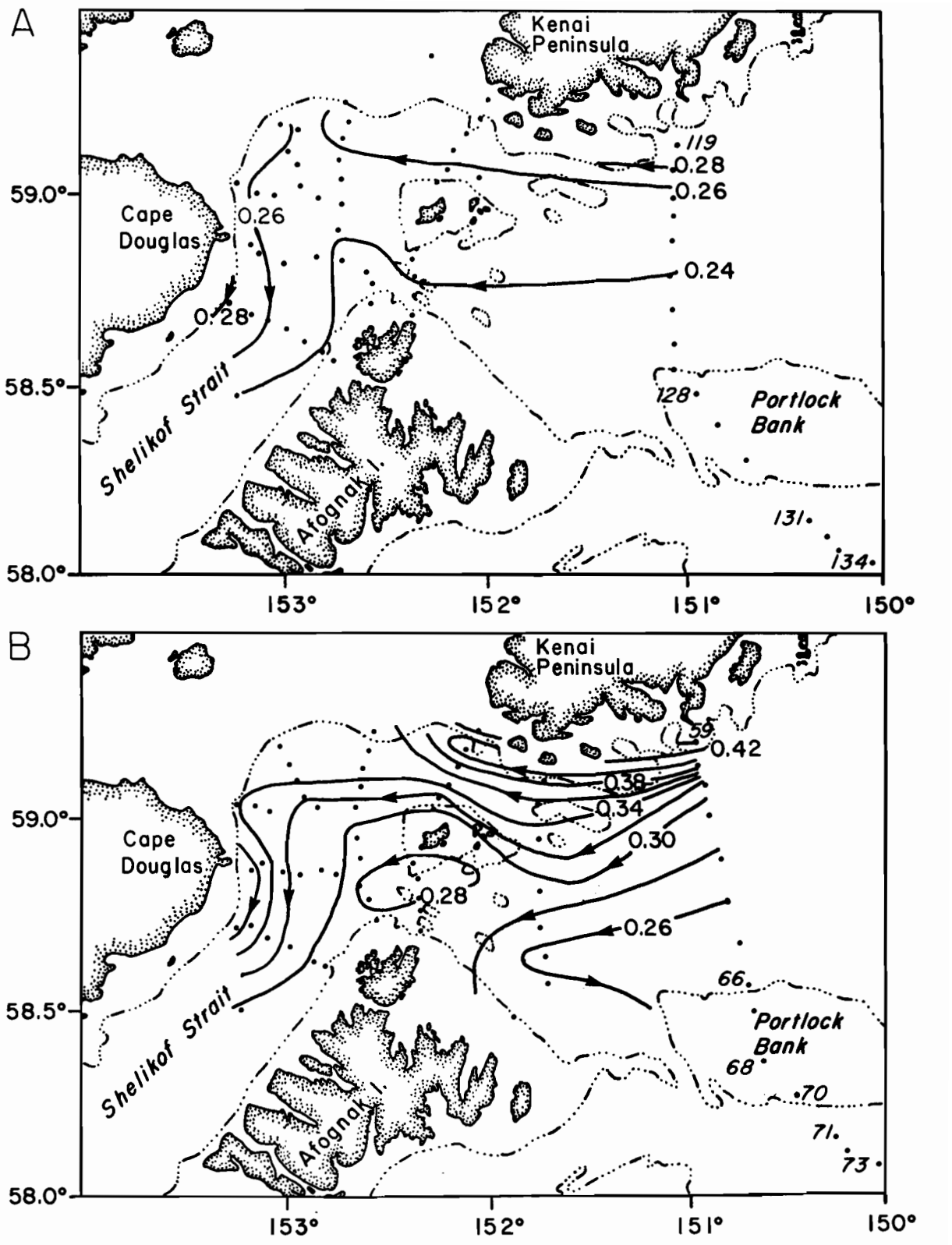

Figure 19. Dynamic topographies depicting flow in the Kenai Current and into lower Cook Inlet during March (upper) and October (lower) 1978.

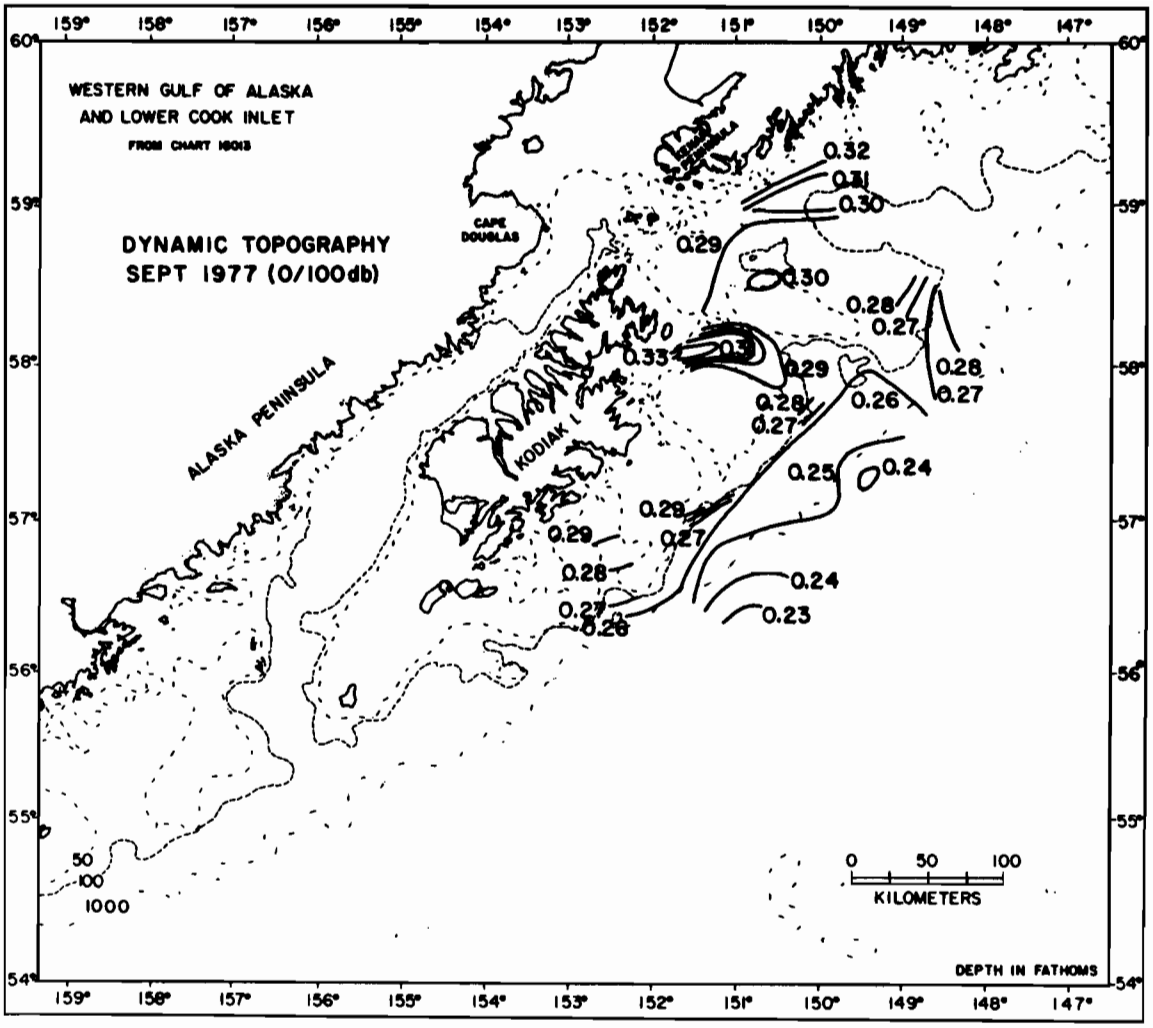

Figure 20. Dynamic topography of the 0/100-db surface in the northwest Gulf of Alaska in September 1977. Contour interval is 0.01 dyn m.

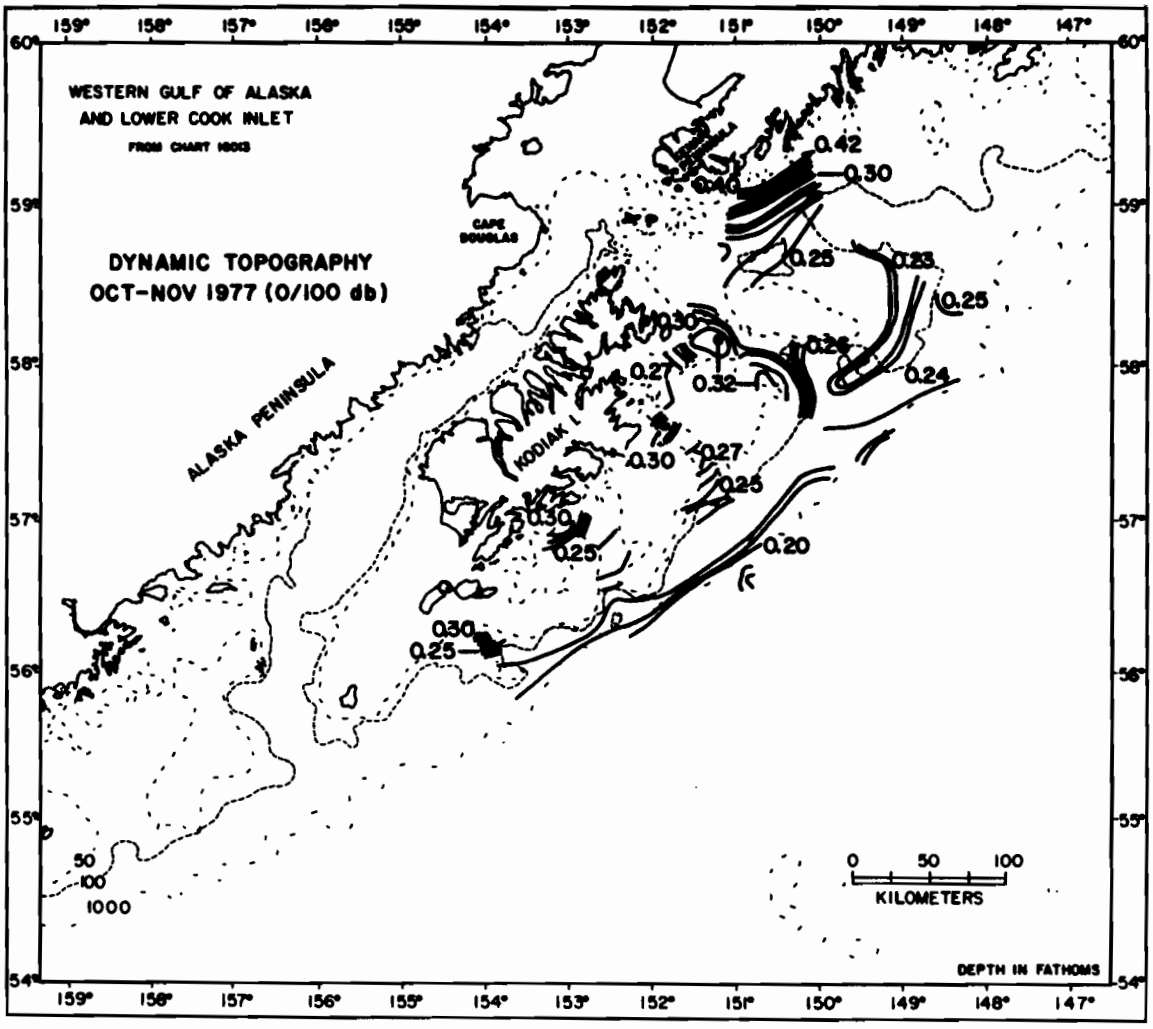

Figure 21. Dynamic topography of the 0/100-db surface in the northwest Gulf of Alaska in October-November 1977. Contour interval is 0.01 dyn m.

revealed erratic flow directions and weak net speeds (~5 cm sec^{-1}) (cf. drogues 1473 and 1157, Fig. 14). During September and October a southward extension of this coastal flow appeared east of Kodiak and Afognak Islands and may have contributed to formation of a well-developed (relief of about 0.04 dyn m) gyre-like feature between Portlock and North Albatross Banks. Relief across the coastal flow itself was about 0.05 dyn m in March and September, but had increased threefold by October. The salinity distribution (not shown) suggested that this increase in dynamic relief was due to coastal freshwater addition which resulted in depressed salinities along the coast. This was in agreement with Favorite and Ingraham (1977), who suggested westward baroclinic flow near the entrances to lower Cook Inlet and Shelikof Strait during April-May 1972.

Vertical sections of temperature, salinity, and sigma-t along the CTD sections off the Kenai Peninsula (stations 59-68, 70-73 in October 1978; stations 119-134 in March 1978) are presented in Figures 22 and 23. The October sections display a narrow band (~20 km) of warm, dilute, low-density water adjacent to the Kenai Peninsula; this strong baroclinicity coincided with the westward coastal flow entering Shelikof Strait. Indications of relatively weak westward flow extend, however, south of this band to about the northern flank of Portlock Bank. The three stations (67, 68, and 70) over Portlock Bank show weak vertical stratification, and the water at station 68 (63-m depth) was completely mixed. South of Portlock Bank, varying isopycnal slopes suggest that peak speeds in the Alaskan Stream occurred seaward of station 73. In March (Fig. 23), gradients across the coastal flow were much weaker than in fall. There were no indications of significant baroclinicity elsewhere. Minimum temperatures were near the surface, rather than near-bottom as in October, and there was significantly

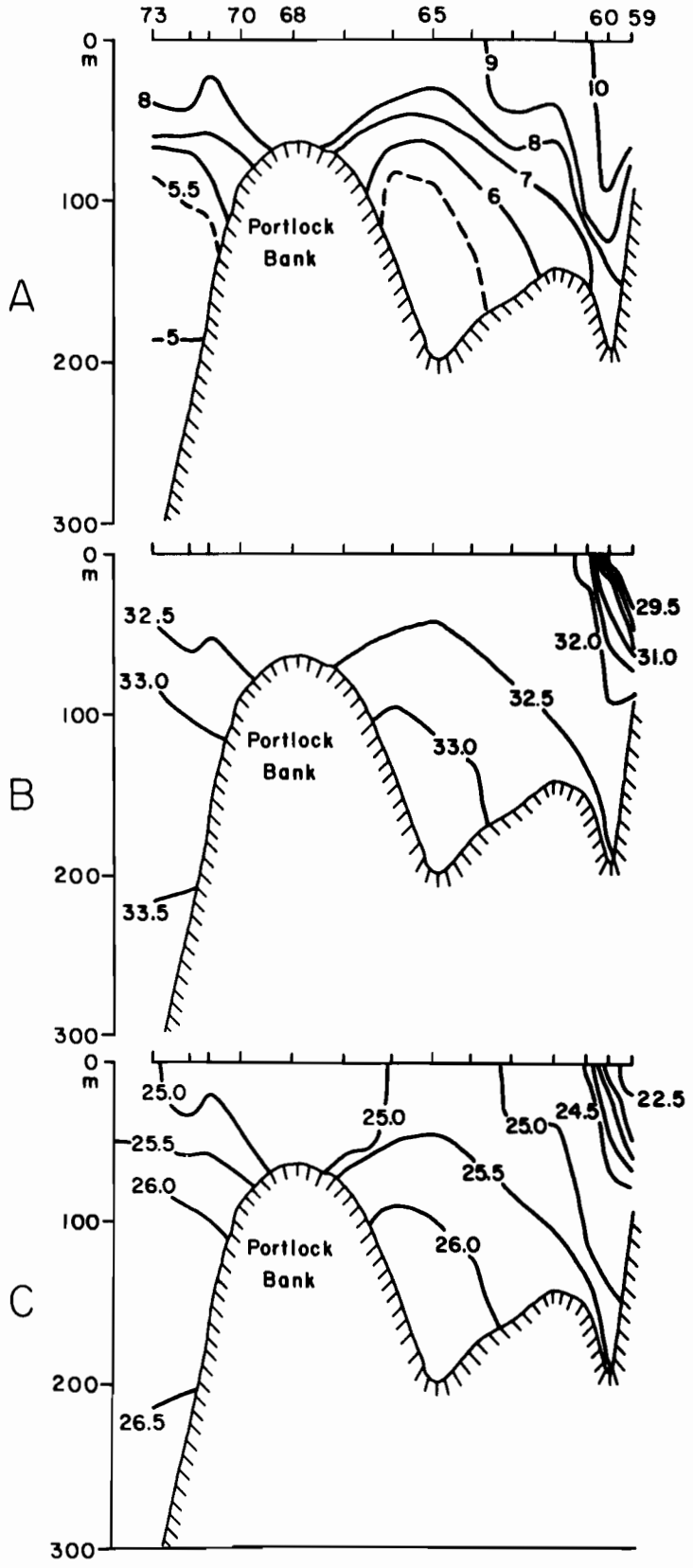

Figure 22. Cross sections of temperature (A), salinity (B) and density as sigma-t (C) across the Kenai Current and Portlock Bank in October 1978. Right-hand side of the section is north.

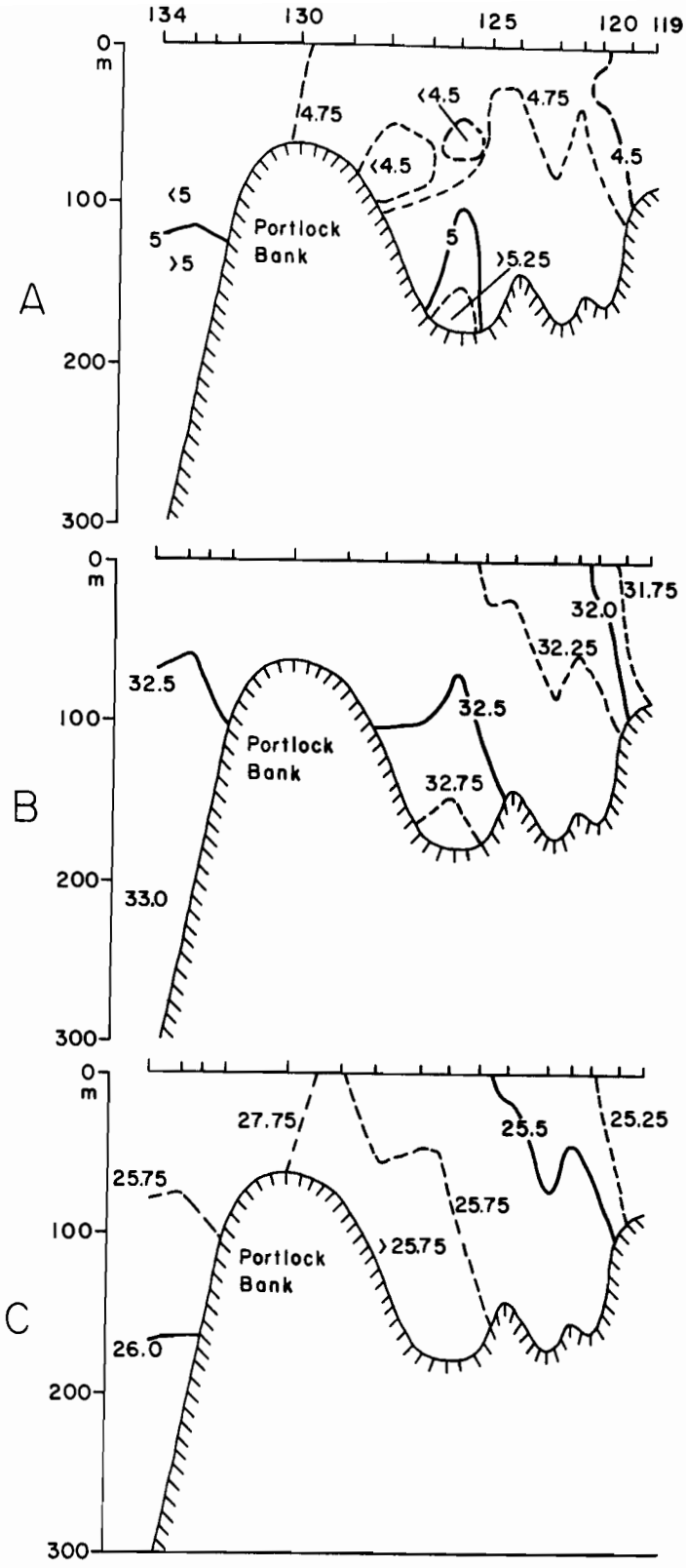

Figure 23. Cross sections of temperature (A), salinity (B) and density as sigma-t (C) across the Kenai Current and Portlock Bank in March 1978. Right-hand side of the section is north.

lower stratification than that observed in fall. The homogeneous water atop Portlock Bank extended about 15 m deeper than in October, which suggests that total mixing (presumably a combination of wind mixing near the surface and tidal mixing near the bottom) was more pronounced in winter than in summer-fall, a result consistent with physical reasoning. The intermediate and deep parts of the water column were more saline in October than in March, while coastal flow near the Kenai Peninsula was more dilute during October. This pattern of decreased surface salinity and increased intermediate and deep salinity during fall is consistent in our data and suggests that the saline water is "drawn up" during periods of peak transport in the Kenai Current, perhaps as an interior upwelling in conjunction with buoyancy flux (Pietrafesa and Janowitz, 1979) similar to estuarine circulation.

3.1.4 Shelikof Strait and Lower Cook Inlet

The flow through Shelikof Strait was measured for 5-mo periods during winter 1977-78 and summer 1978. These observations reaffirmed the southwesterly flow and revealed that mean speeds during summer were about half those during winter; winter 1977-78 speeds were in agreement with those measured in 1976-77. We therefore conclude that mean winter currents in Shelikof Strait flow southwest at about 20-30 cm sec^{-1} with slightly higher speeds at the surface than at depth. Limited evidence has also been presented by Schumacher et al. (1978; 1979) that these observed mean flows agreed with baroclinic flow inferred from the 0/100-db dynamic topography (Figs. 19-21).

Baroclinic coastal flow in the Kenai Current has a significant effect on flow through lower Cook Inlet and Shelikof Strait. This is illustrated by 0/100-db geopotential topographies which encompassed both regions during March and October 1978 (Fig. 21). In March, the baroclinic coastal flow

had a dynamic relief of about 0.06 dyn m. It entered Shelikof Strait through passages north and south of the Barren Islands and veered south off Cape Douglas. In October the flow was considerably stronger, with a dynamic relief of about 0.20 dyn m, and a portion of the flow appeared to turn south near Afognak Island without entering Shelikof Strait.

Inflow into northern Shelikof Strait due to the influence of the Kenai Current was supported by the moored current meter observations. Additional evidence was available in the form of satellite-tracked, drogued drift buoy results (Fig. 14), which showed direct evidence of the westward flow through the year. Buoy 0561 indicated a mean speed of about 55 cm sec^{-1} in January. Buoys 1775 and 1473 indicated much lower mean speeds, about 20 cm sec^{-1}, in May-June. The early spring lowering in speed is in agreement with our hypothesis that this flow is largely baroclinic and driven by coastal freshwater input; in early spring, freshwater content in the coastal waters is near its annual minimum.

The persistent westward flow of the Kenai Current into Shelikof Strait exerts a primary control on circulation in lower Cook Inlet. This was first recognized by Muench et al. (1978), who derived a qualitative circulation scheme for lower Cook Inlet using summer 1973 current and temperature-salinity observations (Fig. 24). The prominent westward flow in the southern Inlet is topographically controlled; it follows the path depicted and turns to the south off Cape Douglas. The southward flow from the upper Inlet is due to freshwater input; this flow merges with the westerly flow off Cape Douglas to produce a strong southerly current there. Flow elsewhere throughout the inlet is weak and variable. More recent current data have corroborated this circulation pattern and quantified the mean winter current speeds. Vectors showing the observed mean winter 1977-78 currents in lower Cook Inlet are

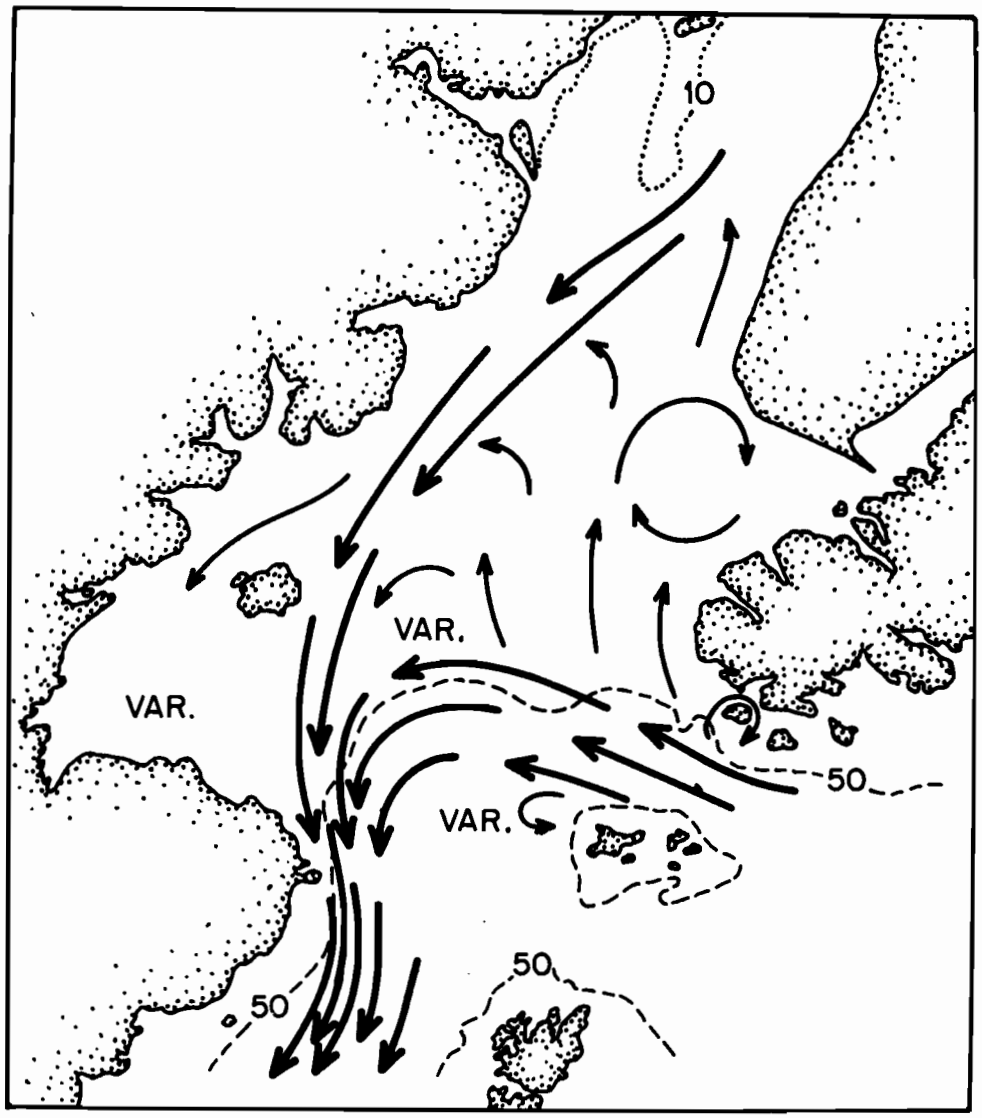

Figure 24. Depiction of qualitative mean flow pattern in lower Cook Inlet derived by Muench et al. (1977) from summer 1973 temperature, salinity and current data. Depths are in fathoms.

depicted on Figure 25. Westerly mean flow across the lower Inlet was about 20 cm sec^{-1}, while southward flow in the western Inlet was 5-10 cm sec^{-1}. Away from these two major flows, mean speeds were only 1-2 cm sec^{-1}.

A similar current observation program was carried out during summer 1978. Preliminary examination of these data has indicated that the flow pattern is the same as during winter. The westerly flow was smaller during summer, and the southerly flow in the western Inlet somewhat larger. Surface current observation carried out in summer 1978 using the CODAR (cf. Section 2.2.4) further substantiated this current pattern; an example of their results is shown in Figure 26.

The circulation depicted on Figure 24 for lower Cook Inlet was also corroborated by drogue results. Westerly drift across the lower Inlet was shown in January, with a mean speed of about 65 cm sec^{-1} (Fig. 14). This relatively high speed, compared with computed mean speeds obtained from moored current meters (Fig. 25), may indicate a current pulse during the observation period. A June drogue track plotted on the same scale did not show sufficient detail for speed computation. The same drogue track was plotted on an expanded scale, however, and compared to a second track on Figure 27. Drogue 1775 followed the bathymetry until 1 June, at which time the data became incomplete. Failure of drogue 1473 to enter Stevenson Entrance from the east suggests that a counterflow may have occurred during June. Drogue 1421 also indicated a westerly flow, though somewhat north of the earlier track and with apparent cross-isobath flow from 1-9 June. We would expect to see this sort of departure of drogue tracks from our conceptual mean flow; the drogues follow instantaneous flow. Both drogues yielded mean westward speeds of order 15 cm sec^{-1}, in agreement with summer mean flows observed using moored current meters.

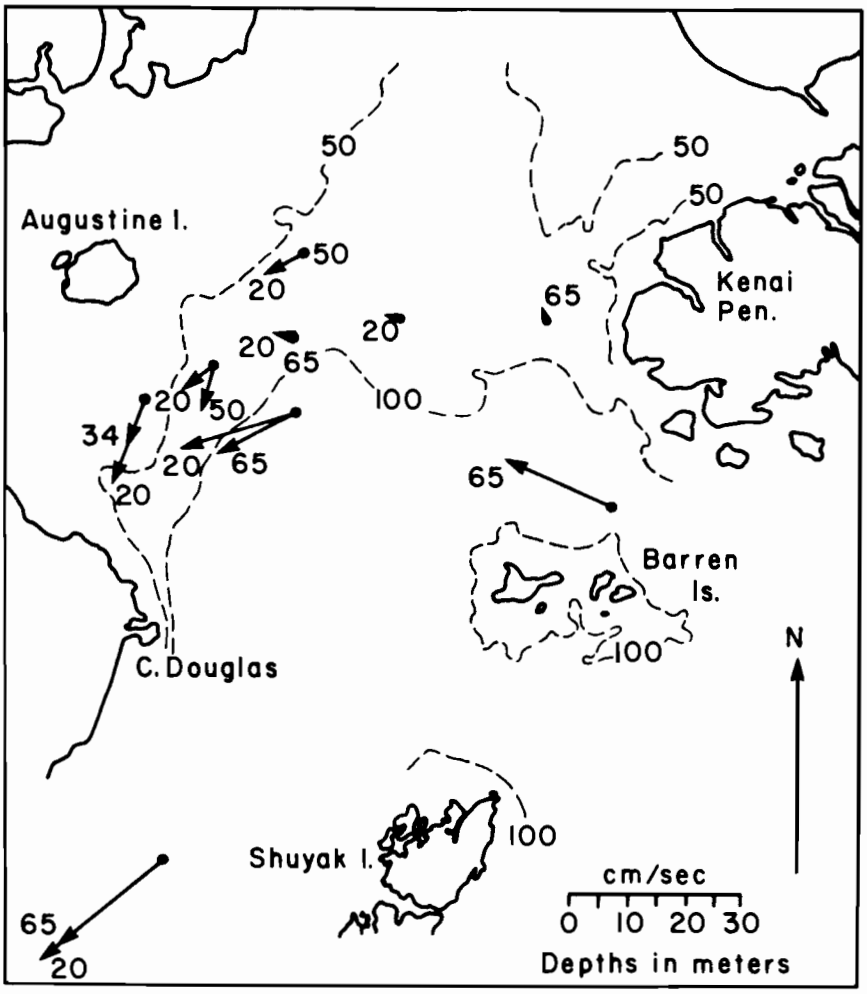

Figure 25. Observed mean current vectors in the lower Cook Inlet region during winter 1977-78. Statistics for individual moorings are given in Appendix A. Numbers indicate current meter depths in meters.

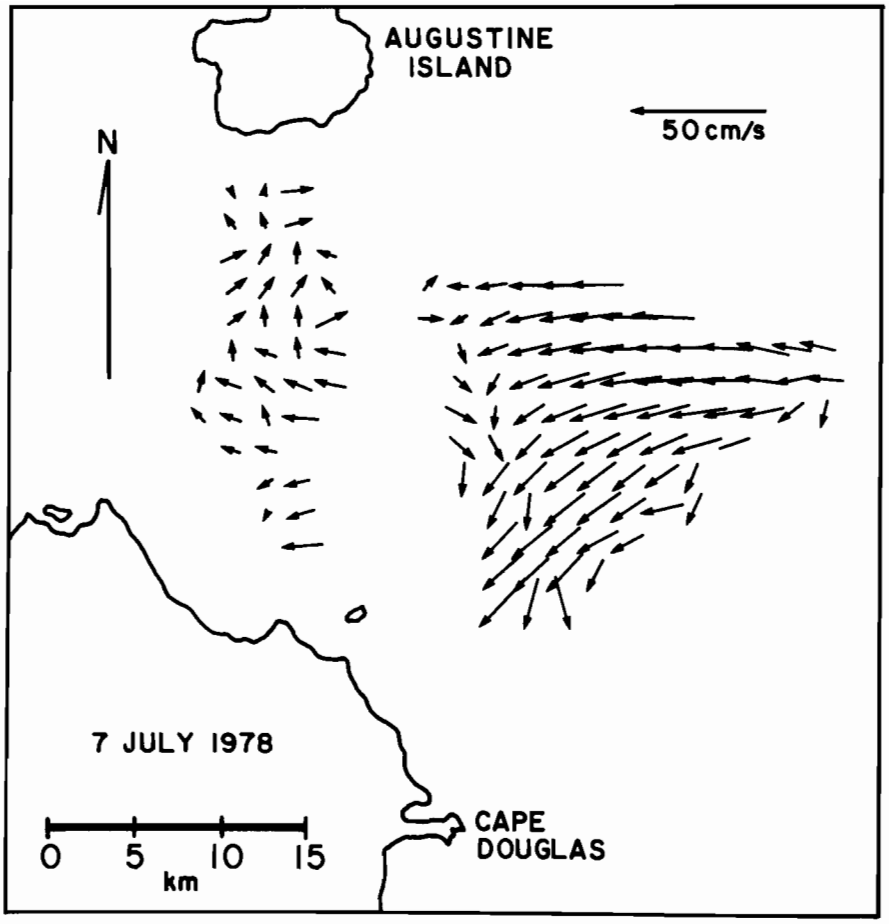

Figure 26. Twenty-four-hour mean surface currents observed on 7 July 1978 in lower Cook Inlet using the surface wave radar unit. Data are from Dr. A. S. Frisch, NOAA/WPL.

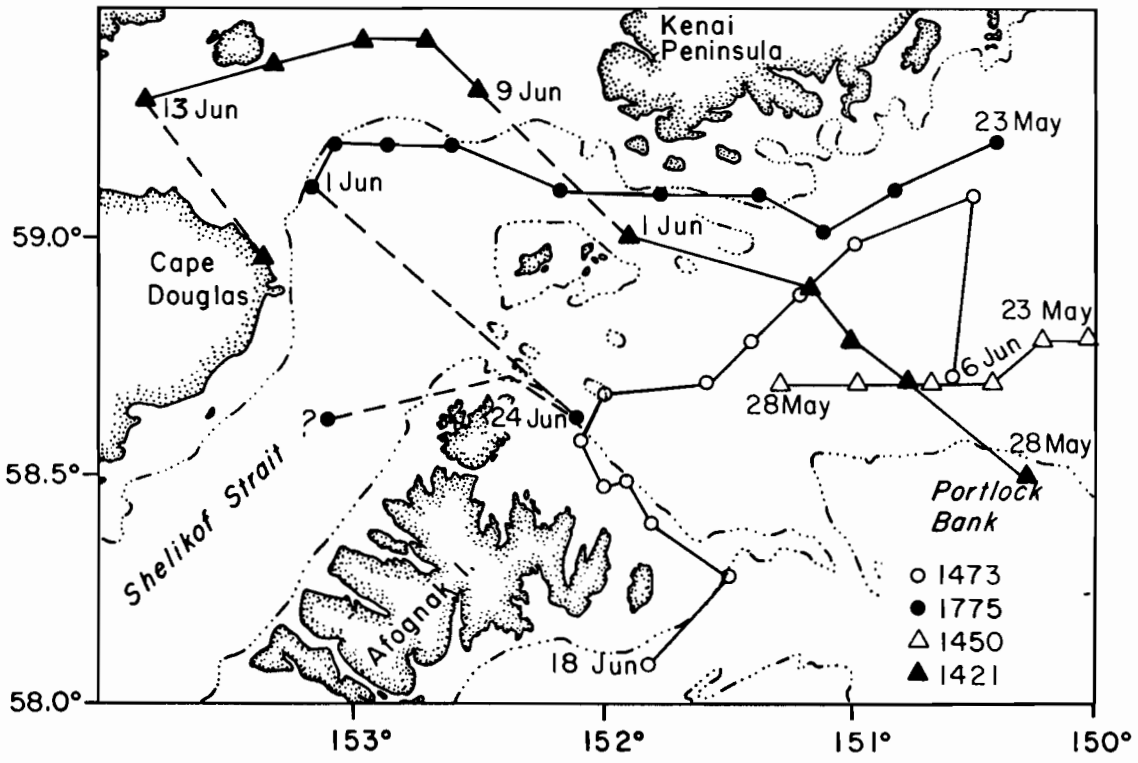

Figure 27. Details of drogued buoy trajectories in the lower Cook Inlet region in 1978. Buoy locations are plotted at 1-day intervals.

3.1.5 The Bank and Trough Region

The area of complex bank and trough bathymetry south of Kodiak Island is of interest because we expect *a priori* that the topography exerts a control both on currents and on vertical mixing processes. To supplement the current data obtained from mooring WGC2 (cf. Fig. 13), moorings were deployed in the Kiliuda Trough region during winter 1977-78 and summer 1978 (cf. Section 2.2).

Whereas results from WGC2 located approximately the inshore edge of the Alaskan Stream, moorings in Kiliuda Trough defined the effect of the bank-trough-bank configuration on currents. Winter mean currents observed are shown on Figure 28. There was a clearly defined shoreward flow on the upstream (northeastern) side of Kiliuda Trough, just inside the 91-m (50 fm) isobath. Current speeds here were of order 10 cm sec^{-1}. Along the axis of the trough, there was a weak ($\sim$5 cm sec^{-1}) shoreward mean flow which showed a tendency to curve left toward the head of the trough. Inward flow into the trough was supported qualitatively by release and recovery data from seabed drifters which indicated a shoreward flow of bottom water into the trough (Fig. 29). Flow at the head of the trough was dominated by a relatively strong ($\sim$20 cm sec^{-1}) southwesterly alongshore flow. The overall tendency was for a cyclonic circulation pattern over the trough. This is reasonable dynamically because of the high-latitude tendency for streamlines to parallel isobaths and hence conserve potential vorticity. The inshore portion of the Alaskan Stream would, in tending to follow isobaths, flow shoreward along the northeastern side of the trough as observed. The southwesterly coastal flow near the head of the trough may be, in part, a baroclinic effect due to coastal freshwater addition, either locally or more likely as part of the Kenai Current. This tends to augment the topographically controlled flow.

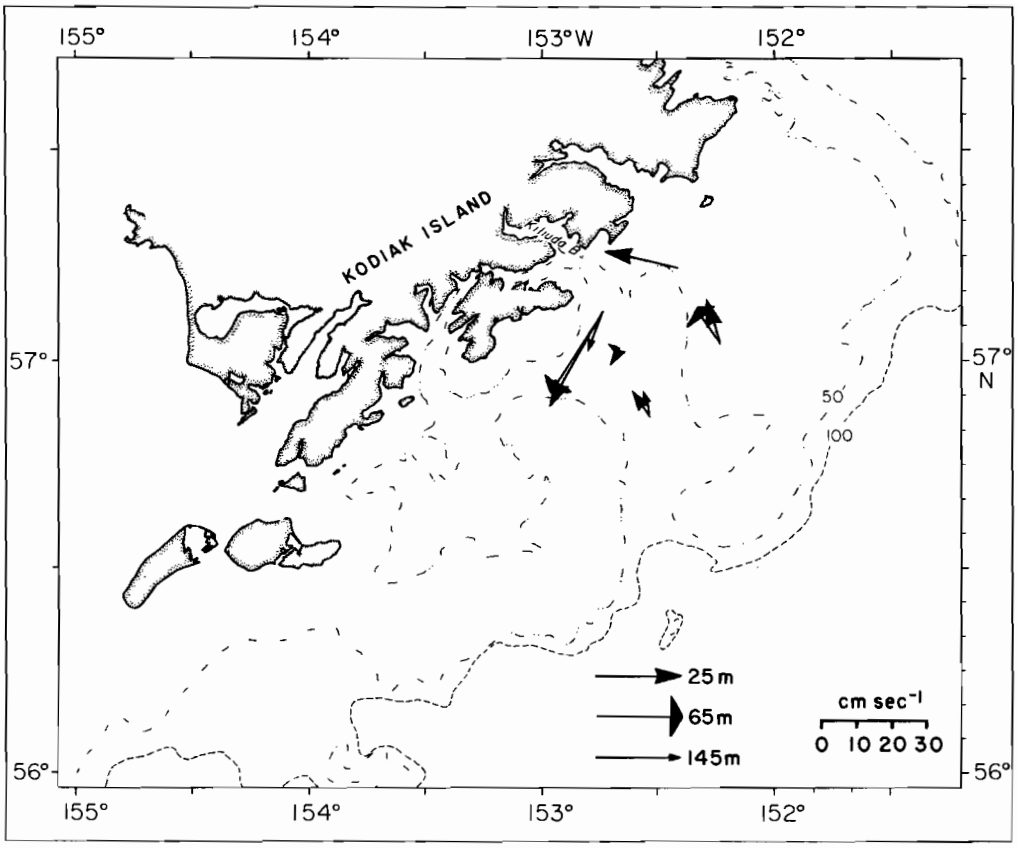

Figure 28. Mean currents observed in the bank-trough region south of Kodiak Island during winter 1977-78. Mooring statistics (moorings K6-K10 A-series) are given in Appendix A.

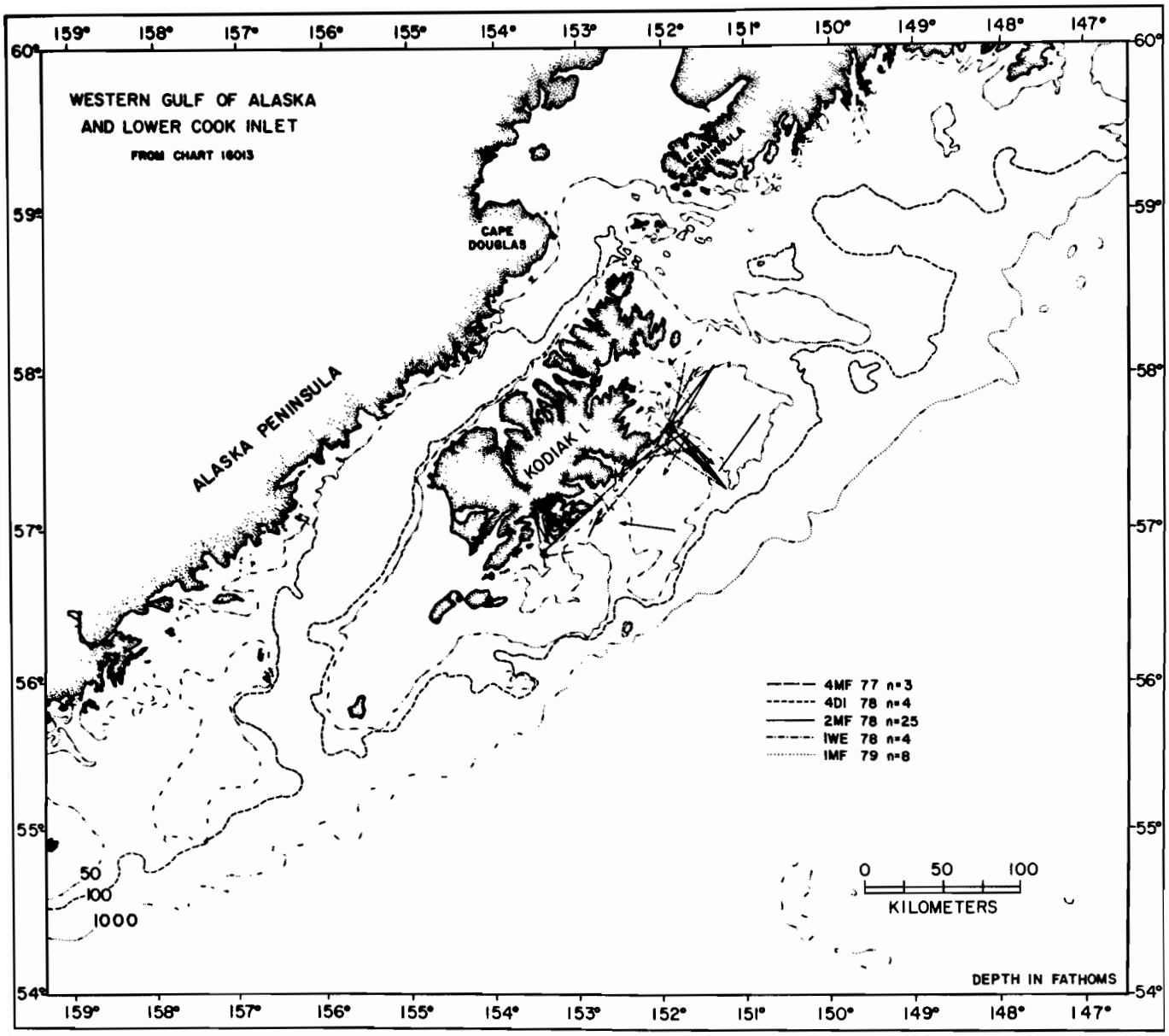

Figure 29. Deployment and recovery locations of seabed drifters, showing inferred directions of movement. Specific positions and dates of deployment and recovery are listed in Appendix C. The figure includes drifters recovered through September 1979, while Appendix C contains recoveries as recent as February 1980.

Sufficient temperature and salinity data were obtained on the banks east of Kodiak Island to allow speculation on processes which influence temperature and salinity distribution. As these banks are bounded on the north by the Kenai Current and on the south by the Alaskan Stream, we might expect considerable complexity there. Of major interest is the vertical density stratification, which reflects vertical mixing processes and mechanisms (such as freshwater input) that act to maintain stratification. With precipitation (>130 cm yr^{-1}) exceeding evaporation (<50 cm yr^{-1}), a net dilution of surface waters occurs (Jacobs, 1951), so that surface changes in salt content usually provide a positive buoyancy flux. During times of minimum precipitation, surface exchange of heat may result in a negative buoyancy flux. Under conditions of negative buoyancy flux, wind and wave mixing at the surface and tidal mixing from the bottom act to stir the entire water column; conversely, with a sufficient positive buoyancy flux, stratification occurs.

We present the distribution of the sigma-t difference between 50 m and the surface (Figs. 30 and 31) compiled from the two cruises having the most complete spatial coverage. The sigma-t differences for September 1977 are representative of summer conditions, whereas those for October-November 1977 represent fall.

The greatest stratification was associated with the Kenai Current. This was caused primarily by dilute (low density) near-surface water, and values were reduced somewhat by enhanced tidal mixing near the Kenai Peninsula and over the banks. During September 1977, the sigma-t distribution suggests that some portion of the Kenai Current did not enter Shelikof Strait but instead turned south near Afognak Island. The effect of more dilute Kenai Current water, in concert with locally added fresh water, was manifested by increased $\Delta\sigma_t$ along Kodiak Island and southwest extension over Middle

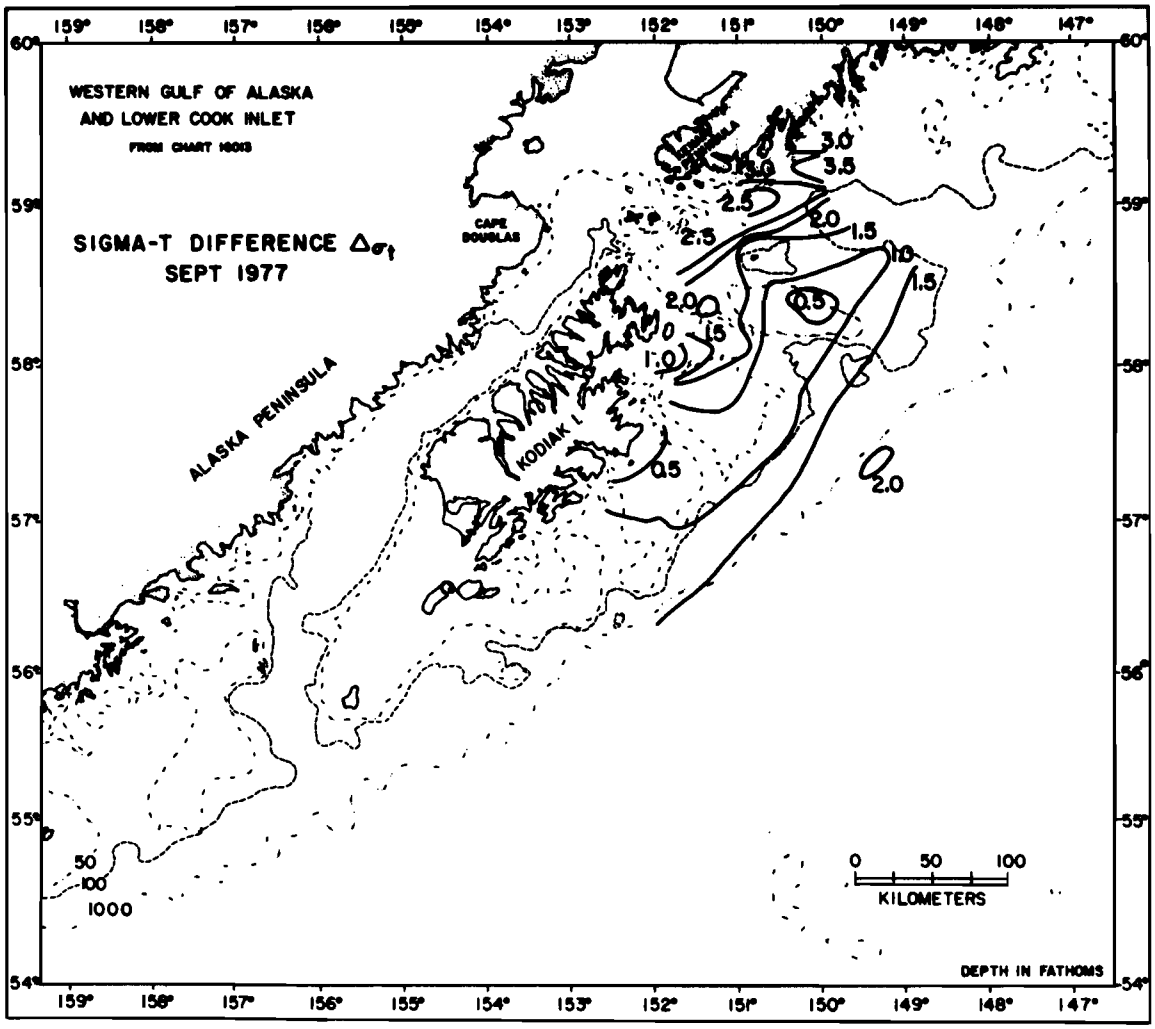

Figure 30. Difference in density (as sigma-t) between the surface and 50-m depths on the banks south and east of Kodiak Island in September 1977.

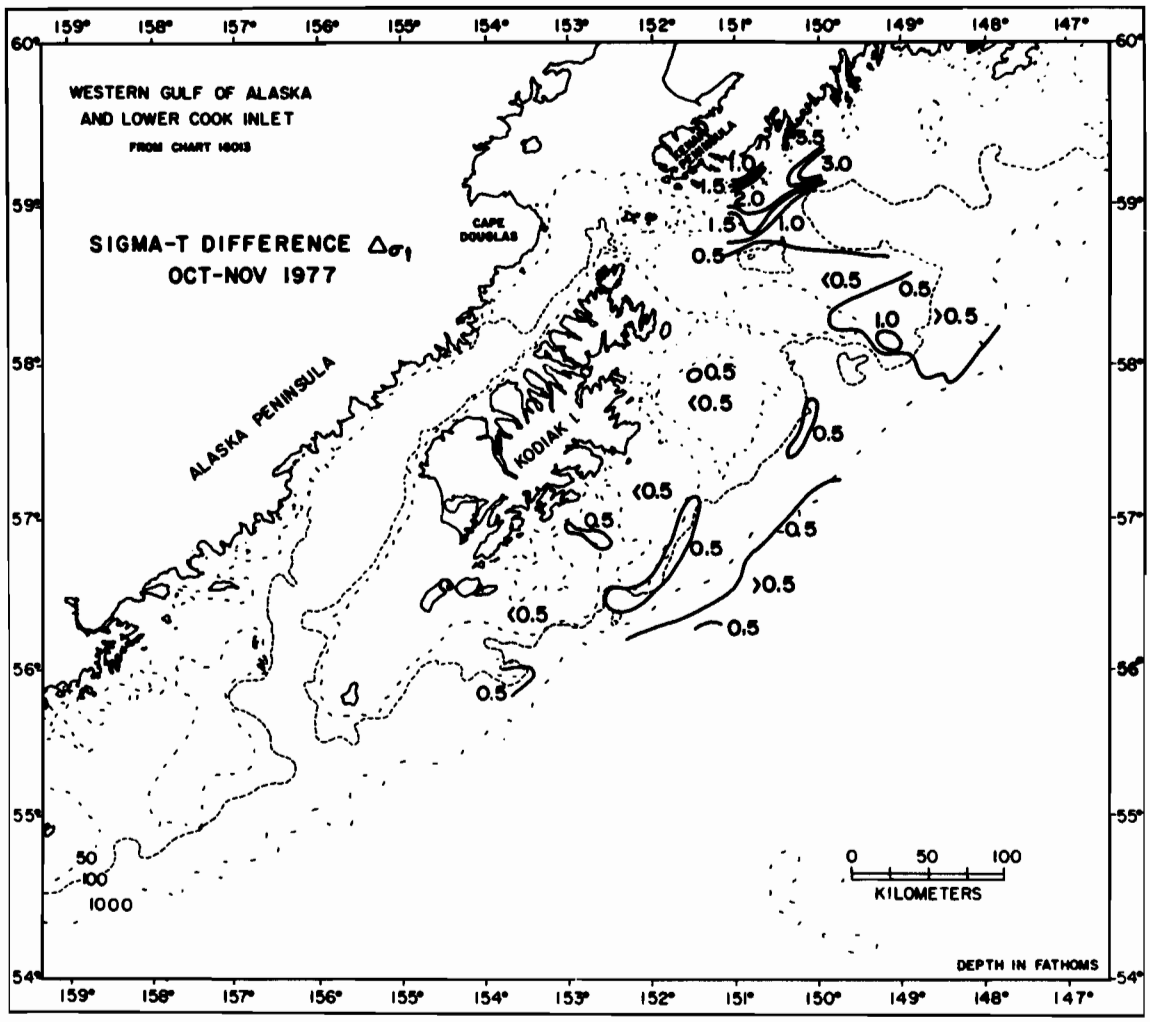

Figure 31. Difference in density (as sigma-t) between the surface and 50-m depths on the banks south and east of Kodiak Island in October-November 1977.

Albatross Bank. During October-November 1977 the wind stress changed from weak northeast to strong southwest, surface cooling became an important factor, and stratification was reduced.

Mechanisms other than thermohaline convection can influence stratification. For example, on 17 October, after occupation of stations 203 and 202.1 over Portlock Bank (Fig. 32), work was discontinued because of high winds from the north (wind speeds > 25 m sec^{-1}). These two stations were reoccupied 41-42 hours later. The storm had produced marked cooling and an increase in salinity of the upper ocean. Although the cooling rates are plausible as a result of surface heat exchange (about 0.6 cal cm^{-2} min^{-1} was estimated from bulk formulas), the large changes in salinity and almost complete homogeneity of the water suggest that a combination of processes including localized upwelling and vertical turbulent mixing occurred in response to the storm. These data point out that the upper ocean may vary widely over short time spans.

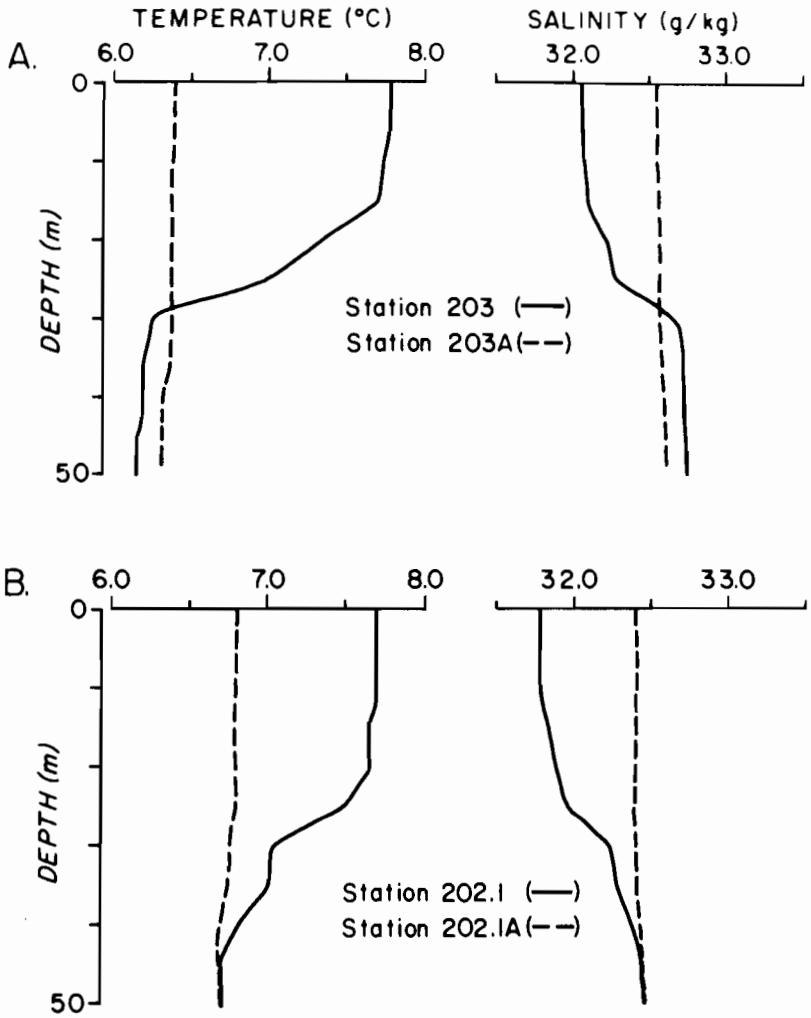

Figure 32. Vertical profiles of temperature and salinity before (solid line) and following (dashed line) a severe storm over Portlock Bank.

3.2 Behavior of Low-Frequency Current Fluctuations

3.2.1 Introduction

In this section, we discuss prominent current fluctuations having periods longer than diurnal tidal, or about 24 hours, but less than seasonal. Currents throughout the northwest Gulf of Alaska and into lower Cook Inlet are characterized by these fluctuations, which attain dominant control over the flow in regions having weak mean currents. For example, in some locations in lower Cook Inlet and on Albatross Bank where the mean flow was small (< 5 cm sec^{-1}) these fluctuations accounted for more than 90% of the kinetic energy in the nontidal water motion, so they must be of paramount importance in material transport. In regions of strong mean flow (> 20 cm sec^{-1}), such as Shelikof Strait, the fluctuations are relatively less important when compared with the mean flow. Figure 33 illustrates the nature of these fluctuations and exemplifies the pattern found throughout the northwestern Gulf. Time scales for the fluctuations are on the order of a week, though they have no clearly defined periodicity. The records used here as illustration are from near-bottom, minimizing biasing of the current records by surface wave noise or mooring motion.

The way in which these low-frequency fluctuations propagate through the northwestern Gulf of Alaska shelf region is of particular interest. We approach this by discussing selected aspects of the fluctuations in specific subregions, commencing with the outer and mid-shelf regions southeast and south of Kodiak Island (Fig. 1).

3.2.2 The Bank-Trough Region

Winter and summer subtidal current variance spectra from outer Albatross Bank (Station WGC2 on Fig. 6) are shown on Figure 34. These spectra are representative of conditions on the banks seaward of Kodiak Island. Most of

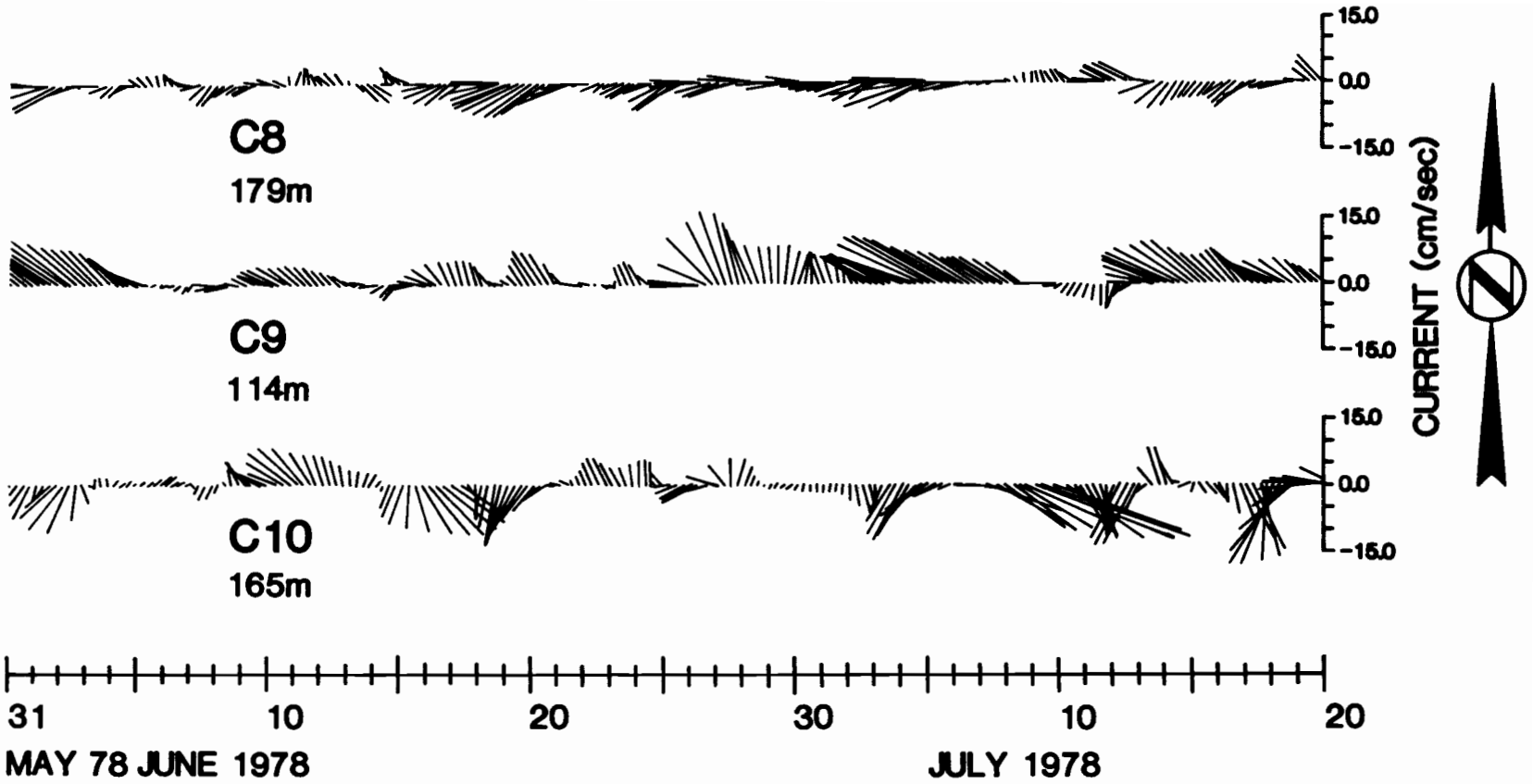

Figure 33. Representative time-series segments of near-bottom currents in Kennedy Entrance (C8), Stevenson Entrance (C9) and northern Shelikof Strait (C10). These records have been low-pass filtered through a 35-h filter to remove the tidal signals.

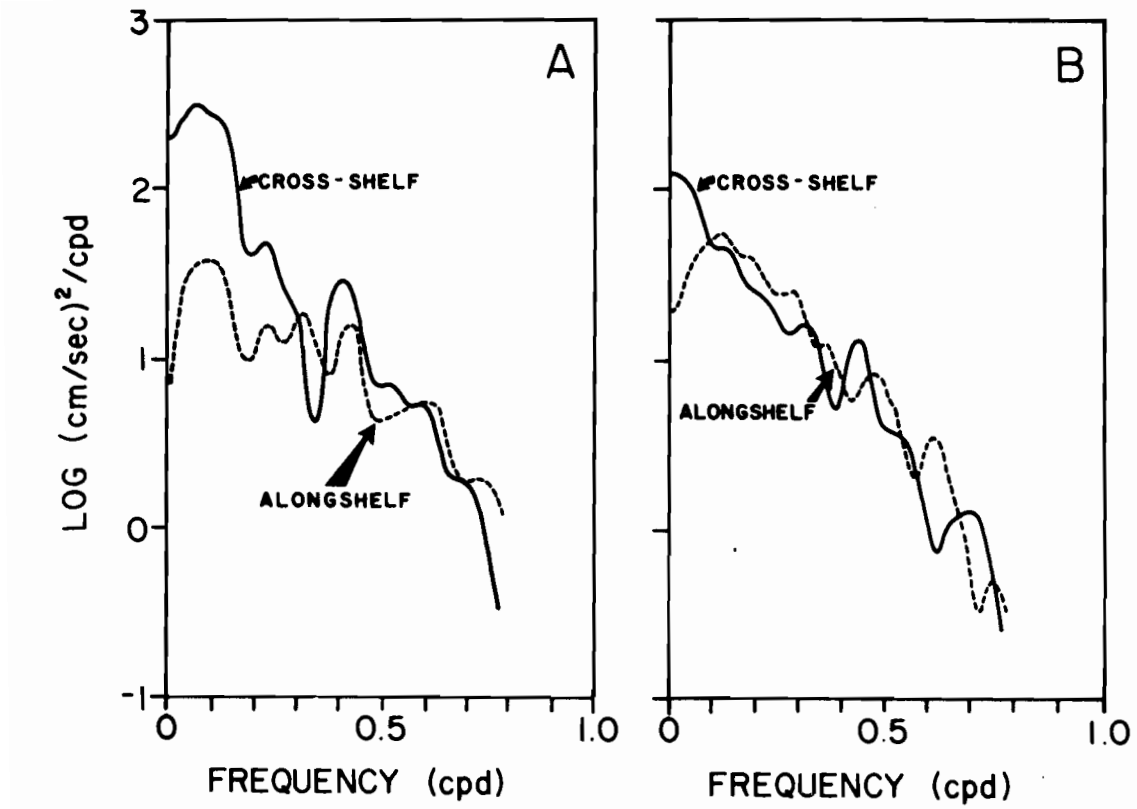

Figure 34. Winter variance spectra at station WGC2 on the banks southeast of Kodiak Island (left) and at station WGC3 off the entrance to Shelikof Strait southwest of Kodiak Island. Both current records were from about 24-m depths. Station locations are indicated on Figure 6.

the low-frequency variance energy is contained in bands below 0.5 cpd, and very low relative amounts of energy occur at 0.75 cpd, the high frequency cutoff. There was a marked change in slope of the spectra at about 0.5 cpd, with variance energy dropping off more sharply at higher frequencies. Shallower observations at the same location indicated higher overall energy levels, while deeper observations showed lower energy levels; the characteristic shapes of the spectra were the same. For comparison purposes, we also show subtidal variance spectra obtained from observations at Station WGC3 just seaward of the southern extremus of Shelikof Strait. The shapes of the spectra at the two locations are similar, though energy levels differ somewhat.

Spectral analyses of the current data from mooring WGC2 on the shelf south of Kodiak Island (Fig. 6) indicated only one significant energy peak; this occurred at about 0.4 cpd or at a period of about 2.5 days and is shown most clearly on the cross-shelf spectra (Fig. 34). Analysis of the current records from moorings WGC1, 2, and 3 have indicated that this peak was coherent in the alongshelf direction, and that motions of this period propagate to the northeast with speeds of about 5 m sec^{-1}. The peak was most pronounced in the cross-shelf component, being in many cases absent entirely from the alongshore component. It decreased in magnitude with increasing depth of observation. It is impossible to discern whether this peak was more energetic on Albatross Bank than elsewhere; overall energy levels were lower on Albatross Bank, and it is possible that a 2.5-day peak of similar magnitude existed at other locations (such as at WGC3 off Shelikof Strait) but was masked by the higher overall spectral energy.

While the WGC series of current moorings were designed to obtain long-term, large-scale information on alongshelf coherency south of Kodiak Island, a more recent series of moorings was deployed in the complex topographic

bank and trough region southeast of central Kodiak Island (cf. Fig. 9), providing further definition of the low frequency flow. The low-pass (35-h) filtered current time series from the 1977-78 winter experiment is shown in Figures 35 and 36. The characteristic low-frequency pulses were clearly present but were manifested in different fashions at different locations relative to the banks and troughs. At stations 6 and 7 on the bank and particularly at station 8 in the shoreward portion of the trough, the pulses were primarily in speed with little directional variation. In the central portion of the trough at stations 9 and 10, however, the pulses were manifested as large variations in both speed and direction leading to frequent reversals. While the records from stations 6 and 7 over the bank suggested that events there were correlated, pulses in the trough were not. It is possible that the instruments deployed in the trough were sampling different flow regimes, as these instruments were in the vicinity of an apparent transition from alongshelf flow on the open shelf to cross-shelf flow connected with the trough.

Analysis of variance contained in different frequency bands in the bank-trough region indicated a flatter distribution than observed farther offshore at WGC2. Subtidal variance was distributed approximately evenly across the band, with a more gradual tapering off of energy levels at higher frequencies than was observed at WGC2, and there were no spectral peaks significant at the 95% confidence level.

3.2.3 Shelikof Strait

Shelikof Strait may be defined as an alongshore channel, and we suspect that, due to its confining lateral boundaries, its fluctuating flow might have somewhat different characteristics than to the southeast upon the open shelf. A winter 1976-77 current observation program in Shelikof Strait obtained

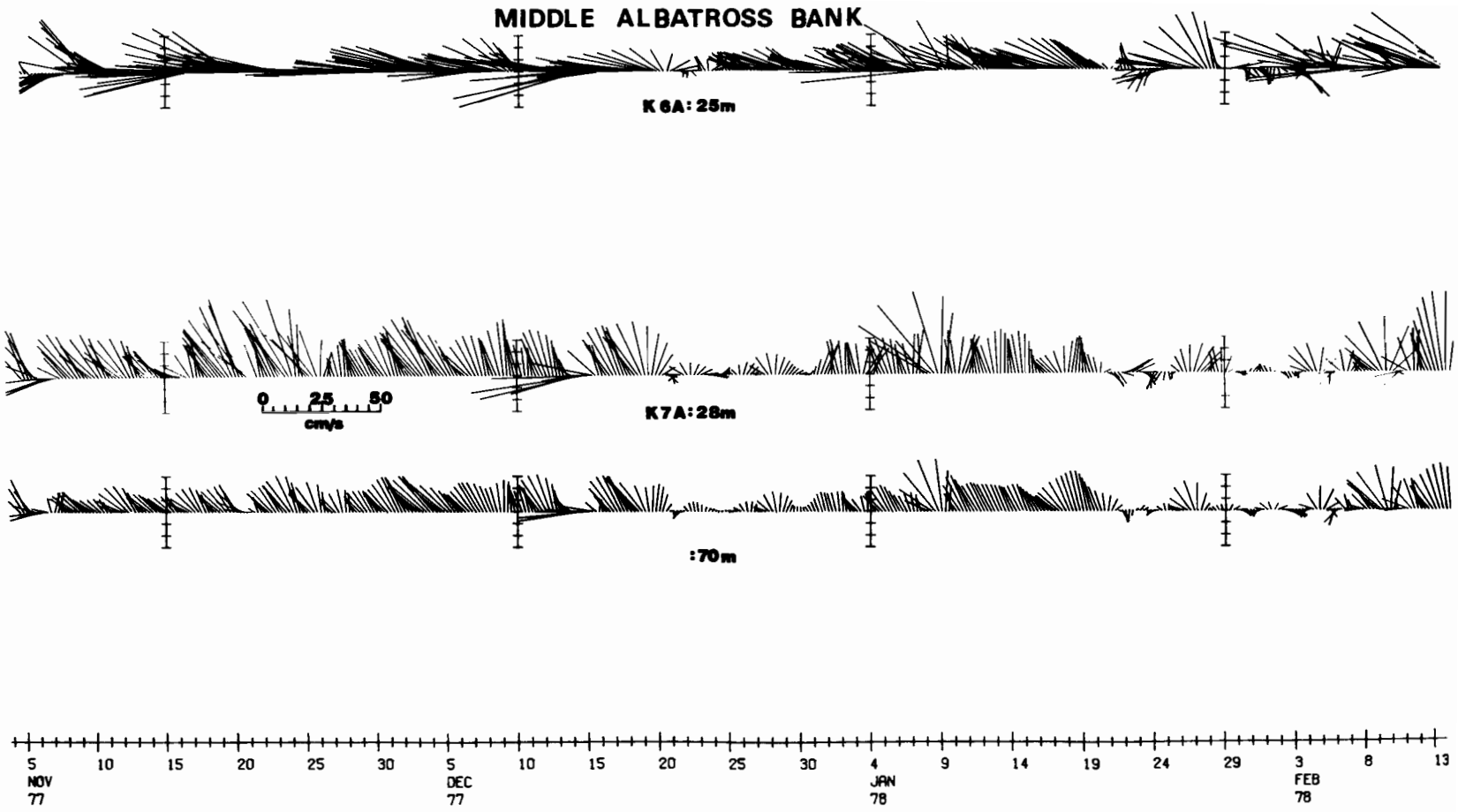

Figure 35. Low-pass (35-h) filtered currents during winter 1977-78 over the bank area south of Kodiak Island. Station locations are indicated on Figure 9.

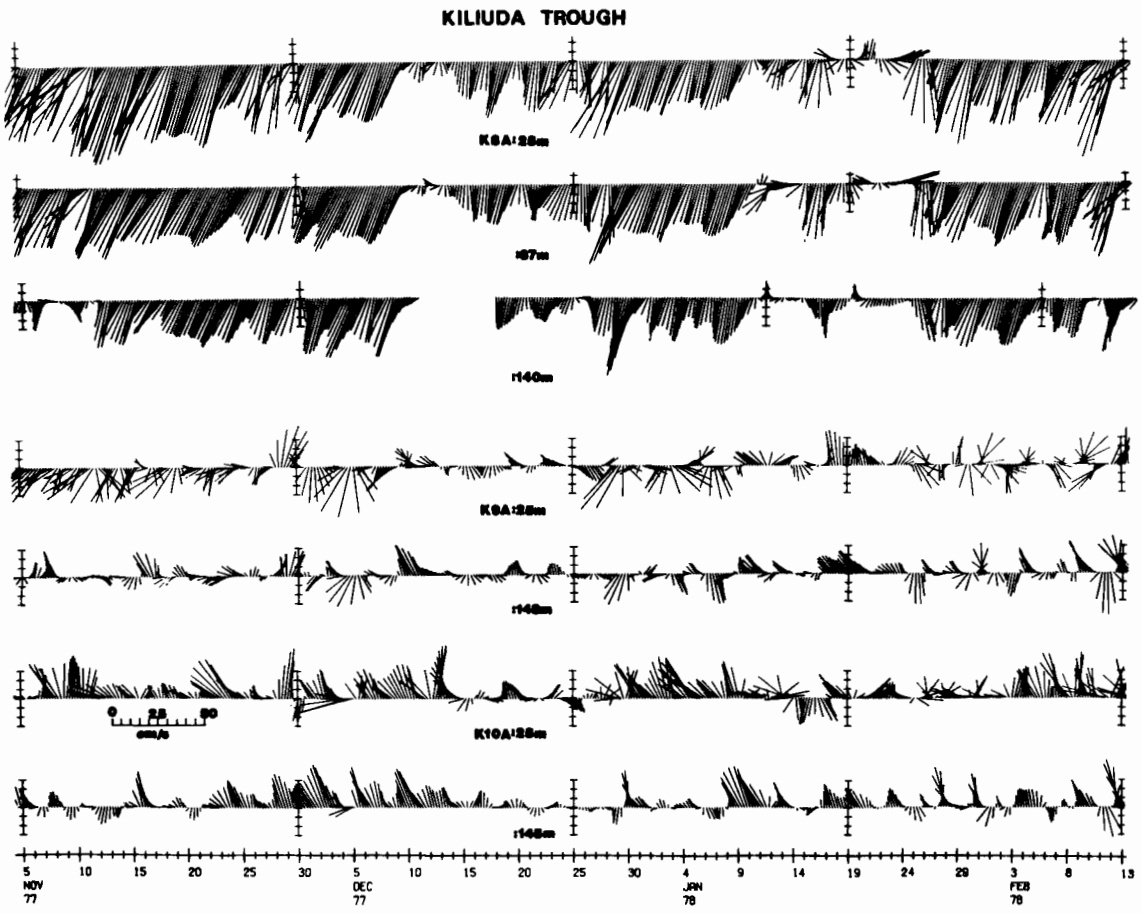

Figure 36. Low-pass (35-h) filtered currents during winter 1977-78 in Kiliuda Trough south of Kodiak Island. Station locations are indicated on Figure 9.

time-series records from the northeast and southwest ends of the Strait, providing data for a comparison of motions through the Strait (cf. Fig. 7). Representative segments of the low-pass (35-h) filtered time series from the two ends of the Strait are shown in Figure 37. Due to the strong winter mean flow through the Strait, the fluctuations were evidenced as pulses in speed rather than as changes in direction. A generally good visual correlation is evident between the records at both ends of the Strait, as we would expect due to the confining lateral boundaries; volume continuity requires that an inflowing pulse at the upstream end of the Strait result in a corresponding outflow at the downstream or southwestern end.

Spectral analyses have been applied to the records from K1 and K2 and indicate a significant shift in cross-channel variance energy from higher and lower frequencies toward a spectral band between 0.1 and 0.3 cpd (Fig. 38). In general, subtidal variance was greater at the downstream than at the upstream end of the Strait. This downstream amplification of cross-channel fluctuations in flow was indicated also on infrared satellite photographs. A representative image is shown in Figure 39, and reveals a wave-like feature defined by the boundary between the low-temperature water from Cook Inlet and the warmer water from the Gulf of Alaska. This boundary appears to oscillate with larger amplitudes towards the southwest end of the Strait before it loses its identity. The same feature has been commonly observed on satellite imagery by G. Hufford (NOAA/NESS, Anchorage, AK 99510). We point out that although the temperature boundary which we use as a tracer loses its identity, it does not necessarily follow that the wave-like feature has ceased to exist.

Application of coherency analyses to the 100-m deep records from K1 and K2 at opposite ends of the strait reveals a confusing picture (Fig. 40).

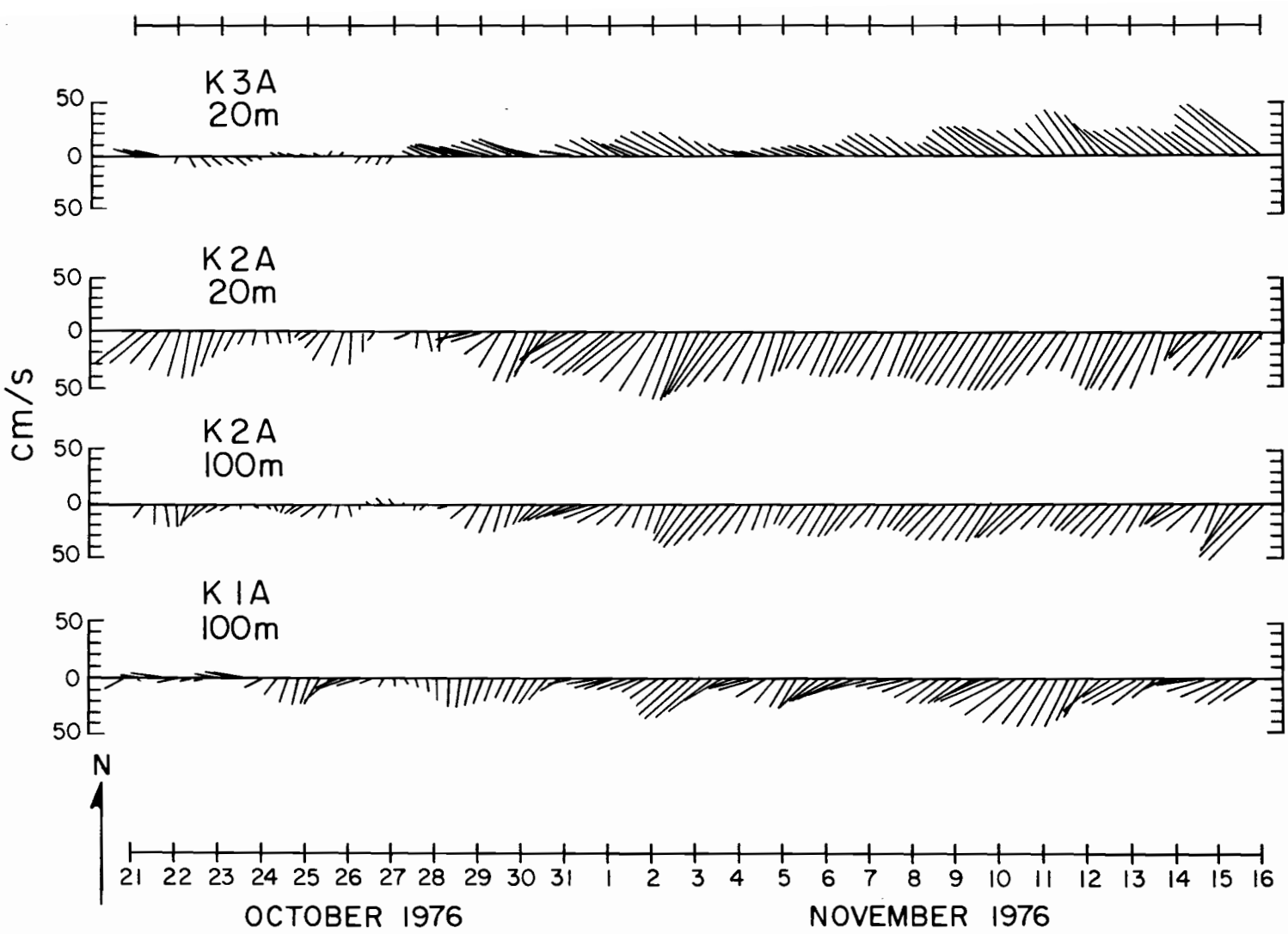

Figure 37. Representative winter segments of low-pass (35-h) filtered current data from northeastern Shelikof Straight (K2A and K3A) and from the southwestern end of the strait (K1A), illustrating continuity of low-frequency flow events through the Straight. Station locations are indicated on Figure 7.

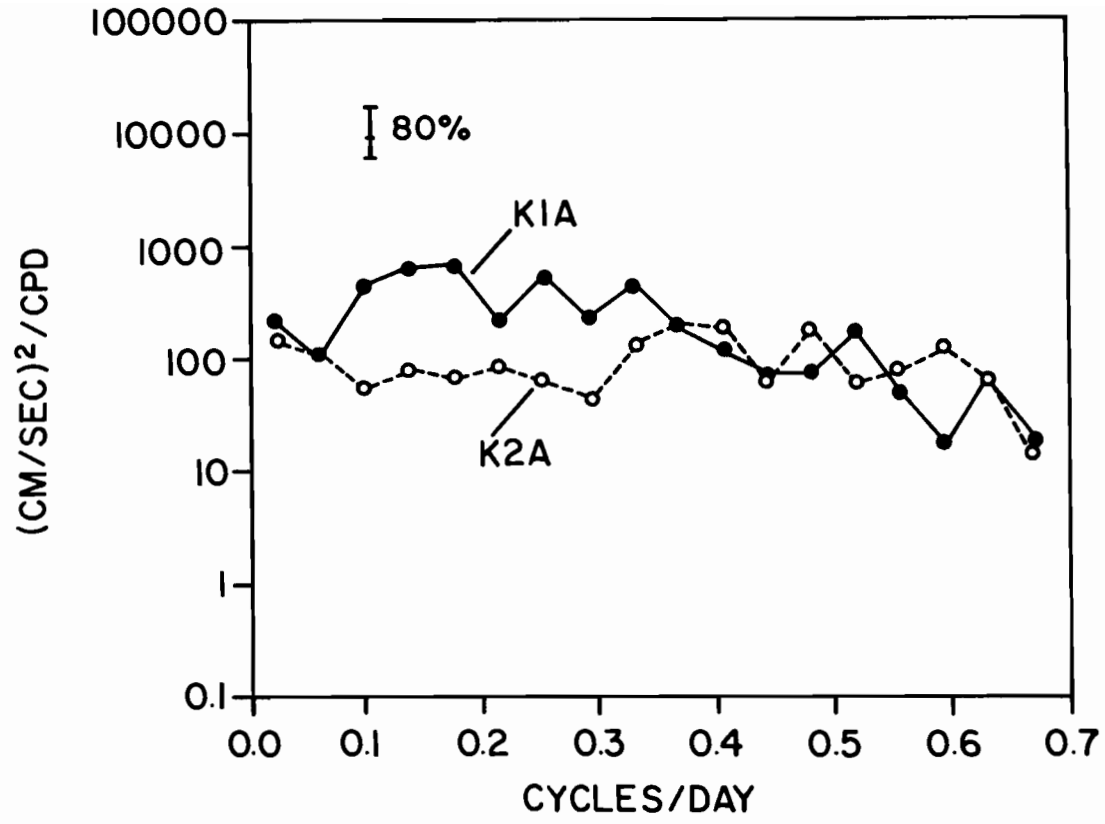

Figure 38. Variance spectra from the northeastern end (K2A) and the southwestern end (K1A) of Shelikof Strait for the cross-channel component of the 100 m deep records, showing the shift of energy into the 0.1-0.35 cpd band from K2A to K1A. Data were obtained during winter 1976-77, and station locations are indicated on Figure 7.

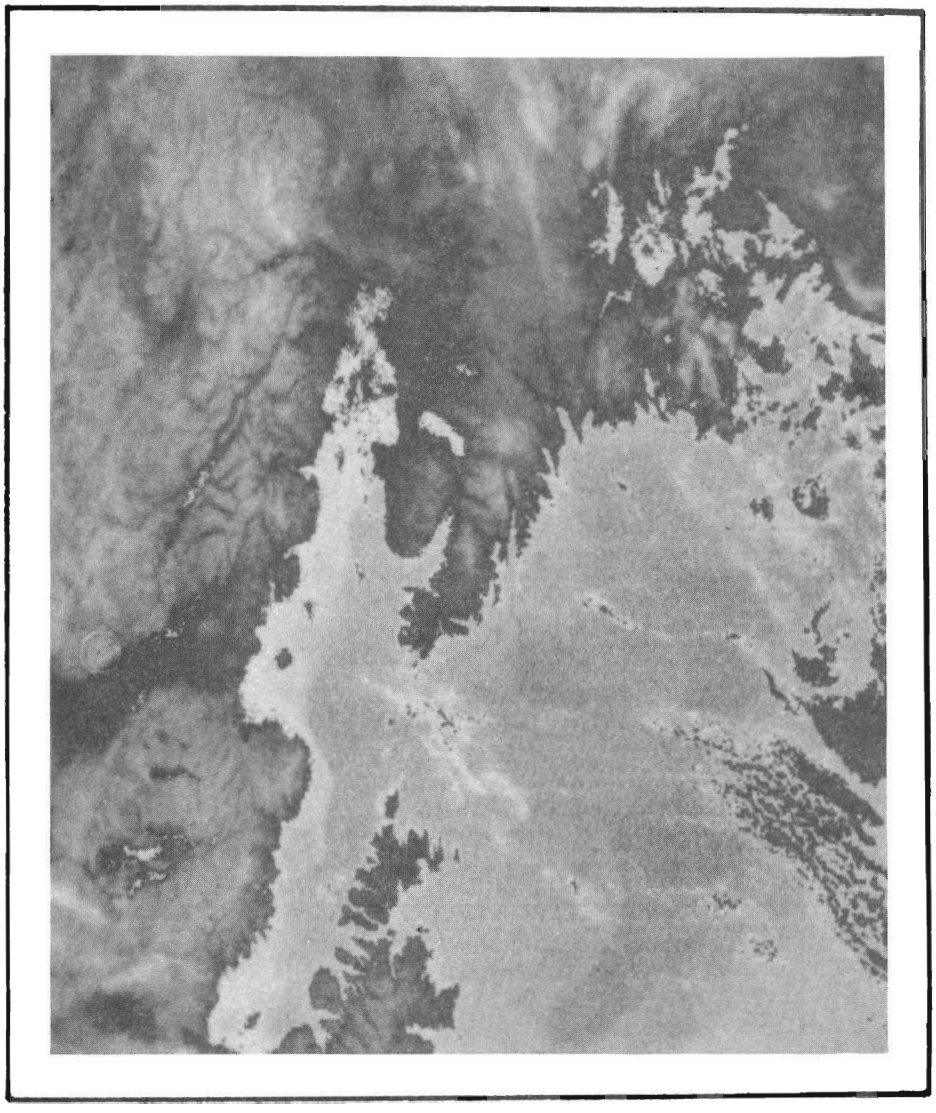

Figure 39. Infrared satellite image of the northwest Gulf of Alaska on 25 February 1977, showing undulating feature defined in northeastern Shelikof Strait by the boundary between cold water (light colored) from Cook Inlet and warmer (darker) water from the Gulf of Alaska.

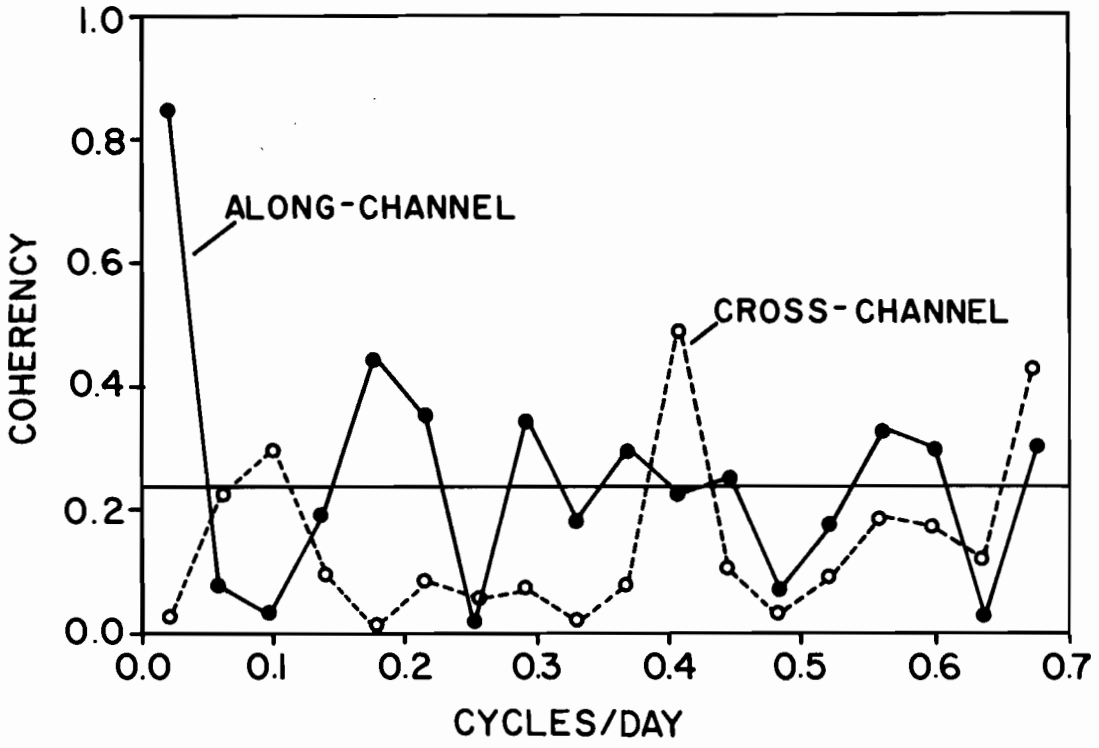

Figure 40. Coherency between cross-channel flow components at northeastern end (K2A) and southwestern end (K1A) of Shelikof Straight using winter 1976-77 data. Station locations are indicated on Figure 7.

The along-channel flow was coherent, as expected, at very low frequencies. The only other significant peaks were at about 0.2 cpd, and at about 0.4 cpd where a cross-channel peak corresponded to our ubiquitous 2.5-day peak. The correlations which are apparent from the time series shown in Figure 37 apparently relate to nonperiodic phenomena, and do not lend themselves to stationary statistical analysis. Based on the above, we conclude that there is generally a good correlation between the along-channel current fluctuations through Shelikof Strait, and that there is a significant coherency between the cross-channel fluctuations at 2.5-day periods. The 2.5-day period pulses are periodic in nature, and manifest themselves in the surface temperature field as wave-like features observable on satellite imagery.

Data obtained from northeastern Shelikof Strait during winter 1977-78 were adequate to test for vertical coherency in the fluctuating flow. Coherency analysis of the entire 5-months record indicated that the flow was vertically coherent throughout the subtidal frequencies. We conclude from this that these pulses are primarily barotropic in nature.

3.2.4 Lower Cook Inlet

A somewhat more detailed analysis of low-frequency fluctuations was possible for lower Cook Inlet than for other regions because of the relatively dense array of current meters used there (Fig. 8). Representative segments of the low-pass filtered currents from six stations in the lower Inlet are shown on Figure 41. It is clear from these plots that the time scales of variability are the same as for other regions considered, on the order of a week, and that the fluctuations are the controlling features of nontidal currents in lower Cook Inlet. At station C4, for instance, it is impossible

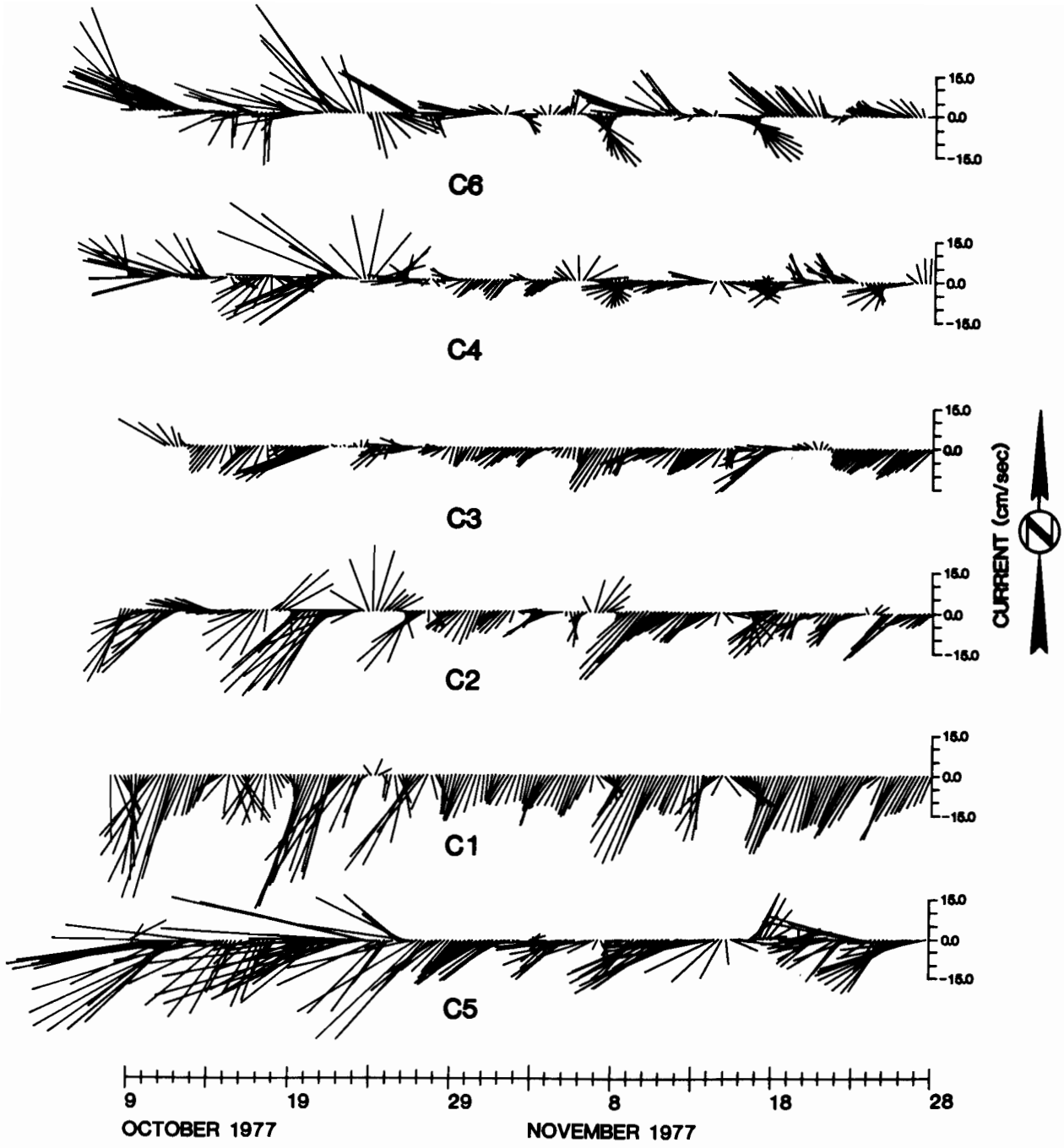

Figure 41. Representative segments of low-pass (35-h) filtered current records obtained from 20 m in lower Cook Inlet. Station locations are indicated on Figure 8.

to detect mean flow direction from a visual inspection of the time-series plot, as the flow was dominated by events. Comparison between the time series shown on Figure 41 reveals a confused pattern of correlation between fluctuations at different locations. For example, a northerly flow event occurred on about 25 October at stations C1, C2 and C4 but not elsewhere. Station C3 showed, in particular, little correlation with events elsewhere in the lower Inlet. Computation of horizontal coherencies between the 20-m records produced no consistent results.

Vertical correlations between the low-frequency pulses varied over the Inlet. At stations C3 and C4 vertical correlations were poor (Fig. 42), even though the records were vertically separated by only 30 and 45 m, respectively. Station C1 showed, conversely, excellent visual correlations in the vertical (Fig. 43) during winter, with correlations somewhat less evident during summer. Station C10, in northern Shelikof Strait, showed high visual correlation in the vertical during both winter and summer. Further analyses are in progress.

Seasonal changes in the low-frequency fluctuations are illustrated by the records from stations C1 and C10 (Fig. 43 and 44). The fluctuations were larger in winter than summer, as evidenced particularly well at station C1. There was no significant seasonal change, however, in time scales or in the lack of horizontal correlation.

In an attempt to further "filter" the current data, 7-day running means of speed were computed. These values, plotted in Figures 45 and 46, allow a better visual definition of correlation between the flow events having time scales longer than 1 week, and also reveal the longer term trends. During the winter observations (Fig. 45) the autumn decrease in flow was evident at all stations except C3. A slight increase later in the winter, particularly

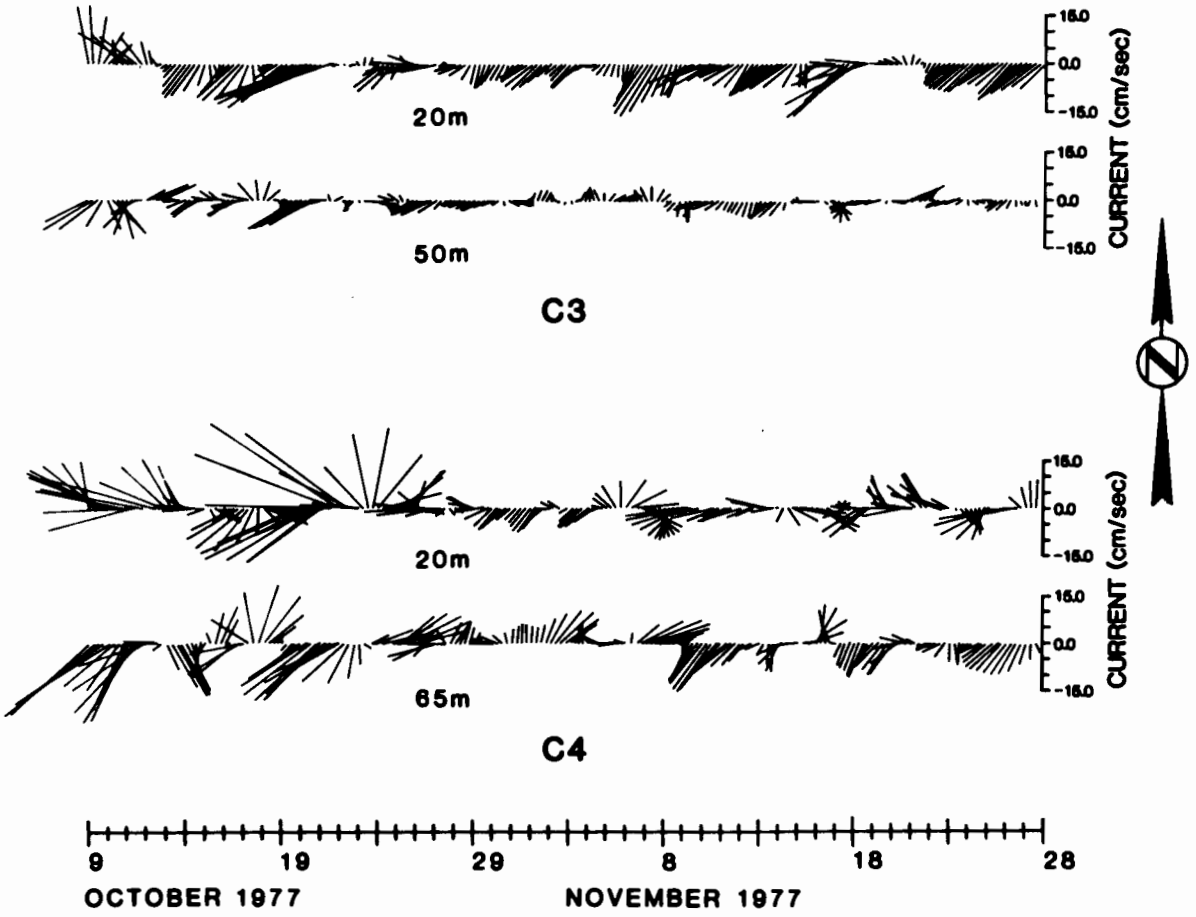

Figure 42. Vertical comparison of low-pass (35-h) filtered current records during winter from two locations in lower Cook Inlet. Mooring locations are indicated on Figure 8.

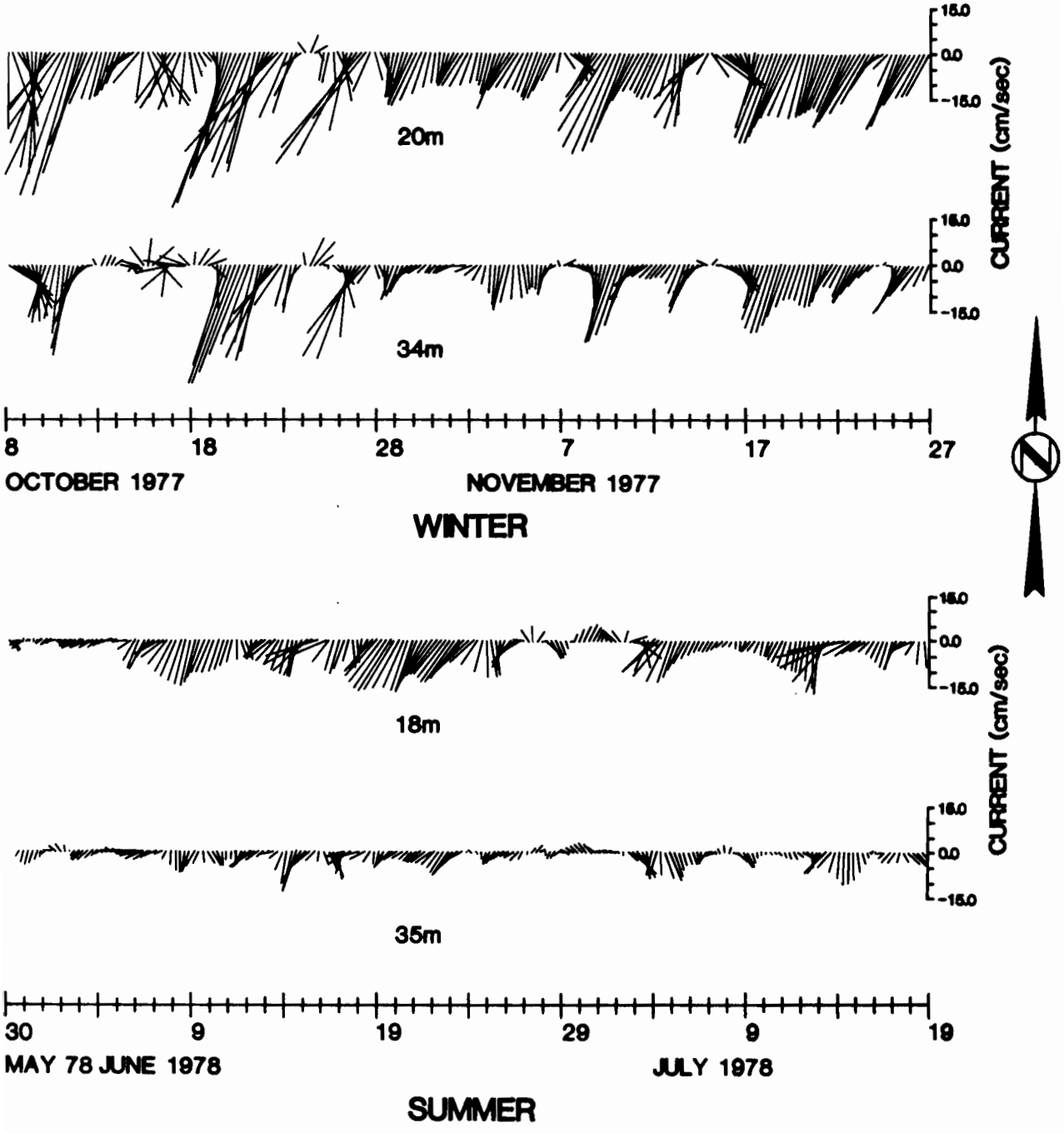

Figure 43. Seasonal comparison of low-pass (35-h) filtered current records from station C1 in lower Cook Inlet at two different depths. Mooring location is indicated on Figure 8.

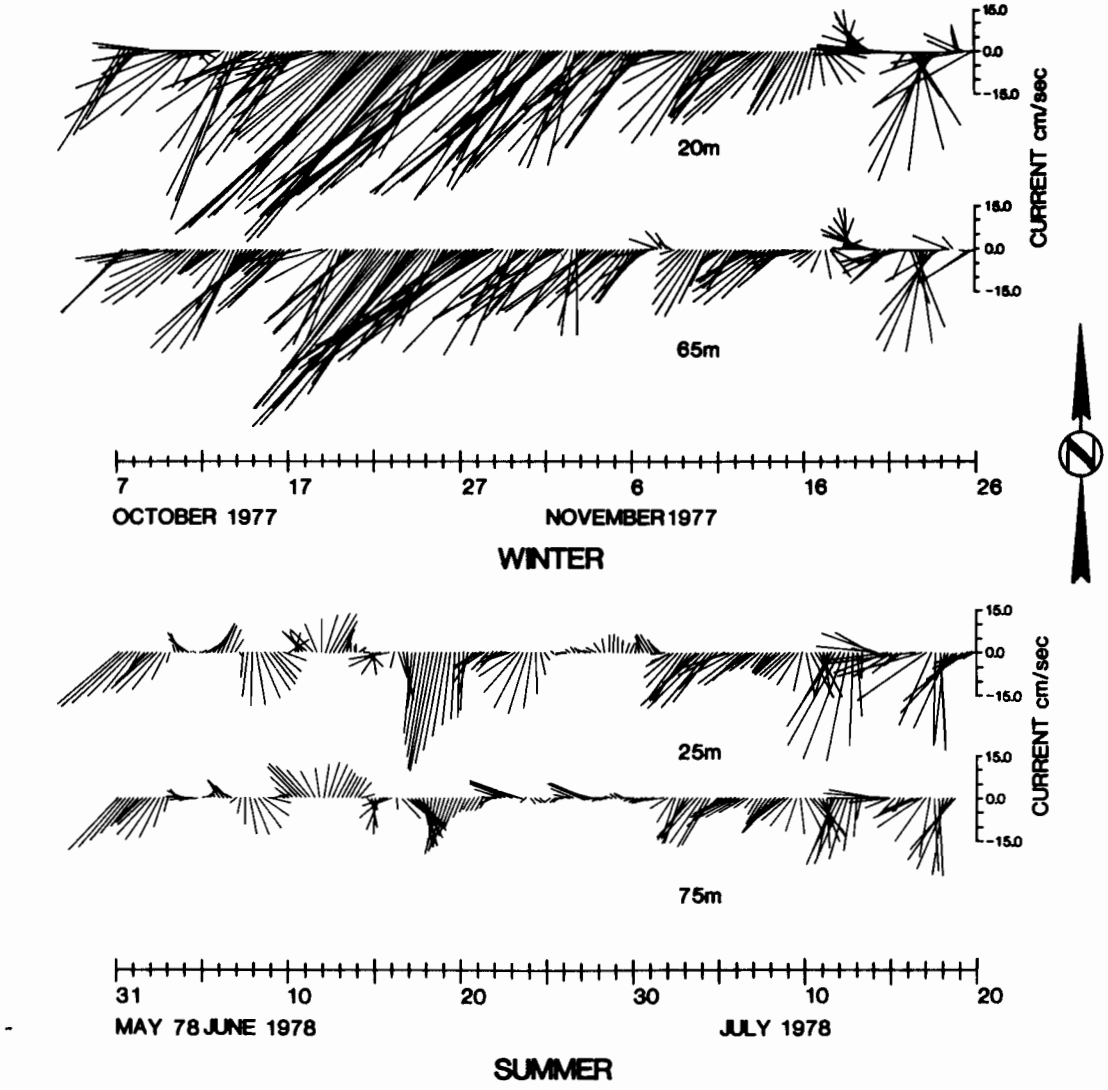

Figure 44. Seasonal comparison of low-pass (35-h) filtered current records from station C10 in northern Shelikof Strait. Mooring location is indicated on Figure 8.

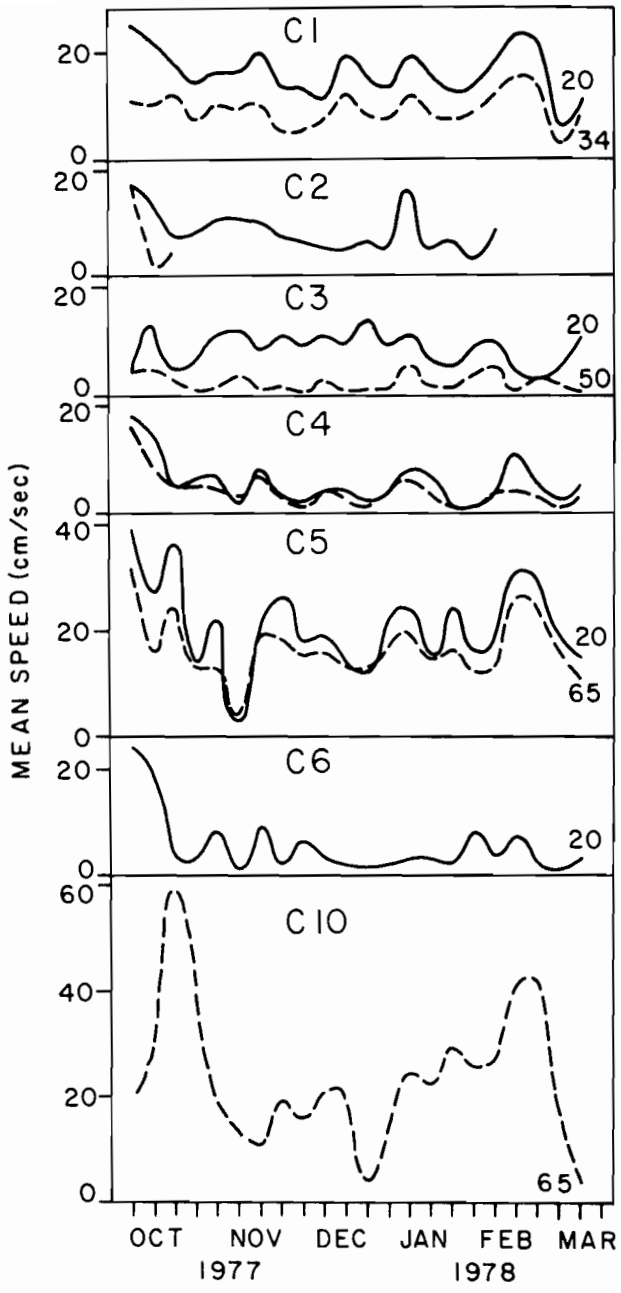

Figure 45. Seven-day running mean speeds at seven stations in lower Cook Inlet. Numbers at right-hand ends of curves indicate observation depths in meters. Station locations are indicated on Figure 8.

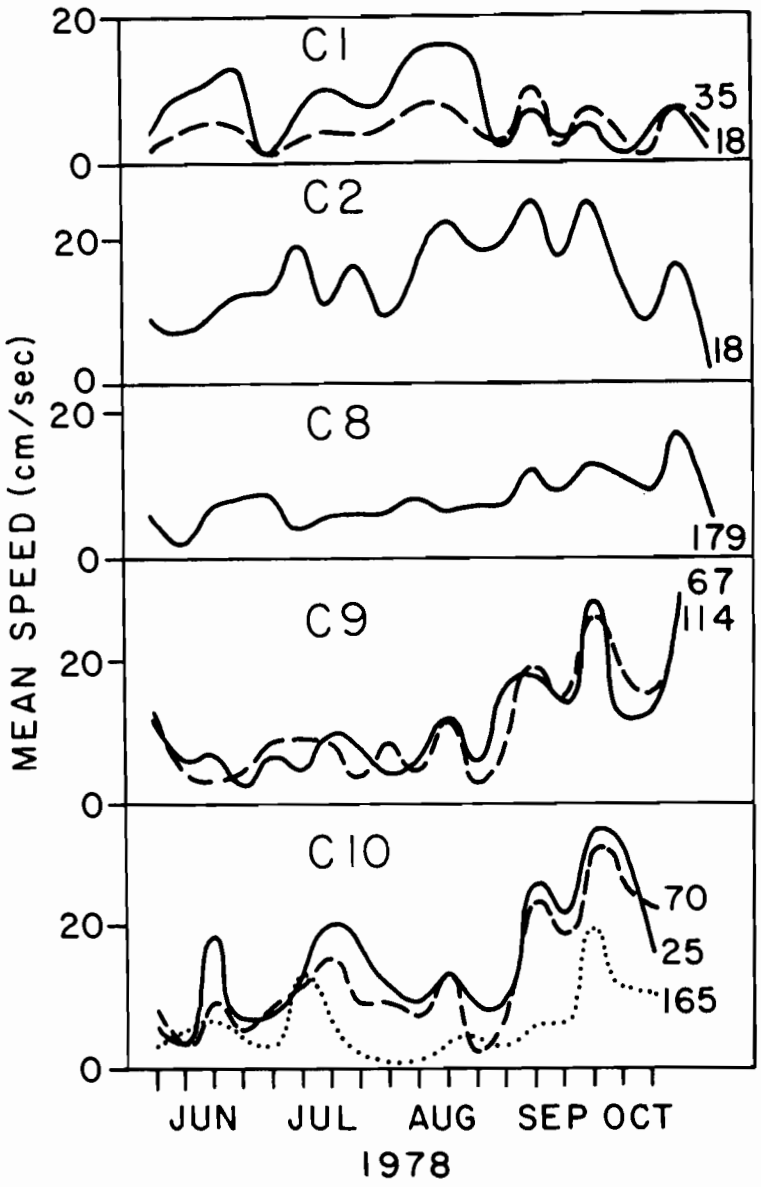

Figure 46. Selected 7-day mean speeds at five stations in lower Cook Inlet during summer 1978. Numbers at right-hand ends of curves indicate observation depths in meters. Station locations are indicated on Figure 8.

apparent at stations C5 and C10, may have been a reflection of winter spin-up of the coastal currents. In addition to the seasonal changes, there were several shorter period (order of weeks) fluctuations that were always correlated at more than one location but rarely at all of them. Stations C5 and C10 were the best correlated, while C3 showed the least correlation with the other records. Generally, vertical correlations were good except for station C3.

Summer current records were relatively incomplete, but indicate the same general patterns that were observed during winter (Fig. 46). The later portion of the records clearly indicates the autumn flow increase consequent to freshwater addition along the Alaskan coast to the east of lower Cook Inlet (Schumacher and Reed, 1980).

The behavior of low-frequency fluctuations in lower Cook Inlet suggests that the pulses tend to follow the same path as the mean flow, that is, an acurate east-west path paralleling the bathymetry. This was manifested as a generally good visual correlation between events at stations C8, C9, C10 and C5. However, these pulses penetrated northward into Cook Inlet only part of the time, so that the frequency of events which can be correlated with those at C5 becomes lower as we progress northward into the Inlet and reaches its lowest value at the northernmost station C3. Conversely, it seems likely that some flow events might be generated in, and confined primarily to, the upper Inlet; these might be evident at the northern stations but not in Shelikof Strait.

The cause of the predominantly aperiodic, low-frequency fluctuations discussed here is uncertain, but is probably related in part to atmospheric forcing. To test for causal factors, selected large events were compared with the local and regional meteorological parameters. Results of these

comparisons were inconclusive, and it is felt that this was probably due at least in part to inadequate meteorological data. As discussed in Section 3.5, the atmospheric pressure field is not necessarily representative of actual winds either inside or outside the Inlet. The existing shore stations have also been shown to bear little relation to over-water winds.

Research into the nature of similar flow fluctuations in other large estuarine systems has revealed that such systems are strongly responsive to atmospheric forcing on the continental shelf outside the mouth of the estuary (Wang and Elliot, 1978; Wang, 1978; Winant and Beardsley, 1979; Holbrook et al., 1979). The meteorology of the lower Cook Inlet region is dominated, particularly in winter, by the northeastward migration of intense atmospheric low-pressure systems. We would expect the coastal sea-level variations attendant upon these cyclonic storms to drive significant flow through lower Cook Inlet and Shelikof Strait. Propagation of these pulses northward into the Inlet would then be subject to modification by bathymetry, stratification and local winds. While we have sufficient information on both the bathymetry and stratification to address this problem, the local wind field during our current observations was not defined due to malfunction of environmental buoy EB-46007, which was located centrally in the lower Inlet so as to define the general wind field there. We retain the hypothesis that the fluctuations are driven primarily by atmospheric events over the continental shelf, with local modification to the flow due to stratification, bathymetry and local winds within the lower Inlet itself. Based on work elsewhere, eddies propagating across the shelf could also contribute to these fluctuations. Quantification of these mechanisms awaits further analysis of current data from within the lower Inlet in combination with regional and local wind data.

3.3 Tides and Tidal Currents

The pressure gage data were analysed for tidal components using the Munk-Cartwright Response method (Munk and Cartwright, 1966) with the tide potential as reference series. Results of these analyses are given in Table 3. These analyses were used, along with historical harmonic constants found in Pearson (1973), Rapatz and Huggett (1977), the International Hydrographic Bureau tables (1966), unpublished National Ocean Survey data, and information obtained from the Tide Tables, to describe tidal characteristics and tidal wave propagation in the study area.

Empirical cotidal charts have been constructed for the M_2 (principal lunar semidiurnal) and K_1 (luni-solar diurnal) constituents (Fig. 47 and 48, respectively). These charts show lines of equal phase, or times of high water, and equal amplitude for each constituent. They have been constructed by interpolation between observed values where stations were close-spaced relative to the tidal wavelength, and by estimation in areas where data were sparse. The M_2 and K_1 are the largest of, and generally representative of, semidiurnal and diurnal constituents, respectively.

Both the diurnal and semidiurnal tides propagate from east to west in the Gulf of Alaska in Kelvin wave fashion as part of a north Pacific amphidromic system. According to the cotidal charts of Luther and Wunch (1975) for the central Pacific, the M_2 amphidrome is located at approximately 25°N and 135°W, and the K_1 amphidrome is at 21°N and 177°E. On the outer shelf, M_2 amplitudes decrease from about 110 cm in the vicinity of Middleton Island to 80 cm near Mitrofania Island. Amplitudes increase to about 160 cm up Shelikof Strait toward Cook Inlet. Large amplitudes are found in Cook Inlet, where the semidiurnal tides are near resonance. Amplitudes are largest on the east side in concurrence with Kelvin wave dynamics (Matthews and Mungall,

TABLE 3

Tidal components derived from pressure gage data using the Munk-Cartwright response method (Munk and Cartwright, 1966) with the tide potential as reference series.

Station	LAT	LONG	O1	P1	K1	N2	M2	S2	FROM	TO	DAYS
K8A	57 07	152 45	24.3 261	12.1 273	36.6 274	19.1 276	92.8 299	29.7 329	77 292	78 001	74
K9A	57 01	152 37	25.4 260	12.9 272	39.2 273	19.0 275	92.7 298	30.5 327	77 292	78 068	141
K10A	56 51	152 26	27.0 260	13.9 273	42.2 274	18.9 275	92.6 298	30.5 328	77 292	78 059	133
C1B	59 11	153 19	32.1 271	16.6 286	50.6 287	36.7 303	172.9 326	64.6 002	78 148	78 291	144
C4A	59 17	152 54	34.0 269	17.6 284	53.6 286	37.7 303	177.0 327	65.5 002	77 280	78 074	160
C9B	58 47	152 16	31.8 262	16.0 276	48.8 277	32.4 282	153.6 305	56.1 341	78 149	78 207	58
MIB	55 25	157 59	28.3 267	14.6 280	44.5 281	17.1 291	81.3 314	27.2 343	77 301	78 065	129
WGC2C	57 27	150 30	29.8 256	15.5 271	47.1 273	20.3 271	98.4 295	32.2 325	76 070	76 160	90

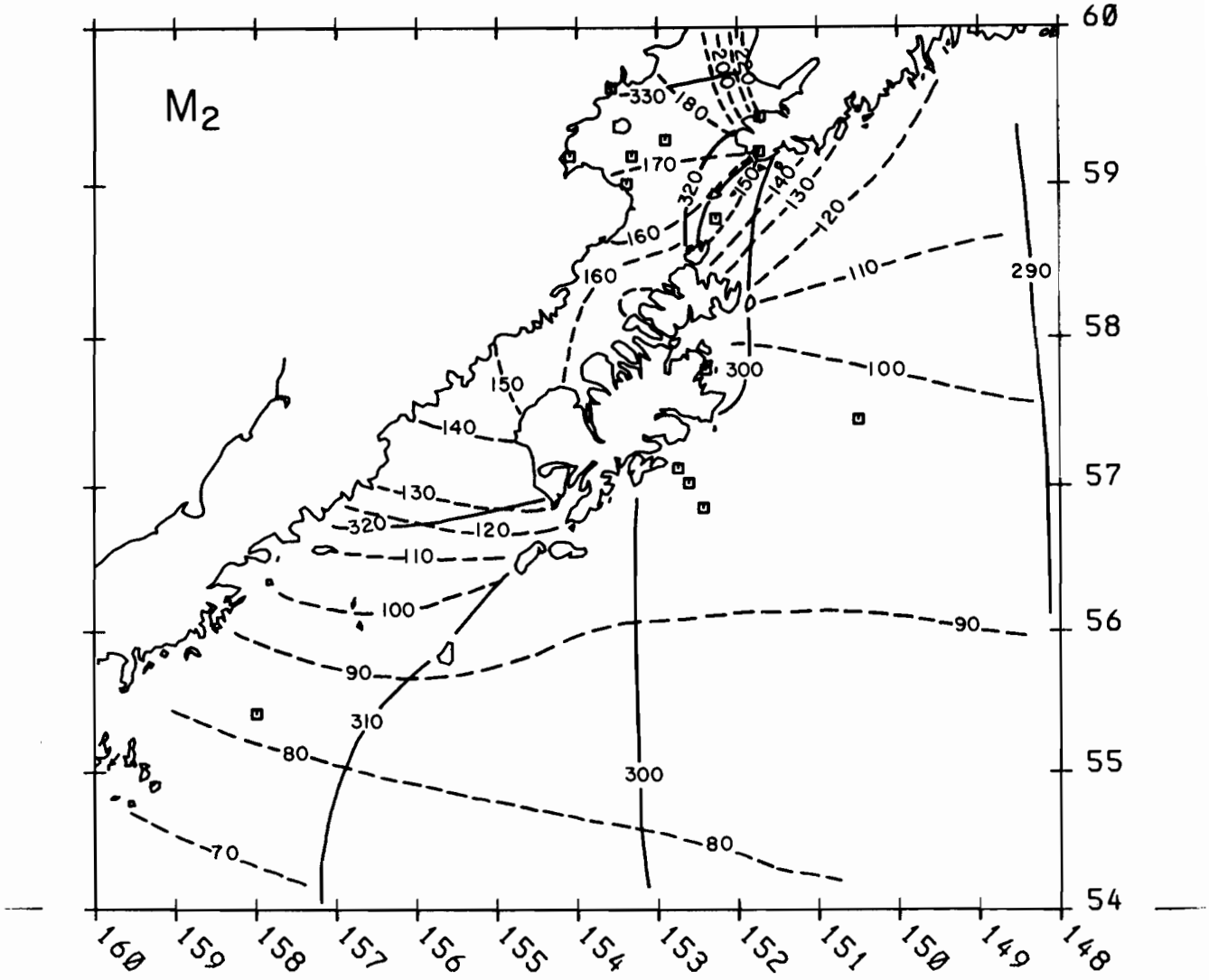

Figure 47. Cotidal chart for the M_2 tides. Solid lines are cophase lines referred to Greenwich. Dashes are coamplitude in cm.

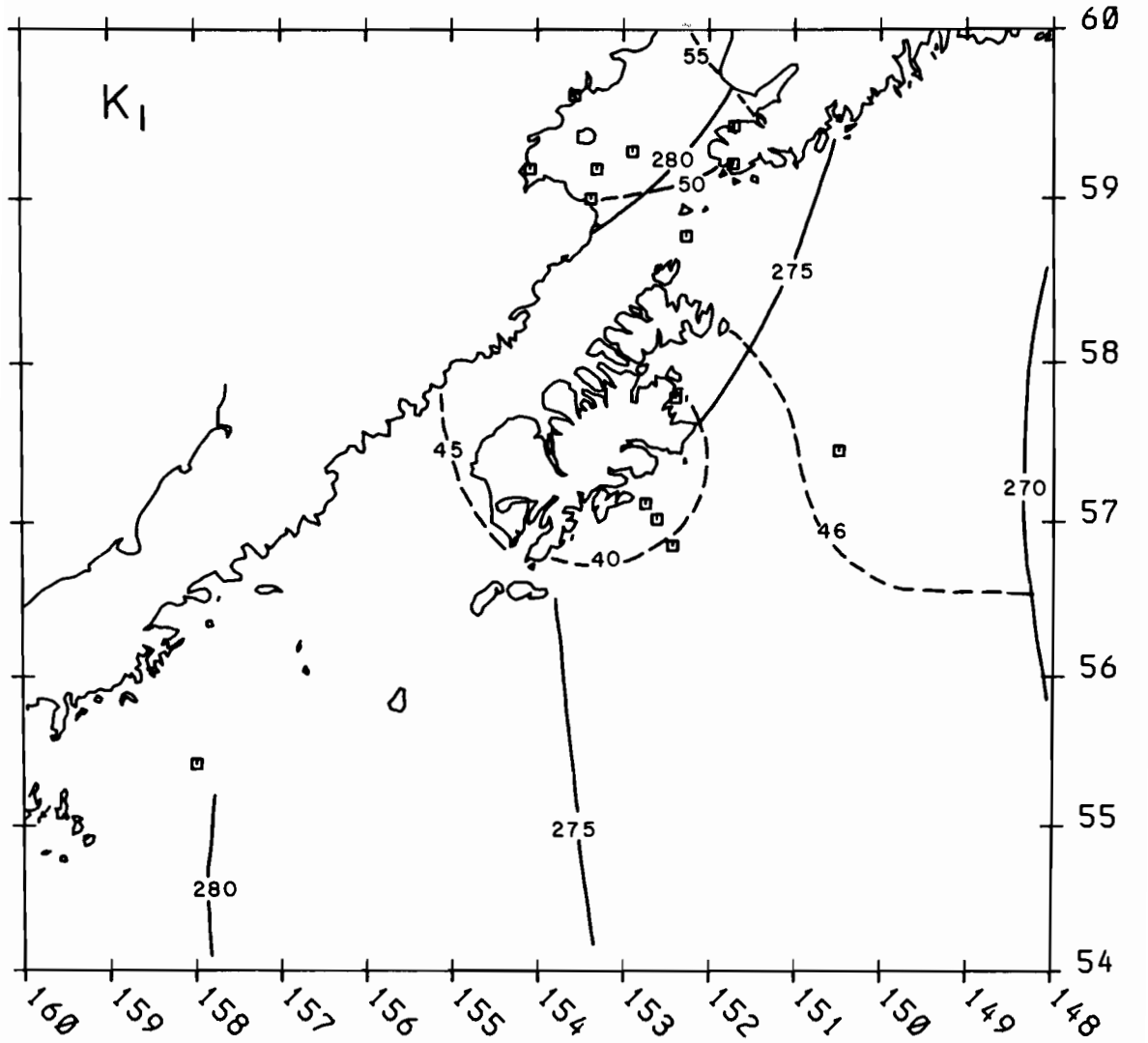

Figure 48. Cotidal chart for the K_1 tides. Solid lines are cophase lines referred to Greenwich. Dashes are coamplitude in cm.

1972). M_2 amplitudes increase from 154 cm at C9 in Stevenson Entrance to 179 cm at C4 in lower Cook Inlet to near 400 cm in the upper Inlet. The K_1 amplitudes are much more uniform in the western Gulf area, ranging from 40 to 50 cm, with somewhat higher values in Cook Inlet.

Tide type may be defined by the ratio of the sums of the amplitudes of K_1 and O_1 to M_2 and S_2:

$$F = \frac{K_1 + O_2}{M_2 + S_2} \quad .$$

F values of 0.25 to 1.5 denote mixed, predominantly semidiurnal tides which are found throughout the Gulf of Alaska region. This type of tide has two high and two low waters per day, but with pronounced inequalities in the high and/or low waters. In the western Gulf, F varies typically from 0.5 to 0.7, with lower values in Cook Inlet where the semidiurnal tide is predominant.

The average spring tide range, defined as $2.1(M_2 + S_2)$, decreases from about 3 m near Middleton Island to 2.5 m near Mitrofania Island, but increases to 5 m and higher in Cook Inlet.

Figure 49 is a plot of the observed bottom pressure for the month of November 1977 at station K9, which is typical of the outer shelf region. The mixed, predominantly semidiurnal tide is evident. Note the large range (3.8 m) observed on the 12th and 13th. This occurred when the new moon, lunar perigee, and extreme lunar declination approximately coincided.

The east and north components of current were analysed for tidal constituents using the response method. Predicted tidal heights from station K9 formed the reference series. The component constituents were then combined in an ellipse representation.

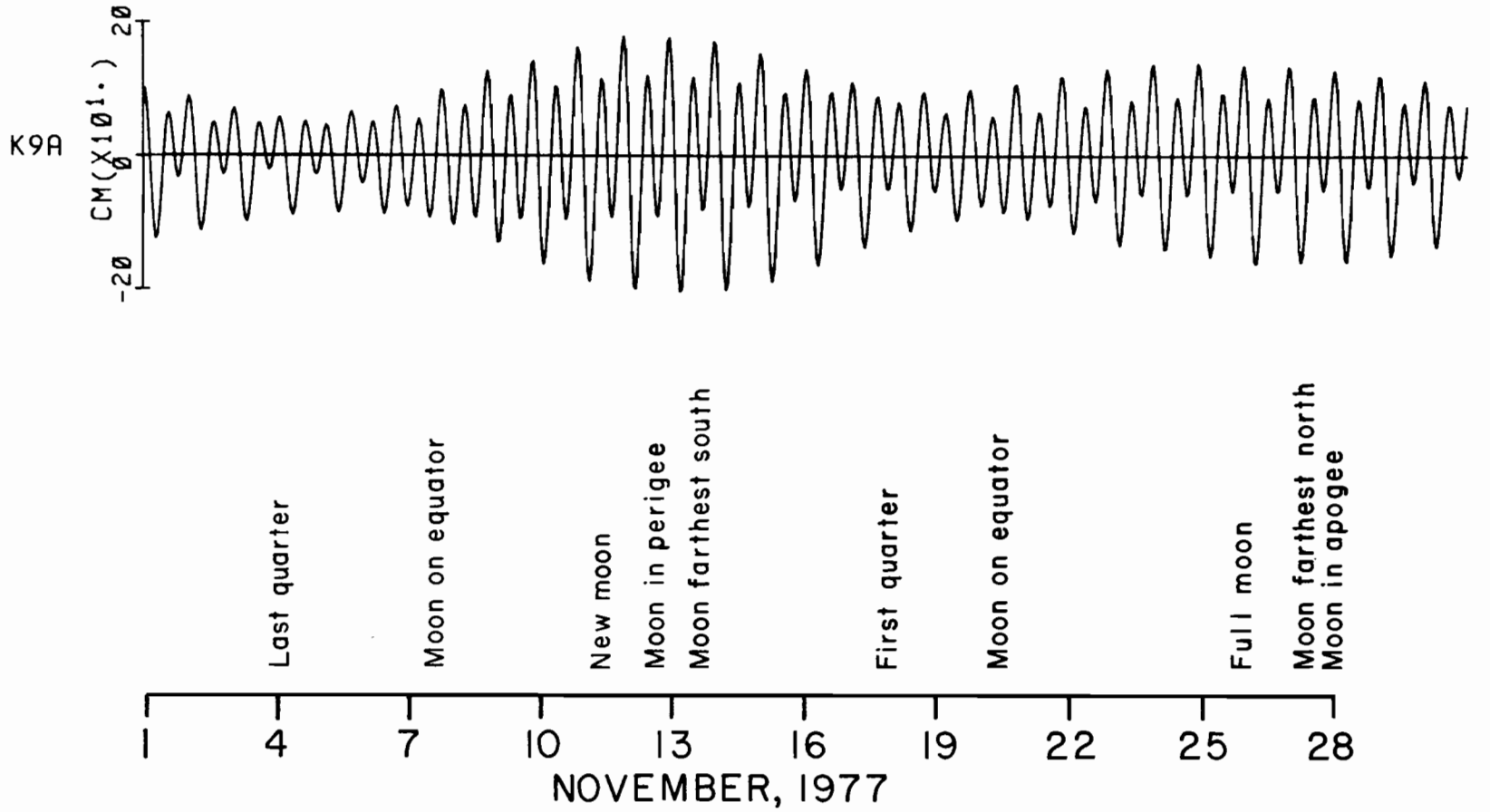

Figure 49. Observed bottom pressure at station K9 for November 1977. Station location is indicated on Figure 9.

In order to minimize possible effects of wave-induced mooring noise, records from summer are presented where possible. However, rotor pumping is not thought to be significant, as discussed in Section 3.1. The results are presented in Table 4. Tidal current ellipses for the M_2 and K_1 constituents are presented in Figures 50 and 51.

The M_2 ellipses show a great deal of spatial variability. Large M_2 tidal currents are found over North Albatross Bank, in Kennedy and Stevenson Entrances and southwest of Kodiak Island. M_2 tidal currents are particularly large in eastern lower Cook Inlet and in upper Cook Inlet. Currents are smaller in central and western lower Cook Inlet, although no further evidence was found of the extremely low tidal currents found at one station in central lower Cook Inlet by Muench et al. (1978). Unusually small M_2 currents are found over Middle Albatross Bank and in northern Shelikof Strait. The small currents over Middle Albatross Bank are evidently the result of Kodiak Island acting as a barrier to the incident tide wave, as the cophase lines roughly parallel the bathymetry there. In northern Shelikof Strait an antinode exists, where the tide wave entering Cook Inlet around the north end of Afognak Island meets the tide wave which has arrived from around the south end of Kodiak Island. The point of meeting, where no M_2 current should exist, is somewhere near station C10. The tidal current there is extremely weak and variable. The semidiurnal tide has standing wave characteristics in Shelikof Strait and over Albatross Bank, while it is more progressive across Portlock Bank and in the entrances to Cook Inlet.

The diurnal K_1 tide exhibits a more uniform speed distribution than M_2. Speeds are very low in Shelikof Strait because, as in the case of the M_2 tide, the waves coming around Kodiak and Afognak islands meet in Shelikof Strait and form an antinode. There is little decrease in the diurnal tidal current

TABLE 4

Tidal current components for four major species derived from current data using the Munk-Cartwright Response method (Munk and Cartwright, 1966) and predicted tidal heights from station K9 as the reference series.

Station	Bottom Depth (m)	Meter Depth (m)	Latitude		Longitude		Start Date (YR/JD)		O_1 Major H	O_1 Major G	O_1 Minor D	O_1 Minor H	O_1 R	K_1 Major H	K_1 Major G	K_1 Minor D	K_1 Minor H	K_1 R	S_2 Major H	S_2 Major G	S_2 Minor D	S_2 Minor H	S_2 R	M_2 Major H	M_2 Major G	M_2 Minor D	M_2 Minor H	M_2 R	Record Length (Days)
K1A	228	100	57	45	154	44	76	290	1.2	239	44	0.3	C	3.0	221	51	0	A	5.7	277	49	.1	A	14.9	239	51	.3	C	163
K2A	164	20	58	37	153	05	76	290	2.0	222	30	0.1	A	3.7	272	3	.3	C	3.8	199	201	2.6	C	11.8	195	218	5.3	C	163
K5A	95	20	56	33	152	39	76	292	11.6	92	217	5.0	C	18.4	121	223	9.5	C	4.7	246	327	2.5	C	14.1	210	333	7.8	C	158
K6B	82	32	57	14	152	23	78	141	10.2	57	234	4.3	C	17.9	87	239	7.9	C	3.3	350	40	1.9	C	7.9	329	47	6.3	C	138
K7B	84	29	57	06	152	13	78	141	10.5	43	219	4.6	C	16.9	B1	227	7.8	C	2.9	14	50	2.6	C	8.0	284	344	6.6	C	136
K8B	155	30	57	07	152	43	78	141	5.2	71	210	0.4	A	7.7	91	223	1.3	A	1.4	311	340	1.3	C	3.5	256	330	2.5	C	136
K9A	157	25	57	01	152	37	77	292	6.7	69	218	0.8	A	13.3	93	224	1.3	A	1.9	284	323	1.3	C	4.5	236	327	2.2	C	141
K10B	153	24	56	50	152	24	7B	141	6.4	68	224	1.5	C	11.6	98	226	4.2	C	1.6	335	320	1.1	C	3.7	264	320	1.5	C	136
K11B	83	25	56	02	155	06	7B	142	6.8	177	308	.1	A	9.2	206	303	.9	A	20.6	238	329	12.5	C	59.9	208	327	35.6	C	68
K13B	115	2B	56	24	156	49	78	142	2.7	155	62	.1	C	4.8	175	62	.2	C	10.4	287	38	2.9	C	24.3	247	41	5.6	C	138
WGC2C	185	24	57	27	150	30	76	070	4.6	150	322	3.B	C	7.7	189	340	6.5	C	5.9	309	304	2.2	C	16.2	289	311	5.6	C	90
WGC2D	93	20	57	34	150	49	76	160	10.4	226	44	7.2	C	16.2	236	34	12.3	C	11.9	298	328	7.3	C	32.4	265	324	22.3	C	132
WGC3D	112	20	55	12	156	57	77	119	3.5	139	24	1.5	C	5.8	178	15	4.2	C	13.8	280	337	8.1	C	36.8	243	341	25.3	C	132
C1B	40	18	59	11	153	19	78	148	3.6	237	34	3.4	C	6.5	229	323	4.8	C	13.6	294	313	5.9	C	33.2	261	306	19.1	C	87
C4A	84	19	59	17	152	55	77	280	6.3	222	14	2.3	C	9.7	242	4	3.7	C	16.8	330	355	6.2	C	46.3	302	357	18.9	C	160
C5A	128	20	59	10	152	56	77	280	3.9	192	355	0.3	A	5.4	222	344	0.5	A	10.2	326	338	0.9	C	28.0	297	338	4.5	C	160
C6B	77	26	59	19	152	38	78	148	6.9	199	8	2.8	C	11.4	213	359	3.7	C	22.7	315	358	7.3	C	57.3	287	356	19.5	C	143
C7B	68	17	59	18	152	10	78	148	8.9	161	358	2.6	C	15.9	184	358	2.5	C	36.8	299	358	4.8	C	98.0	269	357	17.4	C	142
C8B	190	64	59	02	152	03	78	149	8.7	179	301	3.3	A	13.1	207	302	3.7	A	28.0	307	300	2.5	C	70.0	278	295	5.8	C	83
C9B	124	66	58	47	152	16	78	149	10.0	191	293	2.5	C	15.4	205	296	1.9	C	27.2	298	295	1.5	C	70.5	268	291	9.6	C	139
C10B	175	25	58	30	153	12	78	148	2.1	265	58	0.3	A	1.7	307	35	0.1	A	3.3	48	25	1.7	C	8.3	4	35	3.4	C	134
C12A	50	20	59	32	152	14	78	148	9.3	201	9	1.1	C	15.1	212	6	2.0	C	29.8	319	7	0.4	C	79.7	294	6	4.4	C	81
C13A	68	26	59	28	152	41	78	14B	9.5	222	23	4.2	C	14.3	235	22	4.5	C	26.5	335	16	9.8	C	74.1	308	13	28.0	C	141
M2	110	50	55	25	157	59	77	301	4.2	179	25	2.2	C	6.9	213	35	3.8	C	6.1	298	5	2.9	C	16.3	263	358	8.4	C	129
M4	118	70	55	46	157	31	77	301	3.9	172	35	1.2	C	5.8	196	33	1.7	C	7.4	295	16	2.6	C	19.6	260	15	7.6	C	129

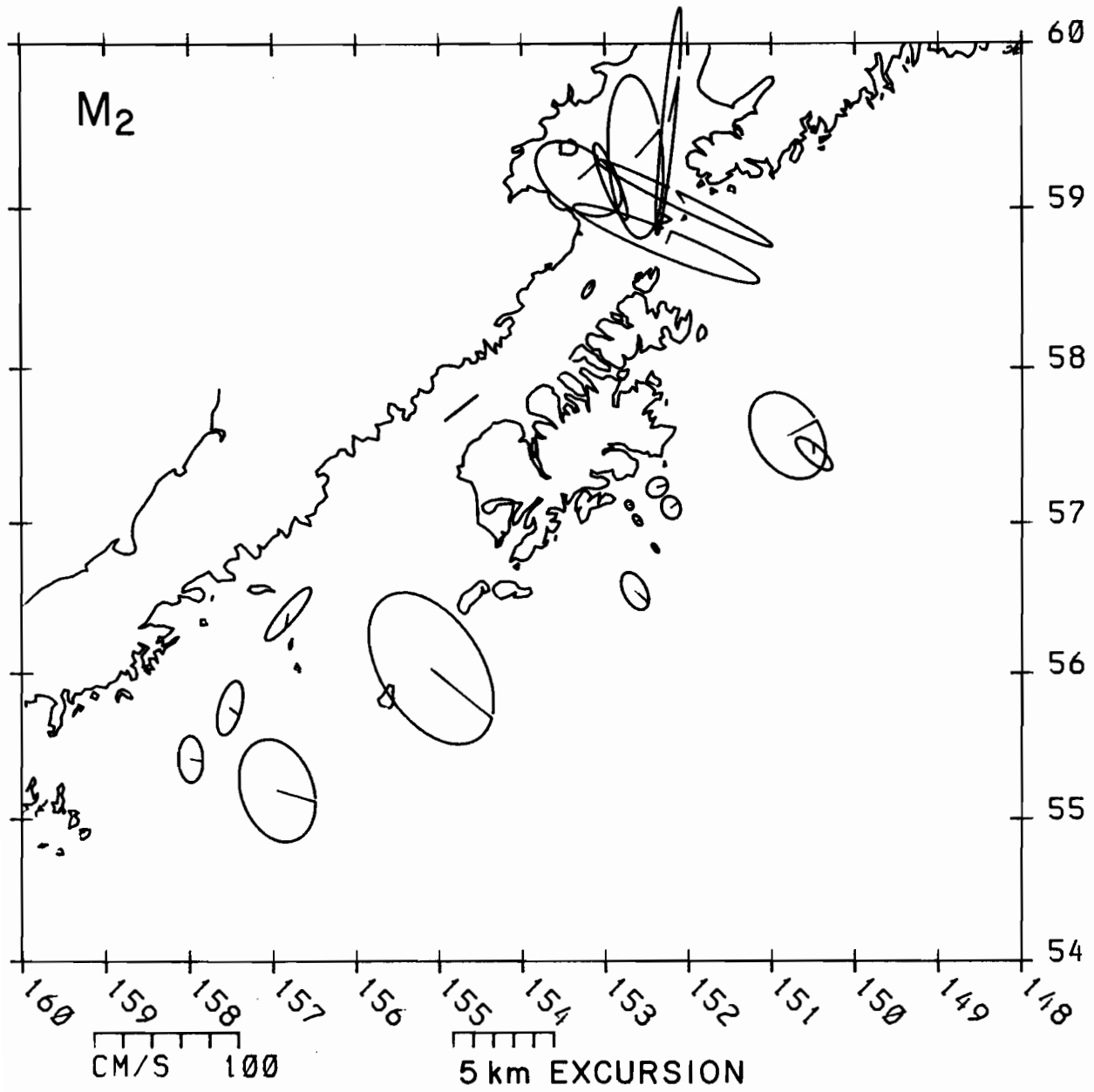

Figure 50. M_2 current ellipses for selected stations in the northwest Gulf of Alaska. Ellipses are centered at station locations; lines radiating from the centers indicate constituent current vectors when the M_2 Greenwich equilibrium phase angle is 0°.

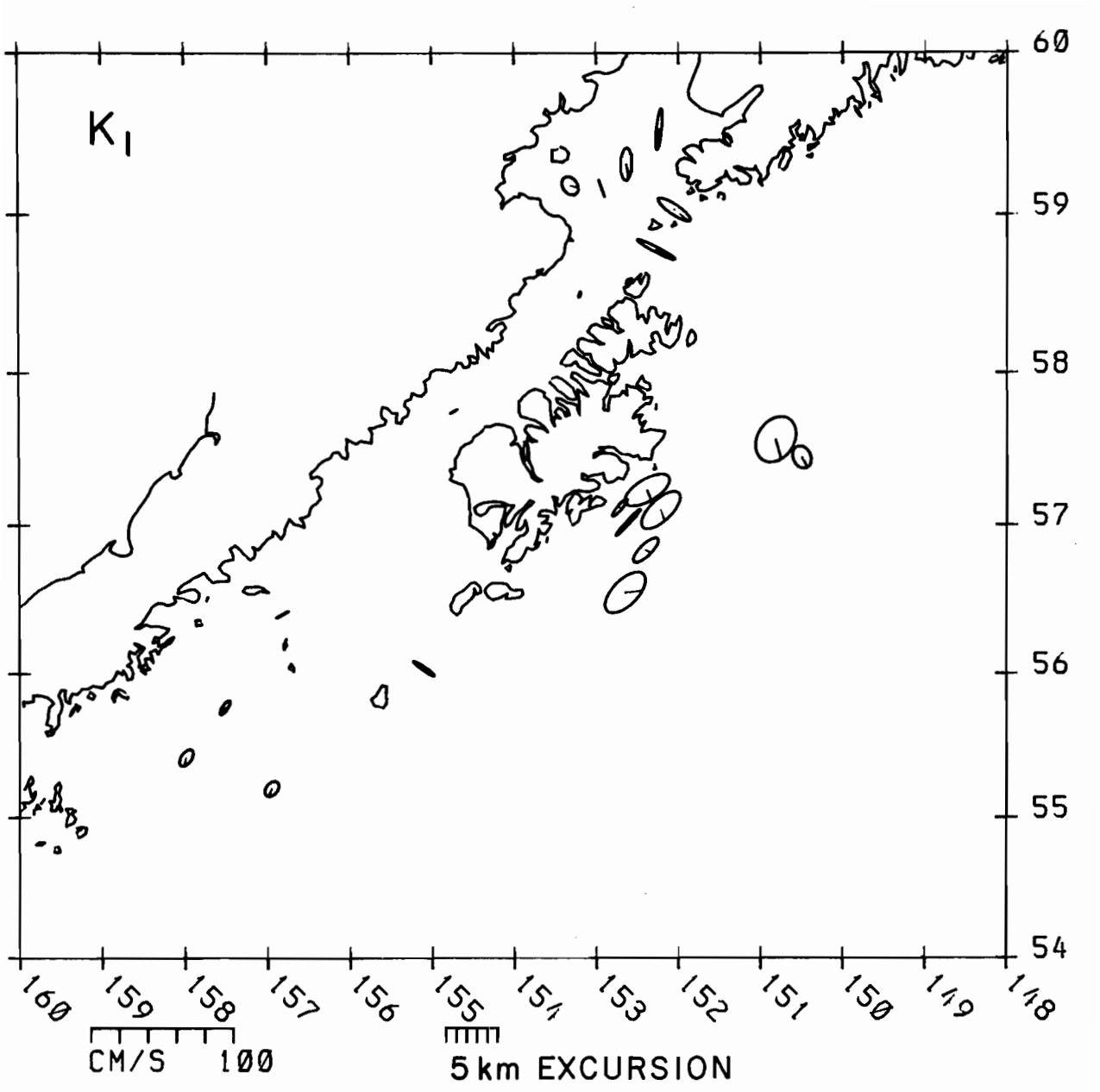

Figure 51. K_1 current ellipses for selected stations in the northwest Gulf of Alaska. Ellipses are centered at station locations; lines radiating from the centers indicate constituent current vectors when the K_1 Greenwich equilibrium phase angle is 0°.

at Middle Albatross Bank, which results in predominantly diurnal tidal currents (F>1.5). Elsewhere the currents are mixed predominantly semidiurnal or regular semidiurnal (F<.25).

In assessing the environmental impact of pollutants, the tidal excursion is important in relation to the proximity of potential impact areas. The tidal excursion in kilometers, over one-half of a tidal period (the flood tide for instance), is:

$$H\int_{o}^{\pi}\cos\sigma t dt = H\frac{T}{\pi}$$

where H is the amplitude, σ is frequency and T is period. For the semidiurnal tide this is approximately 0.14H (H in cm sec^{-1}, and excursion in km). Thus the mean spring tide excursion, where H = 1.05 (M_2 + S_2), is 20 km at C7 in eastern lower Cook Inlet, 15 km at C8 in Stevenson Entrance, 12 km at K11 southwest of Kodiak Island, and only 1.5 km at C10 in northern Shelikof Strait. At Middle Albatross Bank, where the currents are predominantly diurnal, the excursion is .29H, so during extreme lunar declination when H = K_1 + O_1, the excursion over one-half of a diurnal cycle at K7 is about 8 km.

3.4 Current Energy Partition With Frequency

In the following section, we present speed and horizontal kinetic energy (HKE) characteristics from current records collected during the bank-trough experiment (Tables 5 and 6), from North Albatross Bank (Table 7) and from the lower Cook Inlet/Shelikof Strait experiment (Table 6). Coastline and shelf-break orientation are used to define positive alongshelf and cross-shelf as 225°T and 315°T for all records from the bank-trough, north Albatross Bank (WGC series) and C10, 300°T and 030°T for C8B and C9B; and 090°T and 000°T for the lower Cook Inlet records (C3A and 3B and C4A and 4B). Velocities from 35-h filtered records were decomposed along these axes and are presented as speeds. Variance along an axis was used to determine standard deviation as well as subtidal kinetic energy. The 2.9-h filtered data were used to estimate kinetic energy in tidal frequency bands. We note that the latter estimates are averages over several bands, and as such include energy from sources other than tides. The specific tidal frequences do not indicate seasonal trends, as noted also in Section 3.3. The following equations define our parameters:

$$\text{Kinetic energy of the mean } (\overline{KE}) = \tfrac{1}{2}(\bar{u})^2 + \tfrac{1}{2}(\bar{v})^2$$

where the bar represents mean axis speed;

$$\text{Kinetic energy of subtidal flow } (KE') = \tfrac{1}{2}\sigma_u \text{ or } \tfrac{1}{2}\sigma_v$$

where σ represent variance along each axis.

Moorings WGC2A to 2C represent conditions on North Albatross Bank (Table 7). These moorings were deployed at the shelf-break at a depth of approximately 190 m and the series WGC2D to 2F were deployed approximately 25 km shoreward in about 85 m of water. This shoreward shift in mooring location resulted in a substantial change in flow characteristics and the distribution of HKE. At the shelf-break, alongshelf $\overline{KE}$ was dominant. At the shoaler location, flow retained some tendency to be alongshelf, however, the dominant energy was

TABLE 5

Current statistics in winter for the bank-trough region southeast of Kodiak Island, and mean alongshelf and cross-shelf wind stress for the current observation period. Mooring locations are indicated on Figure 9.

Mooring (meter depth)	Observed Speed (cm/s)		Horizontal Kinetic Energy Distribution (cm^2/s^2)					
			Alongshelf			Cross-Shelf		
	Alongshelf	Cross-shelf	Mean	Subtidal	Tidal	Mean	Subtidal	Tidal
BANK								
K6A (23m)	12.3±11.9	19.1±11.2	75.7	70.2	171.5	186.3	62.3	46.1
(65m)	10.6± 8.0	11.4± 6.4	56.2	32.0	88.5	64.8	20.7	17.4
K7A (28m)	-4.1± 8.4	10.7± 9.2	8.4	35.0	173.5	57.2	42.7	62.5
(70m)	-1.5± 4.6	8.0± 5.6	2.3	10.6	76.9	44.0	15.8	25.2
TROUGH								
K8A (25m)	24.3±12.9	-10.1± 7.2	295.3	82.7	35.5	51.0	26.4	20.8
(67m)	20.9±10.1	- 8.3± 6.3	218.4	50.8	31.2	34.5	20.1	9.9
(140m)*	10.1± 7.3	- 6.4± 5.5	51.0	26.4	18.3	20.5	15.2	5.1
K9A (25m)	4.6±10.4	- 0.6± 7.8	10.6	53.8	68.3	0.2	30.1	17.7
(148m)	0.8± 4.7	2.5± 6.2	0.3	11.0	21.4	3.1	18.5	15.1
K10A (25m)	-0.8± 9.4	8.2± 8.8	0.3	44.0	74.1	33.6	39.0	25.8
(144m)	-1.7± 4.1	5.4± 6.8	1.5	8.4	24.5	14.8	22.9	13.2
	Wind Stress ($dynes/cm^2$)							
EB46008	0.76±1.9	0.61±2.0						

*All records 133 days except K8A (140m) which was 66 days. Observation period began in mid-October 1977.

TABLE 6

Current statistics in summer for the bank-trough region southeast of Kodiak Island, and mean alongshelf and cross-shelf wind stress for the current observation period. Mooring locations are indicated on Figure 9.

Mooring (meter depth)	Observed Speed (cm/s)		Horizontal Kinetic Energy Distribution (cm^2/s^2)					
			Alongshelf			Cross-Shelf		
	Alongshelf	Cross-shelf	Mean	Subtidal	Tidal	Mean	Subtidal	Tidal
BANK								
K6B (32m)	9.6±3.0	12.6±4.8	45.9	17.6	120.2	78.9	11.4	40.3
(72m)	6.6±3.4	5.2±2.6	21.6	1.9	63.1	13.3	3.4	18.5
K7B (29m)	-0.8±4.5	9.0±5.3	0.4	9.9	113.2	40.2	14.0	44.9
TROUGH								
K8B (30m)	17.6±7.1	-2.9±3.3	154.9	25.0	25.3	4.2	5.3	10.4
(75m)	10.8±4.5	-0.9±3.5	58.5	2.9	21.9	0.4	0.2	10.5
K9B (13m)	4.9±6.3	-0.8±8.1	11.9	19.7	81.4	0.3	32.4	43.5
(58m)	3.5±6.4	2.4±7.5	6.1	20.2	76.1	2.8	27.8	24.7
(142m)	1.5±2.4	3.7±3.1	1.1	2.8	8.8	6.9	4.8	15.8
K10B (24m)	2.1±4.6	4.3±4.9	2.2	10.4	47.9	9.1	12.1	16.2
(69m)	0.8±4.4	5.7±5.5	0.3	9.6	44.6	16.0	15.2	23.4
(149m)	-2.5±2.3	5.8±3.6	3.2	2.7	13.5	16.6	6.5	12.3
	Wind Stress ($dynes/cm^2$)							
EB46008	-0.18±0.5	0.04±0.4						

*All records are longer than 125 days, and commenced in late May 1978.

TABLE 7

Selected winter and summer current statistics from the lower Cook Inlet region and from the banks southeast of Kodiak Island. Mooring locations are indicated on Figures 7 and 8.

Mooring (meter depth) Record Length(d):Start	Observed Speed (cm/s) Alongshelf	Cross-shelf	Distribution of HKE (cm^2/s^2) Alongshelf Mean	Subtidal	Tidal	Cross-Shelf Mean	Subtidal	Tidal
NORTH ALBATROSS BANK								
WGC-2A (100m) 66:75265	25.7± 6.5	-0.40±2.9	330.30	21.0	39.1	0.1	4.3	84.5
WGC-2C (24m) 90:76070	21.8±12.7	0.70±5.6	237.60	80.7	116.1	0.3	15.8	80.5
63:76070 (104m)	24.4± 7.9	4.30±3.6	297.70	21.9	31.7	9.4	6.4	74.1
WGC-2D (20m)	3.0± 4.6	1.10±3.4	4.60	10.4	244.9	0.6	5.7	378.5
133:76160 (80m)	0.9± 2.1	-0.90±1.7	0.30	2.1	90.9	0.3	1.4	136.0
WGC-2E (20m) 156:76293	2.2± 9.7	0.60±6.6	2.50	47.5	303.0	0.2	21.6	478.5
WGC-2F (20m)	4.7± 5.5	-0.40±3.9	10.90	15.0	265.5	0.1	7.6	401.0
167:77084 (80m)	1.9± 2.8	-2.00±2.1	1.90	3.8	103.0	2.0	2.2	149.9
LOWER COOK INLET AND SHELIKOF STRAIT								
C-10 (65m) 151:77278	23.8±17.3	1.90±8.4	283.20	149.4	19.6	1.8	35.3	5.2
C-10B (70) 133:78148	11.9±11.0	-0.70±8.1	70.80	60.3	12.1	0.3	8.1	3.8
C-9B (66m) 133:78150	9.6±10.8	-0.40±4.9	46.10	58.9	1600.1	0.1	11.9	69.9
C-8B (63m) 133:78150	20.4±18.2	-4.70±8.2	208.10	165.8	1953.0	11.1	33.7	100.5
C-4 (65m) 150:77280	-1.3± 6.5	-0.70±6.3	0.90	21.2	40.9	0.3	19.8	373.4
C-4B (64m) 133:78150	0.5± 6.7	-1.20±5.4	0.02	16.3	32.8	0.8	16.1	348.0
C-3 (50m) 159:77280	-1.3± 4.2	-0.90±2.9	0.90	8.9	58.5	0.4	4.1	420.0
C-3B (50m) 93:78148	0.6± 4.1	-0.06±2.8	0.20	8.2	43.1	0.0	3.9	334.0

tidal. The alongshelf speeds were consistent during the observation periods of WGC2D and 2F, whereas during winter 1976-77, alongshelf flow was weaker and more variable. Over the bank, subtidal kinetic energy indicated a threefold variation between winter (WGC2E) and nonwinter records. We attribute this to increased meteorological forcing in winter.

Records from C8, 9, and 10 are representative of the Kenai Current (Table 7). Records from C10 and C10B indicate that during October 1977 to March 1978 (C10) both $\overline{KE}$ and KE' were substantially greater than during May to October 1978. This is consistent with our present understanding of coastal flow in the northwest Gulf of Alaska (Schumacher and Reed, 1980). A peak in baroclinic transport (and speed) occurred sometime in October-November; during this period, 7-day average flow down the axis of Shelikof Strait was observed to be as high as ~70 cm sec^{-1}. In December 1977 through February 1978, observed mean wind stress was ~1.2 dyne cm^{-2} in an alongshore direction. The resulting set-up and barotropic transport (and speed) resulted in 7-day average axial speeds in Shelikof Strait of 20 to 50 cm sec^{-1}. Winds from June-September 1978 did not contribute appreciably to transport, and the baroclinic field suggested transports 0.1 to 0.3 of those observed during peak freshwater addition in fall. Records from the entrances to Shelikof Strait (C8B and C9B) indicate that tidal frequencies dominated HKE. However, at lower frequencies and in a mean sense, there was a significant difference between the two entrances. $\overline{KE}$ was four times greater in Kennedy Entrance than in Stevenson Entrance. As suggested by Schumacher and Reed (1980), current records and hydrographic data indicate that the Kenai Current preferentially flows through Kennedy Entrance.

Within lower Cook Inlet proper (C3 and C4 series, Table 7), net flow was not significant in the total energy balance and tides dominated HKE

estimates. We note that subtidal frequencies at both of these locations indicate a less dramatic change from winter (October 1977-March 1978) to summer (May to October 1978) than was observed over the banks. Estimated energy due to subtidal frequencies increased by 25 to 30% in lower Cook Inlet and three- to four-fold over the banks. Orographic effects on the wind field over Lower Cook Inlet appear to diminish seasonal trends, whereas over the banks a strong seasonal change was observed.

The most striking feature of the velocity field is that seasonal differences are small in mean speed components and, in several cases, statistically insignificant. HKE in all three frequency bands is greater in winter, a combination of a more energetic regime or perhaps rotor wave-induced noise. Various authors (e.g., Mayer et al., 1979; Halpern and Pillsbury, 1976) have concluded that rotor pumping can significantly affect speeds recorded by Aanderaa current meters. In order to determine whether the western Gulf current meter data set might be significantly contaminated by such wave-induced noise, successive 29-day harmonic tide analyses were performed for data from the summer (June, July, August) and winter (December, January, February). The following table shows the mean M_2 and standard deviations for those stations which had both summer and winter data at the 20-m depth.

TABLE 8

	C4	C10	WGC2	KG	K7	K8	K10	K.11
Winter Mean	35.2	4.7	30.5	7.4	6.8	2.7	3.8	45.8
S.D.**	.6	.6	.9	.7	.7	.7	.3	.6
Summer Mean	33.3	5.9	29.5	7.4	7.4	2.7	2.4	49.1*
S.D.**	2.8	1.2	2.4	.5	.4	.7	1.0	.8
Winter-Summer	1.9	-1.2	1.0	0	-.6	0	1.4	-3.3

*June-mid July only available
**S.D. = standard deviation.

mean M_2 speeds were computed by

$$A_1 = \frac{U_i^2+V_i^2}{2}^{\frac{1}{2}}$$

where U_i is the major axis M_2 amplitude and V_i is the minor axis amplitude for time period i. Five successive analyses were done for each season, with a 14-day overlap between segments. The A_i's were then averaged to produce the seasonal averages shown in the table.

If it is presumed that wave energy is much greater during the winter (and the windstress values shown in Tables 3 and 4 indicate that it is), then these results suggest that wave-induced noise does not significantly affect the speeds recorded from these data sets, at least on a seasonal average. The difference between these results and those of previous studies probably results from the fact that the subsurface float in our studies was deep enough (usually greater than 20 m) to prevent significant contamination by wave noise.

Over Middle Albatross Bank, HKE was greater near-shore (K6) than over mid-bank (K7), and cross-shelf mean HKE dominated in both seasons (Tables 5-6). Over Kiliuda Trough, a similar pattern occurred; however, the along-shelf mean HKE was dominant. Seaward of K8, current records suggest a dramatic change in velocity-field characteristics. Both tidal and sub-tidal HKE were larger than mean HKE.

3.5 Wind Observations

Winds over the ocean can be computed from surface pressure maps in conjunction with a boundary layer model. In general, surface winds are weaker than and aligned to the left of the computed geostrophic wind. Researchers have applied this technique with various degrees of sophistication and success. Agreement between computed winds and measured winds from data buoys are generally good except near the coastline, where a variety of additional physical processes become significant. For example, air flow in Lower Cook Inlet is predominantly down-gradient, that is, at right angles to the left of the geostrophic wind.

In the region of Albatross Bank, east of Kodiak, we found measurements from a data buoy approximately 60 km offshore agreed with calculations. We conclude that coastal influence on winds is not seen that far offshore. Lower Cook Inlet winds were completely dominated by the surrounding mountains.

3.5.1 Orographic Control

We have examined data from buoys located off the northeast Gulf of Alaska coast (EB33, EB45, EB72), Kodiak Island (EB46008, formerly EB49), and lower Cook Inlet (EB46007, formerly EB39), and found that within 50-100 km from shore the winds begin to align with the coastal mountains. The size of the mountain range affects this distance. Within about 25 km of the coast, smaller scale features, such as drainage winds, are felt.

The east coast of Kodiak Island is dominated by mountainous estuaries. Wind measurements from Kodiak and Kiliuda Bay confirm the presence of strongly bimodal winds aligned with the estuary axes. In the winter, these winds are predominantly offshore. However, NDBO buoy EB46008, located 60 km offshore, showed little coastal effect; its measurements agreed quite well with surface winds which were computed by the Fleet Numerical Weather Central

facility. As the mountains of Kodiak are not particularly high, we expect their offshore effect to be correspondingly reduced; however, without other measurements we cannot determine the extent of reduction.

The wind field over lower Cook Inlet, on the other hand, is completely dominated by mountains. We have made a concentrated study of this region to better understand the processes active in such orographically controlled estuaries.

3.5.2 Lower Cook Inlet Meteorology

The mountainous borders of lower Cook Inlet form natural channels for the flow of air (Fig. 52). The major orographic axis extends from the Susitna Valley in upper Cook Inlet southward and into Shelikof Strait, and is oriented at about 30°T. This channel is bounded on the east by the Talkeetna and Kenai mountains and lesser ranges on Kodiak and Afognak islands. It is bounded on the west by the Alaska and Aleutian ranges. The only breaks in this mountainous barrier to air flow occur at Kennedy and Stephenson Entrances and at the Kamishak Gap, a region of relatively low elevation about 50 km wide between Lake Iliamna and Kamishak Bay.

Orographic Channelling. The prevalence of orographic channelling of winds in lower Cook Inlet is clearly seen in wind fabric diagrams (Davis and Ekern, 1977) constructed using data from environmental buoy EB-46007 (cf. Fig. 52 for buoy location). These diagrams are contoured plots indicating the relative concentrations of observations of wind speed and the direction from which the wind blows during a given month. The observations are 8-min means acquired once every 3 hours. Fabric diagrams for four representative months in 1978 are shown in Fig. 53. Lines have been drawn on the diagrams to indicate the directions of the four major orographic axes as seen from the

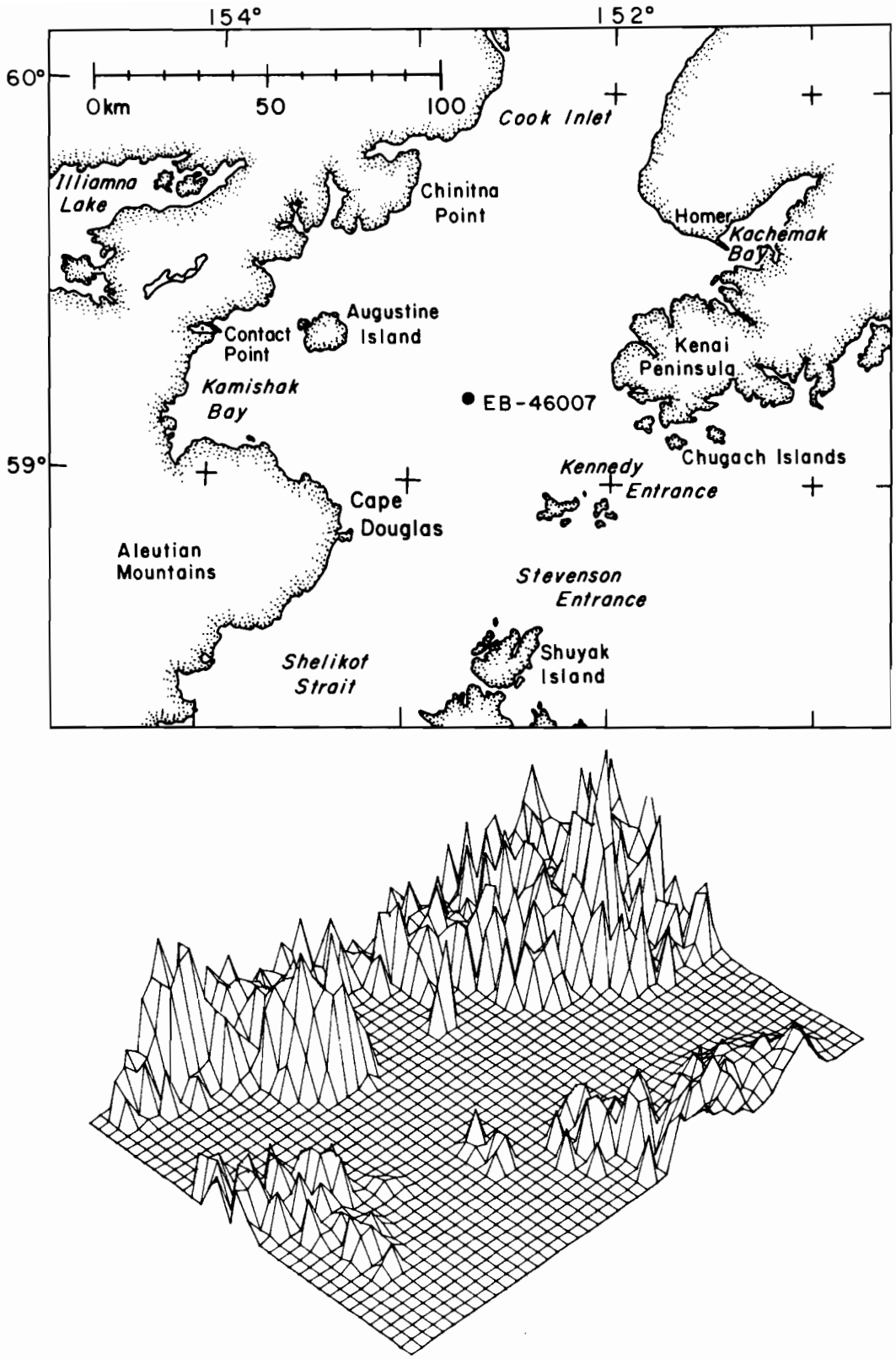

Figure 52. Geographical locations in the lower Cook Inlet region and (lower) a relief map of the same area. The black dot indicates the location of environmental buoy EB-46007.

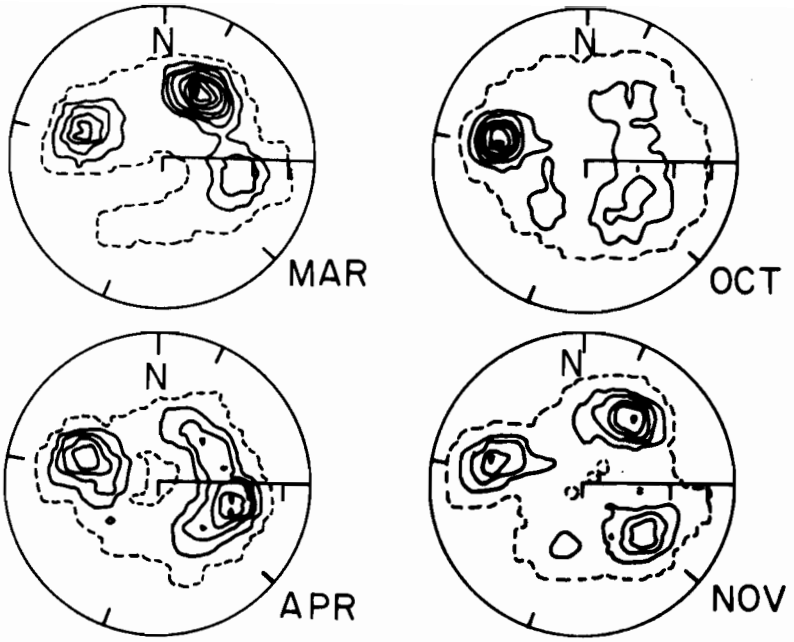

Figure 53. Wind fabric diagrams for EB-46007 in lower Cook Inlet for four months in 1978. The four tic marks on each circle represent the directions of the four channel axes: upper Cook Inlet; Kennedy and Stevenson entrances; Shelikof Strait; and the Kamishak Gap.

buoy. The contours are in intervals of 2% of the observations per percent of the plot area. In March winds were persistently from upper Cook Inlet and closely aligned with the Inlet axis. In April winds blew in both directions through the Kamishak Gap-Kennedy Entrance channel and to a lesser extent from Kachemak Bay and the upper Cook Inlet. In October, winds were almost exclusively from the Kamishak Gap; in November winds originated from all four of the intersecting channels. Little wind was observed from the northwest or southwest, due to the blocking action of the Alaskan and Aleutian ranges.

Though the 4 months that are shown exhibit orographic channeling particularly well, all data obtained show this channeling effect. Given the four major intersecting channels, it is possible to define a minimum of 16 possible flow patterns. Of these, the two which appear most likely to occur are those resulting from the synoptic scale pressure distribution and from interior drainage winds, especially from the Susitna Valley which enters upper Cook Inlet.

Pressure Gradient Forcing. The Geostrophic wind is given by

$$u_g = - \frac{1}{\rho f} \frac{\partial p}{\partial y}$$

$$v_g = \frac{1}{\rho f} \frac{\partial p}{\partial x}$$

where u_g and v_g are the east-west and north-south components of the geostrophic wind, ρ is the air density, f is the Coriolis parameter, and $\frac{\partial p}{\partial x}$ and $\frac{\partial p}{\partial y}$ are the east-west and north-south pressure gradients.

At least three stations are needed to establish the two-dimensional pressure gradient. If more stations are available a plane may be fitted to

the observations using multiple regression techniques. The equation

$$p = ax + by + c$$

is fit where x and y are the positions of each station. The pressure gradients are then

$$\frac{\partial p}{\partial x} = a \quad \text{and} \quad \frac{\partial p}{\partial y} = b$$

If curvature in the pressure field is judged significant, higher order equations may be used. The second order equation is

$$p = a_0 + a_1x + a_2y + a_3x^2 + a_4y^2 + a_5xy,$$

for which a minimum of six stations are required. However, for most applications many more than six stations are needed to adequately define the second order pressure field.

In this study we have used a first-order fit with only three stations: Anchorage, Kodiak, and King Salmon. We would have liked to have used Iliamna, but it reports irregularly and, in addition, a 2-mb bias was found in pressure readings reported for March-June 1978. It was felt that the three chosen stations were spaced around the lower Cook Inlet (Fig. 12) to give a reliable and representative network for determining the regional pressure gradient. There are undoubtedly small-scale gradients that are unresolved by such a widely spaced network. These three stations will also be inadequate when the pressure field is highly curved, for we are assuming that it is well represented by a plane.

The geostrophic wind was determined for 7 months in 1978 and 1979. The hourly pressure readings were filtered with a 3-h triangular filter and sampled every 3 hours. These pressures were then fit with a plane to determine the pressure gradients.

In Figure 54 the direction of the geostrophic wind is plotted against that of EB-46007 for the spring (March through June) and for the winter (November through January). Only points for which the geostrophic wind is

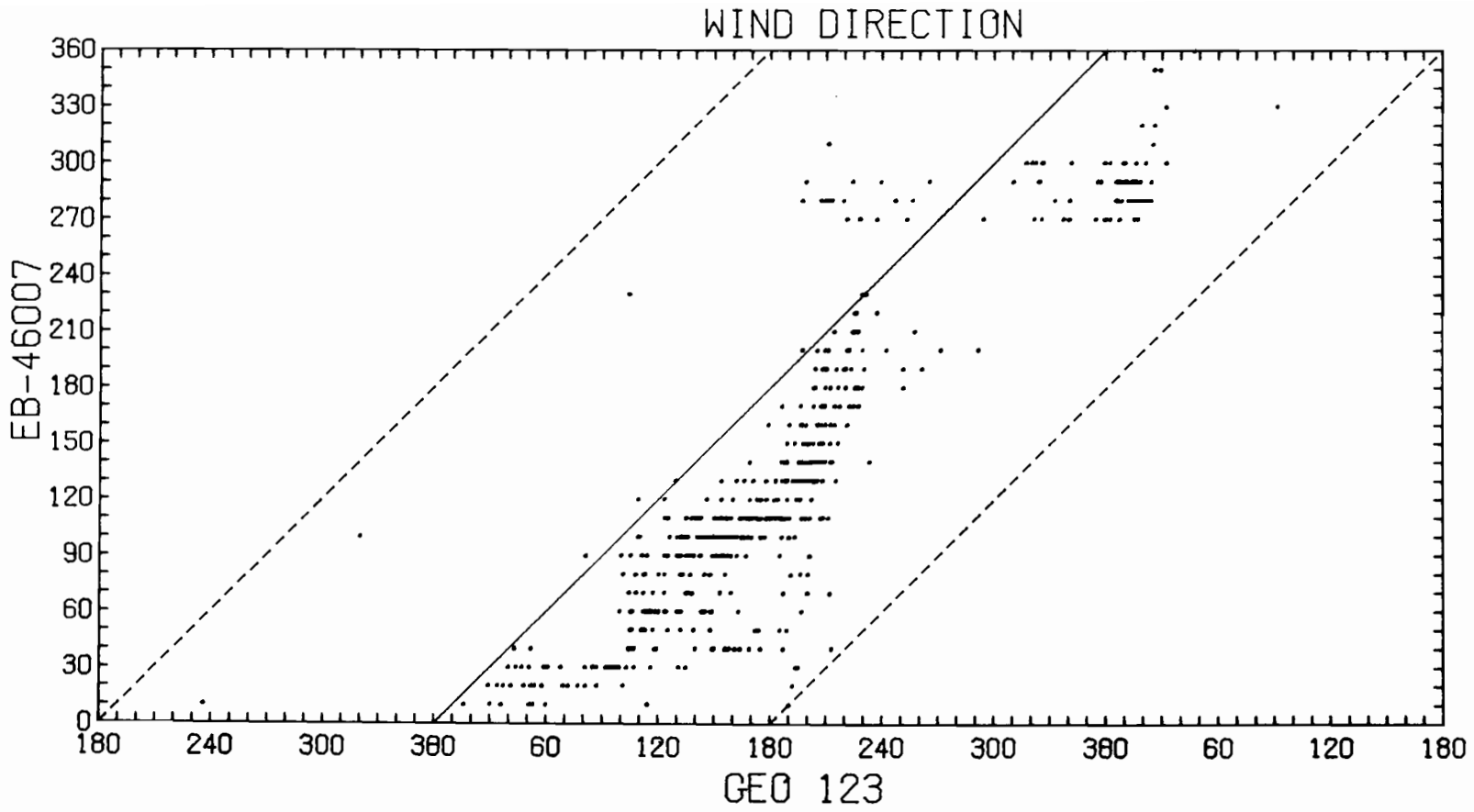

Figure 54. Wind direction at environmental buoy EB-46007 in lower Cook Inlet compared to direction of the geostrophic wind for cases where the geostrophic wind speed was greater than 5 m sec^{-1}.

greater than 5 m sec^{-1} are plotted. The solid line indicates winds which are from the same direction (i.e., the buoy winds are parallel to the isobars); points to the right of the line indicate a component of buoy winds down the pressure gradient, while those to the left indicate a countergradient component.

These figures show clearly the ambiguity often seen in the relation between geostrophic and surface winds in orographically dominated sites; a wide range of surface winds is observed for a given geostrophic wind. For example, with the geostrophic wind from 180° the observed buoy wind can come from virtually any direction. The apparent countergradient flow out of Kamishak Gap may be the result of poor estimation of the local pressure gradient from the three widely spaced stations. Alternately, the pressure field in the Bering Sea could drive air through the Iliamna Gap into lower Cook Inlet and against the pressure gradient there. We have not found that the regional pressure gradient is a good predictor of the local winds. It should be noted, however, that in virtually all cases when the geostrophic wind direction was from 270°-0° in the March-June period or from 240°-40° in the November-December period, westerlies from the Iliamna Gap occurred.

Drainage Winds. Given the presence of adjacent continental land masses whose interior regions are occupied during winter by cold dense air masses, we suspect that drainage or katabatic winds might play an important role in the local wind field in lower Cook Inlet. The magnitude of such winds is dependent upon the cold air reservoir, the external large-scale pressure field and local topographic focussing. These flows are generally colder than the surrounding air and therefore flow beneath the ambient air overlying the water. The distance offshore to which the flow persists depends

upon the water-air heat flux and upon the stability of the overlying air. By far the major winter wind feature in lower Cook Inlet is the drainage wind from the Susitna Valley (Fig. 53), which is supplied by a dominant inland high pressure region to the north.

On a smaller scale, drainage winds appear off virtually every glacier and river valley which enters lower Cook Inlet. An example of such a flow was observed in the vicinity of Cape Douglas (Fig. 55), with the wind originating from 2100-m Mt. Douglas and funneling out of a small valley. Width of both the valley mouth and the flow offshore was about 2 km. Vertical potential temperature profiles obtained within this flow and from nearby undisturbed air over northern Shelikof Strait showed similar structure above about 300 m (Fig. 56). The profile off Cape Douglas exhibited, however, a stable layer which was eroded by sea-air heat flux from the surface to a height of 200 m during its passage from the coastline to a point about 10 km offshore. Environmental buoy EB-46007, located about 40 km off this valley, did not reflect the presence of this flow. In general, the buoy data suggest that katabatic flow seldom, if ever, attains the central part of lower Cook Inlet.

Kachemak Bay, across the lower inlet from Cape Douglas, often exhibits drainage winds because several glaciers terminate at its head. At times, these drainage winds resulted in strong ENE winds at Homer, while winds observed at EB-46007 in the lower inlet were westerly. Shipboard observations suggest that the drainage winds in Kachemak Bay are confined to the southern portion of the bay mouth and seldom persist beyond about 20 km from the bay mouth.

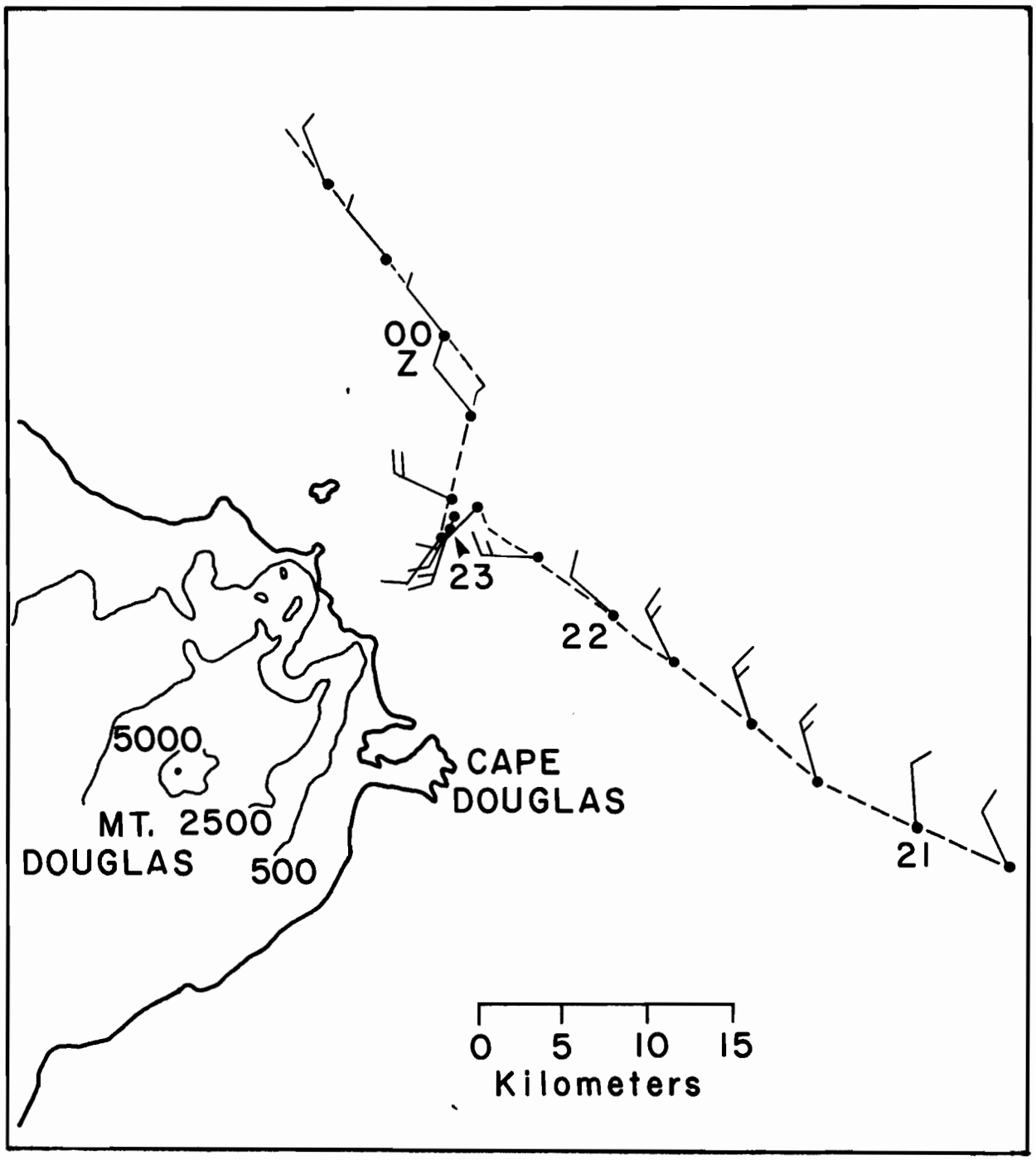

Figure 55. Observations of surface wind velocity in the vicinity of Cape Douglas, lower Cook Inlet, on 17-18 March 1978. Katabatic flow extended offshore from a mountain valley. Elevation contours are in feet above mean sea level.

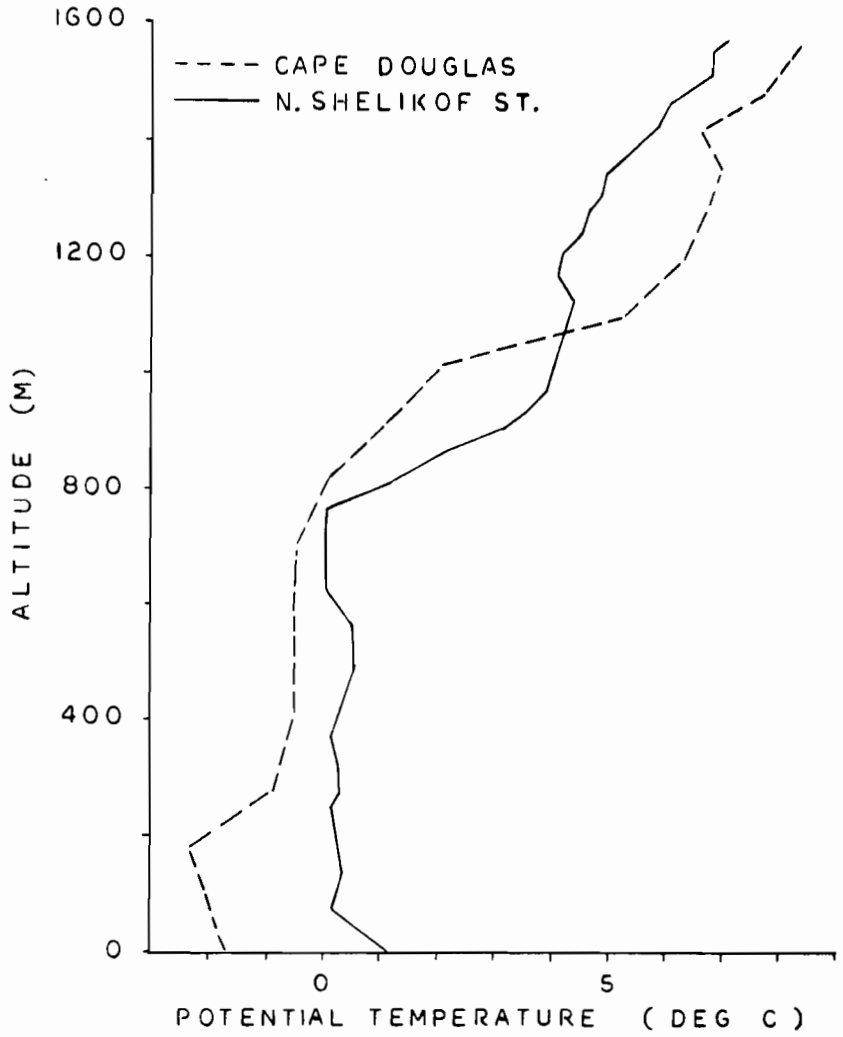

Figure 56. Comparison of vertical potential temperature profiles from airsonde ascents near Cape Douglas and over northeastern Shelikof Strait. A remnant katabatic layer was evident below about 300 m in the sounding from Cape Douglas.

Wake Effects. Given the large vertical relief of land masses surrounding lower Cook Inlet, we would a priori expect to see localized effects of certain of these masses on the air flow. An exceptional example is provided by Augustine Island, which presents a 1300-m high cone-shaped obstacle to local air flow at the eastern edge of Kamishak Bay (Fig. 52). Theoretical and laboratory studies of flow past a cylinder (Hinze, 1959; Batchelor, 1967) have shown that the imposed pressure and velocity distributions generate vortical flow in the lee of the cylinder. Flow on the lee side of an isolated mountain would be expected to show similar characteristics. This supposition was borne out by Scorer (1967), who found that wake effects were present and that the arc sector defining the wake within which lee waves are apparent may vary from 10°-70°. Amplitude of the lee wave disturbances decreases rapidly with increasing height and with distance downstream from the obstacle.

During a period of NNW winds in the lower Inlet, the free stream wind had speeds from 3 to 8 m sec^{-1} and directions from 320-020°T. Assuming a disturbed downstream arc sector of 70° and considering the directional range of the free stream winds, all observed winds to 03 GMT depicted on Figure 57 could be categorized as wake flow. No such confused flow was encountered prior to a station occupation at about 02 GMT some 4 km offshore. Here, in an hour's time and within an area of 2 km^2, wind direction was observed to vary over nearly 360°, suggesting the presence of vortical flow induced by the mountain.

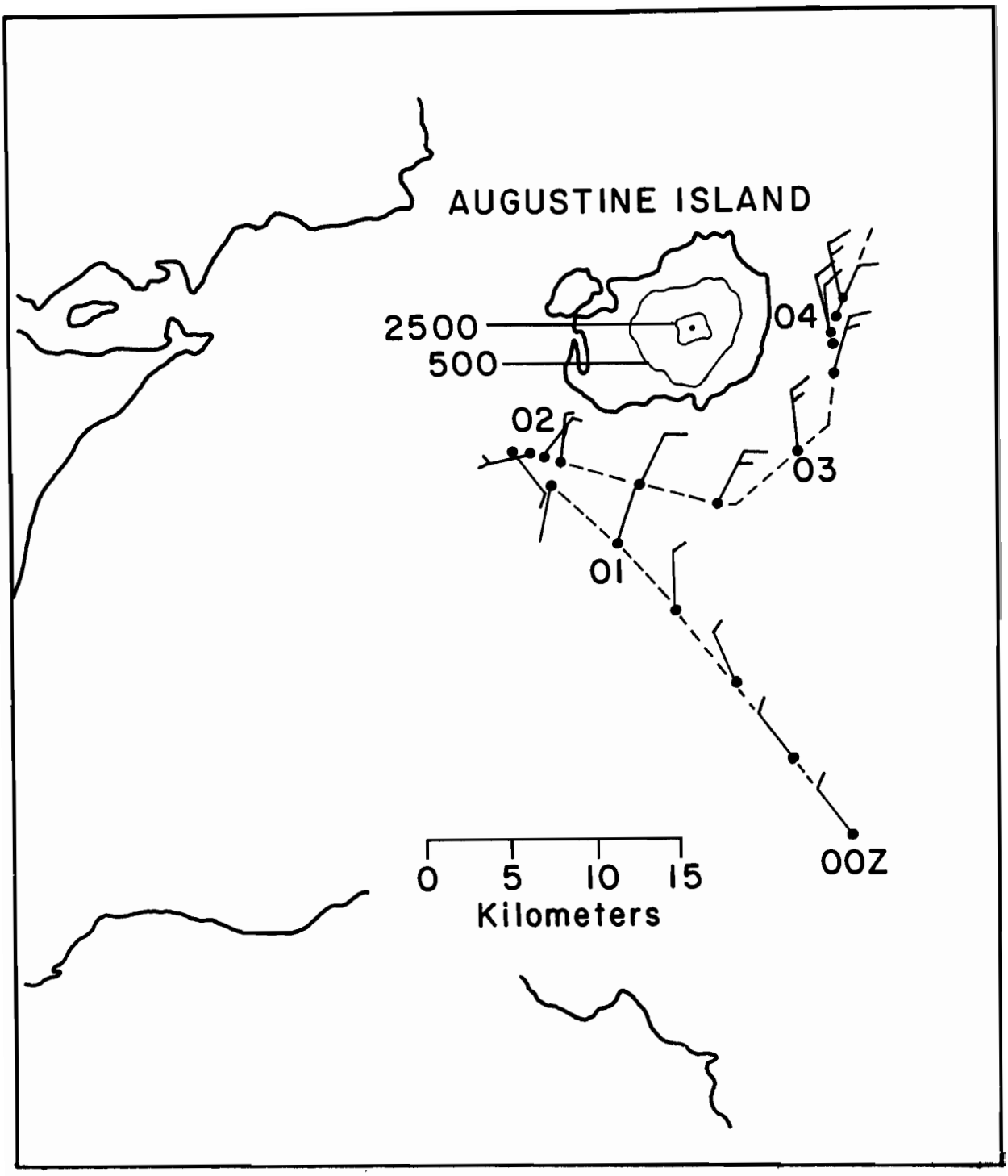

Figure 57. Observations of surface wind velocity in the vicinity of Augustine Island on 18 March 1978. Variable winds at about 02 Z suggest that vortical flow was present in the lee of Mt. Augustine. A quarter flag on the vector shaft designates wind speed below 1.5 m sec^{-1}.

Summary and Conclusion. Winds in lower Cook Inlet are orographically funneled through two perpendicularly oriented channels defined by upper Cook Inlet-Shelikof Strait and Kamishak Bay-Stevenson Entrance. Specific flow patterns appear in most cases to be triggered by the larger scale pressure gradient, though the relationship between geostrophic winds and observed winds is weak and poorly understood at present. Within 20 km of shore, drainage winds emanate from glacier and river valleys. These winds are nearly continuously occurring, but are quickly eroded over water by the sea-air heat exchange. On a yet smaller scale, vortical circulation has been observed in the lee of Augustine Island, a major, centrally located topographic feature in the lower Inlet.

In an effort to provide a more realistic wind input to oil spill trajectory models, we drew surface wind patterns for the lower Cook Inlet based on the weather types of Putnins (1966). Putnins determined 22 different generalized weather classifications for Alaska based on 18 yr of daily synoptic weather charts. For each type he reproduced a representative surface weather chart. For each weather chart, we drew a sketch of what our interpretation of the wind patterns in the lower Cook Inlet would be. This interpretation was based on the data we have analyzed and on our experience in the area. It was, of necessity, tentative and subjective.

The twenty-two wind patterns could be reduced reasonably to five. These five patterns, labeled I through V, are found in Figures 58-62. The wind speeds are indicated in m sec^{-1}. The major guiding principle in the formulation of these patterns is that the wind is predominantly channeled by the orography of the region. We have good evidence that this is true from EB-46007. We have also noted examples where this was not apparently the case, in which the winds seem to be passing across the Kenai Mountains.

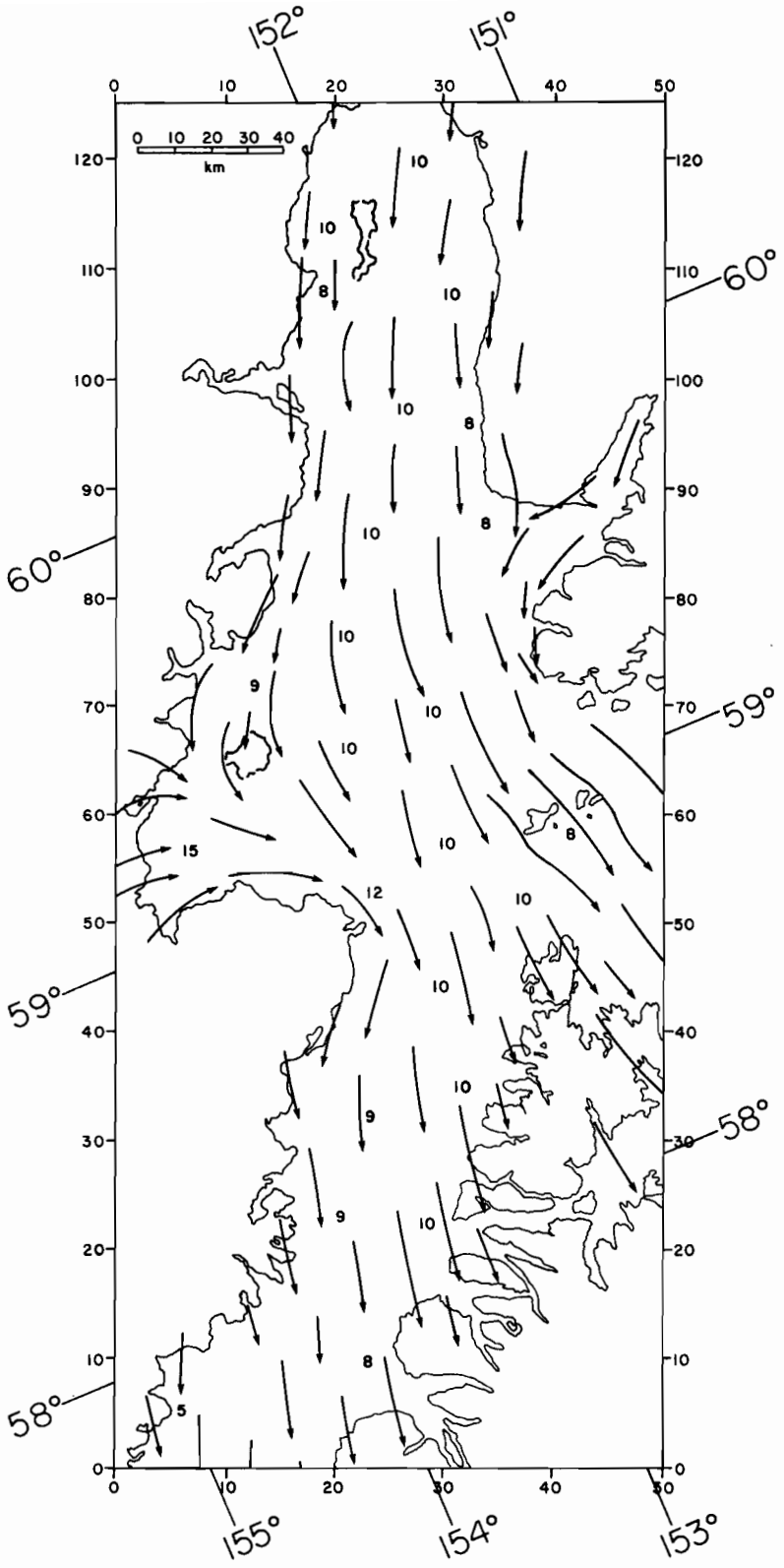

Figure 58. Map I of Putnins' wind type for lower Cook Inlet.

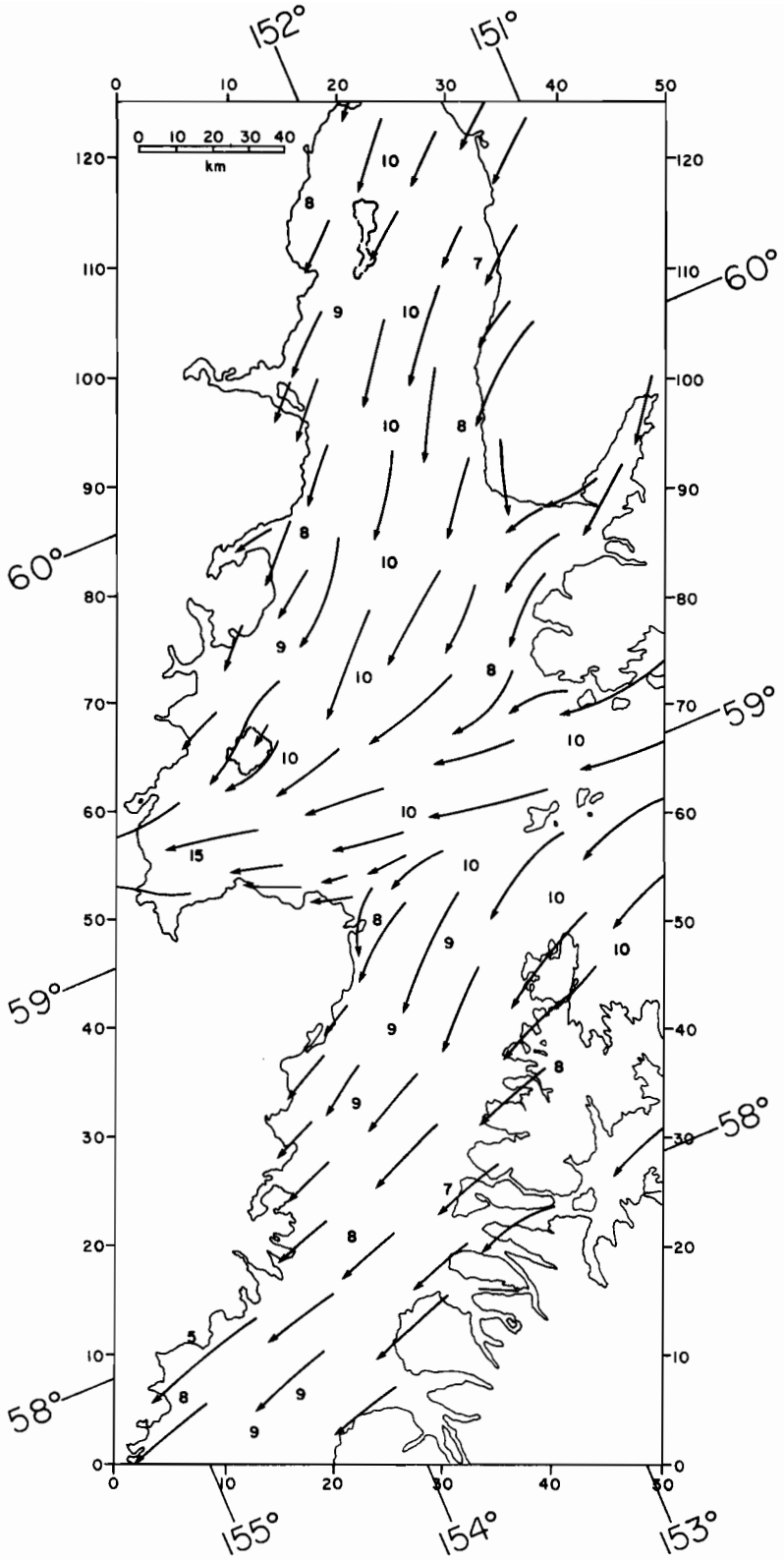

Figure 59. Map II of Putnins' wind type for lower Cook Inlet.

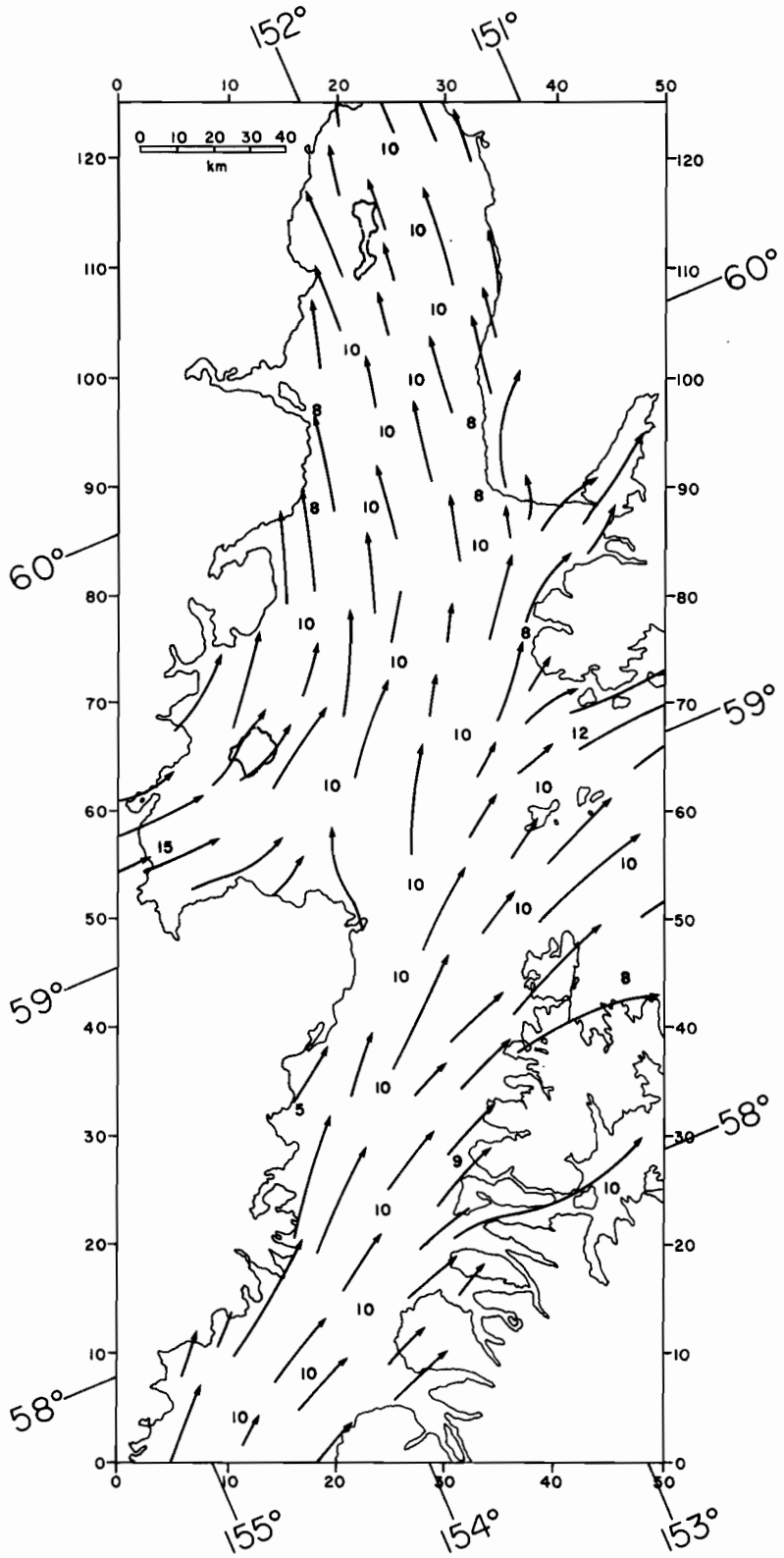

Figure 60. Map III of Putnins' wind type for lower Cook Inlet.

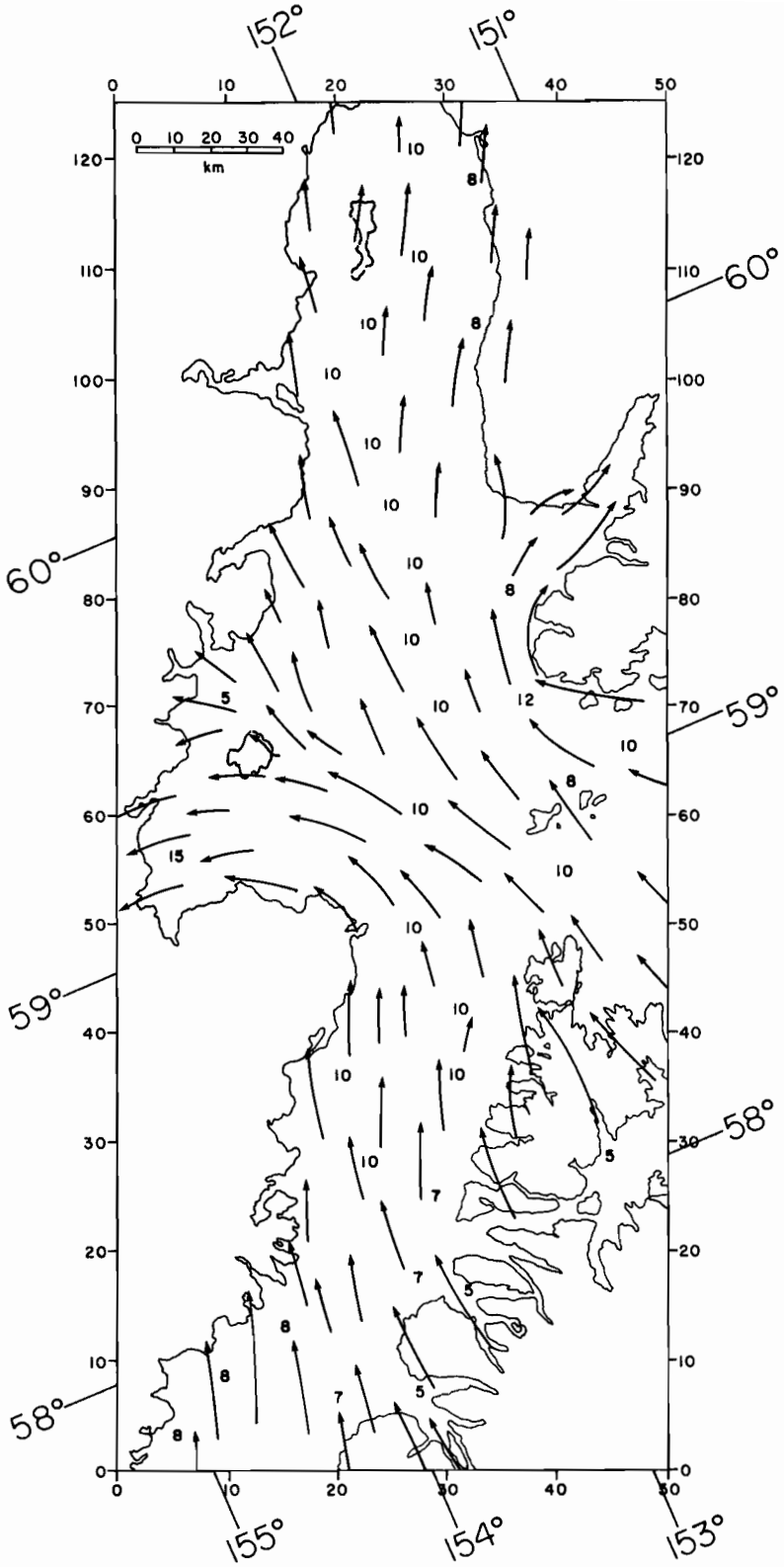

Figure 61. Map IV of Putnins' wind type for lower Cook Inlet.

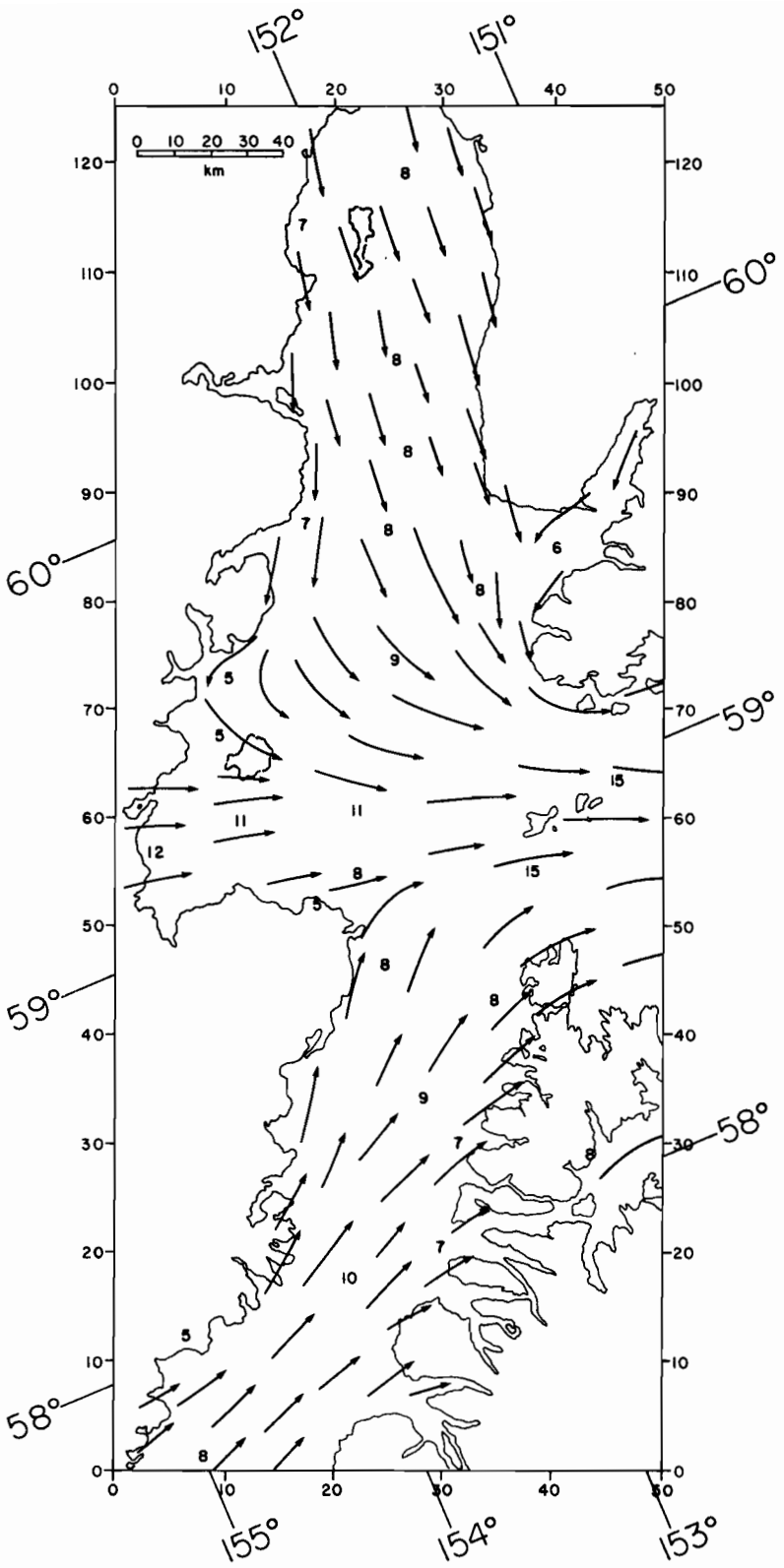

Figure 62. Map V of Putnins' wind type for lower Cook Inlet.

There are undoubtedly many situations which would not be well approximated by one of the five patterns, but nevertheless we feel these patterns show the dominant winds.

Each of Putnins' types is assigned a wind pattern map and a scaling factor for the wind speeds in Table 9. In Table 10 the Putnins types associated with each map are listed with their annual percentage occurrence and the total annual percentage occurrence for each map.

An approximate transition matrix was compiled from Putnins' report. He lists the number of times each classification was followed by each of the other classifications on a month-by-month basis for the 18 yr of records. For example, in January type D (101 occurrences) was repeated 73 times, when followed by type E_1 6 times, by type E 5 times, and by type H 4 times. The compilation was somewhat incomplete in that Putnins ignored sequences that occurred rarely. We summed these monthly figures to give the total number of occurrences of each sequence for the whole 18 yr of record. This matrix was then normalized to give the percent probability of each type following each other type (Table 11).

The above scheme provided a transition matrix based on a long historical record. The study by Putnins was the only one available. There are, however, a number of weaknesses to this approach, especially when applied to the lower Cook Inlet region alone. First, each of Putnins' classifications includes a broad range of different weather situations that may produce quite different local winds. The synoptic map reproduced by Putnins for each type is nothing more than a representative sample, and it cannot be presumed that all situations of the same type will produce similar winds in lower Cook Inlet even though that is our working assumption. It is a bit disheartening to note that the most common type, A', has the least well defined pressure gradients

TABLE 9

Assignation of Putnins' wind types according to patterns (cf. Fig. 58-62), and scaling factors for wind speeds

Type	Map	Scaling Factor
A	II	1.5
A_c	II	1.5
A^c	V	1.0
A''	III	1.0
A'''	IV	1.0
A_1	I	1.5
A_2	IV	1.0
A_3	III	0.3
B	I	1.0
C	II	0.5
D	II	1.0
D'	I	1.5
D_1	II	1.0
E	IV	0.5
E'	IV	0.5
E''	II	0.5
E_1	V	0.5
E_1'	IV	0.5
F	III	1.2
F_1	II	1.0
G	V	1.0
H	I	1.0

TABLE 10

Putnins' wind types associated with each map (Fig. 58-62), annual percentage occurrence of each type, and total annual percentage occurrence for each map

Map	Types and % Annual Occurrence							Total %
I	A_1	B	D'	H				
	6.7	1.0	1.2	7.1				16.0
II	A	A_C	C	D	D_1	E''	F_1	
	7.5	3.7	1.3	6.3	3.6	0.8	0.7	23.9
III	A''	A_3	F					
	5.2	1.1	1.1					7.4
IV	A'''	A_2	E	E'	E_1'			
	1.6	5.9	6.3	8.2	5.3			27.3
V	A'	G	E_1					
	23.2	1.0	1.0					25.2

TABLE 11

Normalized matrix showing the percent probability of each of the Putnins' wind types following each other type.

	A	A'	A''	A'''	A_1	A_2	A_3	A_c	B	C	D	D'	D_1	E	E'	E''	E_1	E_1'	F	F_1	G	H
A	51.7	36.0	4.1		1.1			1.9					1.4	0.5	1.1			2.2				
A'	3.8	68.2	6.0	0.4	7.4	4.5	0.5	1.0						0.7	1.5			1.2				4.8
A''			13.0	39.1		15.3				10.8		4.3	6.6	10.9								
A'''			13.0	39.2		15.2				10.9		4.3		6.5	10.9							
A_1		15.5			50.3	0.7			0.7	5.5	6.9		1.4		3.8			0.7		1.4		13.1
A_2	4.2	21.8	1.9		1.9	49.8		1.2			1.2			1.9	13.8			0.8				1.5
A_3		14.3				20.0	65.7															
A_c	3.5	34.5			6.5	1.7		50.4													1.7	1.7
B		25.0	35.0						20.0					20.0								
C		22.5		6.5	10.0	6.4			6.4	35.4		6.4		6.4								
D							0.6				71.4		1.9	8.2	8.2			5.0		1.6		3.1
D'			5.7		5.7	5.7					11.4	48.6	8.6	8.6	5.7							
D_1	11.4	3.6			1.8								59.6		2.5			1.8				19.3
E	10.0	13.7	4.7	2.3		2.0								40.5	17.4			9.4				
E'	1.7	4.1	1.2		0.5	7.0					6.0		1.2	19.2	54.0	0.5		4.6				
E''																50.0		25.0				25.0
E_1		42.9															57.1					
E_1'	18.2	24.0				1.8		3.1					1.3	7.6	5.8			38.2				
F					26.7	13.4							13.4						46.5			
F_1	50.0																		50.0			
G					100.0																	
H	1.7	16.1			5.8	1.6		5.0					9.8		1.7			3.6				54.7

in the lower Cook Inlet area and is most subject to allowing small changes in the positions of low pressure centers to produce large local wind changes. Furthermore, we have only a limited basis for assigning local wind conditions based on a specific baric situation. Finally, and of the least consequence, the transition matrix determined from Putnins' compilation of monthly sequences was not complete and produced some distortion of the overall frequency of occurrence. For example, type A' occurred 23.2% of the time, while the transition matrix is based on an occurrence of 27.3% of the time.

6. ACKNOWLEDGEMENTS

We acknowledge the aid of a large number of persons, not only in the preparation of this document but in carrying out the field work and analyses which have led to its existence. Of these, special thanks must go to the officers and crews of the research vessels DISCOVERER, SURVEYOR, ACONA, MOANA WAVE and MILLER FREEMAN for laboring under less than ideal conditions to carry out an ambitious field program; the first of this magnitude ever undertaken in these stormy waters. Lynn Long, Sharon Wright, Sally Dong, Cindy Loitsch, Jean Chatfield, Phyllis Hutchens, Joy Golly, and Gini May Flake of NOAA/PMEL are due thanks, also, for their help in analyzing the data and preparing the document. Dr. Tom Royer of the University of Alaska and Mr. Ronald K. Reed of PMEL/NOAA have contributed suggestions which have aided preparation of the manuscript. This study was supported in part by the Bureau of Land Management through interagency agreement with the National Oceanic and Atmospheric Administration, under which a multiyear program responding to needs of petroleum development of the Alaskan continental shelf has been managed by the Outer Continental Shelf Environmental Assessment Program (OCSEAP) Office.

7. REFERENCES

Barrick, D. E., M. W. Evans, and B. L. Weber (1977): Ocean surface currents mapped by radar. Science, Vol. 198, 138-144.

Batchelor, G. K. (1967) An Introduction to Fluid Dynamics. University Press, New York, N.Y., 615 pp.

Brower, W.A., Jr., H. F. Diaz, A. S. Prechtel, H. W. Searby, and J. L. Wise (1977) Climatic Atlas of the Outer Continental Shelf Waters and Coastal Regions of Alaska, Vol. 1, Gulf of Alaska. NOAA/OCSEAP Final Rept. Ru No. 347 (unpublished manuscript). 439 pp.

Burbank, D. C. (1977) Circulation studies in Kachemak Bay and lower Cook Inlet, Alaska. Dept. of Fish and Game, Anchorage, AK (unpublished manuscript). 207 pp.

Charnell, R. L. and G. A. Krancus (1976) A processing system for Aanderaa current meter data. NOAA Tech. Memo. ERL-PMEL 6, NOAA, Boulder, CO. 50 pp.

Davis, B. L. and M. W. Ekern (1977) Wind fabric diagrams and their application to wind energy analysis. J. Appl. Meteor., 16: 522-531.

Dodimead, A. J., F. Favorite and T. Hirano (1963) Review of oceanography of the subarctic Pacific region. Bull. Int. N. Pacific Fish. Comm., 13: 1-195.

Favorite, F. (1964) Drift bottle experiments in the northern North Pacific Ocean, 1962-1964. J. Oceanog. Soc. Japan, 20: 160-167.

Favorite, F. (1967) The Alaskan Stream. Bull. 21, Int. N. Pac. Fish. Comm., Vancouver, B. C. 1-20.

Favorite, F. and D. M. Fisk (1971) Drift bottle experiments in the North Pacific Ocean and Bering Sea 1957-60, 1962, 1966, and 1970. NOAA/ NMFS Data Rep. 67, U.S.D.O.C., Washington, D. C. 20 pp.

Favorite, F., A. J. Dodimead and K. Nasu (1976) Oceanography of the subarctic Pacific region, 1960-1972. Bull. Int. N. Pacific Fish. Comm., 33: 1-187.

Favorite, F. and W. J. Ingraham (1977) On flow in the northwestern Gulf of Alaska, May 1972. J. Oceanog. Soc. Japan, 33: 67-81.

Gatto, L. W. (1976) Baseline data on the oceanography of Cook Inlet, Alaska. Rept. 76-25, U. S. Army Cold Regions Res. and Eng. Lab., Hanover, N.H. 84 pp.

Halpern, D., and R. D. Pillsbury (1976) Influence of surface waves on subsurface current measurements in shallow water. Limnolog. and Oceanog., 21: 611-616.

Hayes, S. P. (1979) Variability of current and bottom pressure across the continental shelf in the Northeast Gulf of Alaska. J. Phys. Oceanog., 9: 88-103.

Hayes, S. P. and J. D. Schumacher (1976) Description of wind, current and bottom pressure variations on the continental shelf in the northeast Gulf of Alaska from February to May 1975. J. Geophys. Res., 81: 6411-6419.

Hinze, J. O. (1959) Turbulence. McGraw-Hill, New York, N.Y., 586 pp.

Holbrook, J. R., R. D. Muench and G. A. Cannon (1979) Seasonal observations of low-frequency atmospheric forcing in the Strait of Juan de Fuca. Proc. Fjord Oceanog. Workshop, Plenum Press, New York, 305-317.

Ingraham, W. J., A. Bakun and F. Favorite (1976) Physical oceanography of the Gulf of Alaska. Environmental Assessment of the Alaskan Continental Shelf, 11, NOAA/ERL, Boulder, CO. (unpublished manuscript).

International Hydrographic Bureau (1966) Tides, Harmonic Constants. Spec. Publ. No. 26, Monaco. 260 pp.

Jacobs, W. C. (1951) The energy exchange between the sea and atmosphere and some of its consequences. Bull. Scripps Inst. Oceanog., 6: 27-122.

Kinney, P. J., D. K. Button, D. M. Schell, B. R. Robertson and J. Groves (1970a) Quantitative assessment of oil pollution problems in Alaska's Cook Inlet. Rept. R-169, Inst. Mar. Sci., Univ. of Alaska, Fairbanks. 125 pp.

Kinney, P. J., J. Groves and D. K. Button (1970b) Cook Inlet environmental data, R/V Acona cruise 065 - May 21-28, 1968. Rept. R70-2, Inst. Mar. Sci., Univ. of Alaska, Fairbanks. 120 pp.

Knull, J. R. and R. Williamson (1969) Oceanographic survey of Kachemak Bay, Alaska. Man. Rept. 60, Bur. Comm. Fish. Lab., Auke Bay, Alaska. 54 pp.

Levanon, N. (1975) (Editor) Special issue on data collection from multiple earth platforms. IEEE Trans. on Geoscience Electronics, Vol. 13.

Luther, D. S. and C. Wunsch (1975) Tidal Charts of the Central Pacific Ocean. J. Phys. Oceanog., 5: 222-230.

Matthews, J. B. and J. C. Mungall (1972) A numerical tidal model and its application to Cook Inlet, Alaska. J. Mar. Res., 30: 27-38.

Mayer, D. A., D. V. Hansen, and D. A. Ortman (1979) Long-term current and temperature observations on the middle Atlantic shelf. J. Geophys. Res., 84: 1776-1792.

McEwen, G. F., T. G. Thompson and R. Van Cleve (1930) Hydrographic sections and calculated currents in the Gulf of Alaska, 1927 to 1928. Rept. Int. Fish. Comm., No. 4. 36 pp.

Muench, R. D., H. O. Mofjeld and R. L. Charnell (1978) Oceanographic conditions in lower Cook Inlet; spring and summer 1973. J. Geophys. Res., 83: 5090-5098.

Muench, R. D. and J. D. Schumacher (1980) Some observations of physical oceanographic conditions on the northeast Gulf of Alaska continental shelf. NOAA Tech. Memo. ERL PMEL-17, NOAA/ERL, Boulder, CO. 84 pp.

Munk, W. H. and D. Cartwright (1966), Tidal Spectroscopy and Prediction. Phil. Trans. Roy, Soc. London A, 259, 533-581.

Pearson, C. A. (1973) Deep sea tide and current observations in the Gulf of Alaska and northeast Pacific. NOAA Tech. Memo. NOS16, NOAA/NOS, Rockville, MD. 18 pp.

Pietrafesa, L. J. and G. S. Janowitz (1979) On the effects of buoyancy flux on continental shelf circulation. J. Phys. Oceanog., 9: 911-918.

Putnins, P. (1966) Studies on the Meteorology of Alaska: First Interim Report (The sequences of baric weather patterns over Alaska). U. S. Dept. Commerce, ESSA/EDS, Silver Spring, MD (unpublished manuscript).

Rapatz, W. J. and W. S. Huggett (1977) Pacific Ocean offshore tidal program. Proc. XV Int. Cong. Surv., Stockholm. 47-80.

Reed, R. K. (1980) Direct measurement of recirculation in the Alaskan Stream. J. Phys. Oceanog., Vol. 10 (in press).

Reed, R. K. and N. E. Taylor (1965) Some measurements of the Alaska Stream with parachute drogues. Deep-Sea Res., 12: 777-784.

Reed, R. K., R. D. Muench and J. D. Schumacher (1980) On baroclinic transport of the Alaskan Stream near Kodiak Island. Deep-Sea Res., Vol. 27 (in press).

Roden, G. I. (1969) Winter circulation in the Gulf of Alaska. J. Geophys. Res., 74: 4523-4534.

Royer, T. C. (1975) Seasonal variations of waters in the northern Gulf of Alaska. Deep-Sea Res., 22: 403-416.

Royer, T. C. and R. D. Muench (1977) On the ocean temperature distribution in the Gulf of Alaska, 1974-1975. J. Phys. Oceanog., 7: 92-99.

Royer, T. C. (1979) On the effect of precipitation and runoff on coastal circulation in the Gulf of Alaska. J. Phys. Oceanog., 9: 555-563.

Royer, T. C., D. V. Hansen and D. J. Pashinski (1979) Coastal flow in the northern Gulf of Alaska as observed by dynamic topography and satellite-tracked drogued drift buoys. J. Phys. Oceanog., 9: 785-801.

Scorer, R. S. (1967) Causes and consequences of standing waves. Proc. Symp. on Mountain Meteorology, Atmos. Sci. Paper 122, Colorado State Univ., Fort Collins, CO, 75-101.

Schumacher, J. D., R. Sillcox, D. Dreves and R. D. Muench (1978) Winter circulation and hydrography over the continental shelf of the northwest Gulf of Alaska. NOAA Tech. Rept. ERL 404-PMEL 31, NOAA, Boulder, CO. 16 pp.

Schumacher, J. D., R. K. Reed, M. Grigsby and D. Dreves (1979) Circulation and hydrography near Kodiak Island, September to November 1977. NOAA Tech. Memo. ERL-PMEL-13, NOAA, Boulder, CO. 49 pp.

Schumacher, J. D. and R. K. Reed (1980) Coastal flow in the northwest Gulf of Alaska: the Kenai Current. J. Phys. Oceanog., 85 (in press).

Thomson, R. E. (1972) On the Alaskan Stream. J. Phys. Oceanog., 2: 363-371.

Wang, D. P. and A. J. Elliott (1978) Non-tidal variability in the Chesapeake Bay and Potomac River: evidence for non-local forcing. J. Phys. Oceanog., 8: 225-232.

Wang, D. P. (1978) Subtidal sea level variations in the Chesapeake Bay and relations to atmospheric forcing. J. Phys. Oceanog., 8: 413-421.

Winant, C. D. and R. C. Beardsley (1979) A comparison of some shallow wind-driven currents. J. Phys. Oceanog., 9: 218-220.

Wright, F. F., G. D. Sharma, and D. C. Burbank (1973) Erts-1 observation of sea surface circulation and sediment transport, Cook Inlet, Alaska. Proc. Symp. on Significant Results Obtained from the Earth Resources Technology Satellite-1, NASA, Washington, D. C., 1315-1322.

Appendix A. Current meter statistics for northwest Gulf of Alaska moorings.

					"In" Water OBS			2.86 hr. Net Drift		35 hr. Net Drift		2.86 Mean	35 Mean	2.86	35	Temp.		Preasure		Salinity	
Mooring	Lat.	Long.	Meter Depth	Bott. Depth	Date	Per. 'Days'	Meter #	Speed	Direc.	Speed	Direc.	Speed	Speed	Var.	Var.	Mean	Var.	Mean	Var.	Mean	Var.
C1A	59.18	153.30	20	42	77-279	160	1810	16.26	198.8	15.94	198.7	38.94	16.93	247.18	90.82	4.52	4.91	26.12	1.48	31.12	0.36
C1B	59.18	153.31	18	40	78-148	87	2504	9.15	202.4	9.34	203.5	31.54	10.38	162.59	27.72	8.64	2.77	20.39	1.48	31.40	0.31
C1A	59.18	153.30	34	42	77-279	160	2512	9.04	198.4	8.98	198.7	25.07	10.73	146.52	51.81	4.66	4.65	40.41	1.85	31.08	0.25
C1B	59.18	153.31	35	40	78-148	143	3286	4.36	193.5	4.34	192.7	18.15	6.22	83.56	15.04	9.04	2.21	38.03	1.02	30.45	0.78
C2A	59.23	153.03	20	64	77-279	128	2355	8.18	226.6	8.14	226.6	35.45	11.64	256.60	65.48	5.79	3.72	28.59	1.70	31.37	0.25
C2B	59.23	153.13	18	62	78-148	143	3176	14.64	218.3	14.57	218.4	40.81	17.42	416.01	83.94	9.07	2.07	18.53	1.60	30.33	1.92
C2A	59.23	153.03	50	64	77-279	21	2498	8.03	196.4	10.04	197.1	25.15	18.39	163.79	79.10	8.55	0.12	58.47	2.38	31.52	0.11
C2B	Bad data		48				2505														
C3A	59.40	152.89	20	59	77-280	159	2494	8.21	234.2	8.30	233.6	46.35	9.51	380.48	27.25	5.23	3.68	25.43	2.19	31.42	0.26
C3B	59.41	152.89	25	64	78-148	143	598	17.14	231.8	17.25	231.8	52.14	18.82	603.78	54.93	9.10	1.98	23.49	1.77	0.00	0.00
C3A	59.40	152.89	50	59	77-280	159	2359	1.59	230.9	1.70	229.7	28.42	4.49	212.49	8.86	5.32	3.26	53.89	2.41	31.38	0.11
C3B	59.41	152.89	55	64	78-148	97	3180	0.58	109.8	0.64	94.9	24.56	4.09	179.98	7.89	8.15	1.38	51.08	1.82	30.96	0.76
C4A	59.28	152.90	20	84	77-280	159	1452	3.19	272.9	3.15	273.1	40.11	9.03	317.37	48.24	5.80	2.94	19.32	1.87	31.43	0.26
C4B	59.28	152.92	19	83	78-153	138	3294	2.90	243.7	2.97	245.7	26.40	5.56	551.80	27.38	0.00	0.00	0.00	0.00	0.00	0.00
C4A	59.28	152.90	65	84	77-280	159	1672	1.56	241.3	1.55	238.8	26.35	7.07	217.17	33.56	5.95	2.68	65.14	2.97	31.65	0.07
C4B	59.28	152.92	64	83	78-150	141	3290	1.41	166.4	1.33	157.8	26.95	6.61	199.31	29.01	8.27	1.26	62.69	1.50	31.13	0.48
C5A	59.17	152.94	20	128	77-280	159	1804	20.77	249.8	20.96	250.3	34.95	23.93	269.56	162.62	6.04	2.59	17.49	1.46	31.52	0.25
C5B	59.17	152.90	27	135	78-148	115	2156	18.96	251.6	19.06	251.8	44.81	23.14	796.84	258.46	8.40	1.68	0.00	0.00	28.63	1.68
C5A	59.17	152.94	65	128	77-280	159	1981	16.15	240.1	16.29	240.1	30.61	19.03	148.49	87.95	6.10	2.27	62.33	2.09	31.73	0.08
C5B	Bad data		72				3184														
C5A	Bad data		122				2168														
C5B	59.17	152.90	127	135	78-148	123	1815	2.35	199.1	2.46	199.8	15.05	6.18	85.25	23.02	7.00	0.54	128.55	1.78	32.06	0.07
C6A	59.30	152.64	20	71	77-280	162	1817	2.41	280.5	2.48	275.0	46.34	9.09	444.15	66.96	5.96	3.00	21.72	2.16	31.57	0.23
C6B	59.31	152.63	26	77	78-148	142	3173	0.88	256.9	0.65	256.1	46.31	7.49	518.61	38.89	8.84	2.01	0.00	0.00	25.74	1.81
C6A	Bad data		65				1818														
C6B	59.31	152.63	71	77	78-148	143	3295	3.09	119.2	3.22	118.7	25.38	5.44	193.44	11.60	8.41	1.33	70.82	1.81	30.89	0.75
C7A			20			Not recovered															
C7B	59.31	152.18	17	68	78-148	142	2249	4.19	310.0	4.17	310.0	71.69	7.48	1505.49	42.07	8.61	1.84	31.39	0.39	21.87	1.82
C7A	59.32	152.20	65	71	78-281	118	1986	1.48	343.0	1.52	352.8	53.43	4.16	902.31	7.52	6.59	2.13	63.02	2.25	0.00	0.00
C7B	59.31	152.18	62	68	78-148	142	2500	1.80	237.3	1.81	237.2	38.91	3.56	598.15	4.68	8.31	1.16	67.52	1.68	31.86	0.21
C8A	Lost		20				1806														
C8B	59.0	152.06	63	190	78-149	138	3179	22.26	287.3	22.09	287.4	61.54	23.50	1607.82	353.61	7.79	0.82	63.53	5.67	31.96	0.04
C8A	59.04	152.06	65	191	77-277	19	1681	28.10	295.9	27.34	294.0	52.83	29.34	866.77	96.04	8.12	0.17	72.07	61.37	32.05	0.04
C8B	59.03	152.06	64	190	78-149	82	2252	14.24	284.2	14.21	283.8	51.96	15.55	978.58	70.36	7.26	0.57	63.96	3.85	31.95	0.03
C8A	Inst. Failed		180				1680														
C8B	59.03	152.06	179	190	78-149	138	1682	7.84	258.3	7.84	258.7	39.83	8.63	262.40	20.18	6.65	0.27	179.39	1.63	32.39	0.03
C9A	Lost		20																		
C9B	58.78	152.27	66	124	78-149	138	1973	10.84	299.9	10.58	299.6	52.51	13.18	965.86	102.87	6.78	0.47	66.82	1.69	32.22	0.05
C9A	Lost		65																		
C9B	58.77	152.27	67	124	78-149	138	2501	10.64	297.3	10.38	296.8	52.11	13.05	976.83	104.88	6.76	0.46	68.24	1.89	32.28	0.05
C9A	Lost		107																		
C9B	58.78	152.27	114	124	78-149	138	2248	11.68	300.3	11.35	300.5	34.38	12.04	362.54	74.83	6.09	0.33	115.55	1.13	32.41	0.07
C10A	58.50	153.19	20	170	77-278	159	1683	27.66	228.9	27.80	229.6	33.20	31.01	470.82	382.87	5.82	1.69	26.44	1.66	31.92	0.21
C10B	58.50	153.20	25	175	78-148	134	3171	14.70	221.4	14.43	221.6	20.08	17.67	182.55	118.26	8.59	1.77	21.26	2.00	31.19	1.07
C10A	58.50	153.19	65	170	77-278	159	1982	23.34	228.8	23.43	229.4	27.29	25.73	294.65	254.31	5.87	1.06	72.26	1.46	32.15	0.05
C10B	58.50	153.20	70	175	78-148	134	3175	12.48	221.3	11.95	221.4	17.15	15.28	119.84	94.07	7.36	0.97	66.25	2.14	31.52	0.78
	Bad data		157				1824														
C10B	58.50	153.20	165	175	78-148	134	1669	4.77	201.8	4.28	200.4	11.13	9.29	67.06	49.37	5.42	0.26	18.08	0.39	32.49	0.03
C11A	Lost		34																		
C11B	59.56	151.66	82.4	87	78-149	20	1451	1.37	336.4	1.39	333.7	10.23	1.61	13.72	0.77	5.54	0.04	80.01	2.78	32.04	0.00
C12A	59.53	152.23	20	50	78-148	81	2358	4.03	41.4	3.85	42.4	54.82	4.55	990.82	4.21	7.93	1.31	19.98	2.80	31.76	0.14
C13A	59.47	152.68	26	68	78-148	141	3293	5.14	190.6	5.15	189.2	59.65	8.92	704.34	22.41	8.92	1.79	22.21	1.50	31.08	0.23
C12A	59.53	152.23	46	50	78-148	141	3291	4.02	31.0	3.97	30.1	42.81	4.60	651.61	4.25	8.73	1.71	46.71	2.14	30.58	1.47
C13A	Bad data		56.6				2356														

Appendix A. Continued

					"In" Water OBS.			2.86 hr. Net Drift		35 hr. Net Drift		2.86 Mean	35 Mean	2.86	35	Temp.		Pressure		Salinity	
Mooring	Lat.	Long.	Meter Depth	Bott. Depth	Date	Per. 'Days'	Meter #	Speed	Direc.	Speed	Direc.	Speed	Speed	Var.	Var.	Mean	Var.	Mean	Var.	Mean	Var.
K1A	Inst. failed		20				1988														
K1A	57.75	154.73	100	228	76-290	164	1820	27.12	237.8	27.55	237.3	32.87	31.05	247.26	135.66	6.47	0.35	108.94	1.00	32.15	0.03
K2A	58.62	153.08	20	164	76-290	165	1975	41.92	214.3	42.50	214.0	46.17	43.96	588.39	408.45	6.52	0.80	29.24	2.03	31.80	0.12
K2A	58.62	153.08	100	164	76-290	165	2163	26.21	223.2	26.73	228.0	30.19	28.55	249.26	180.05	6.46	0.42	111.02	1.62	32.06	0.03
K3A	58.76	152.17	20	198	76-289	37	1451	33.34	296.6	32.38	296.8	61.12	33.58	1352.74	266.94	7.41	0.35	24.82	3.32	31.88	0.14
K3A	Bad data		100				1806														
K4A	Lost mooring						1816														
K4A	Lost mooring						1976														
K5A	56.55	152.66	20	95	76-292	157	2359	14.73	191.9	15.04	192.1	29.75	18.11	140.44	73.29	10.75	0.43	0.00	0.00	28.20	0.01
K5A	56.55	152.66	80	95	76-292	157	1809	13.30	184.0	13.49	184.2	19.04	14.49	110.78	67.47	5.72	0.15	92.23	0.25	32.70	0.05
K6A	57.22	152.43	23	75	77-292	141	2249	21.63	282.6	21.52	282.9	33.17	24.32	178.69	145.05	5.02	1.41	23.47	0.52	32.40	0.06
K6B	57.23	152.39	32	82	78-141	137	3296	15.72	278.1	15.63	278.0	23.14	16.21	117.14	41.39	7.77	1.38	31.03	0.75	31.38	1.75
K6A	57.22	152.43	65	75	77-292	141	2248	14.67	272.5	14.53	272.5	21.23	16.18	91.98	62.67	5.27	1.21	66.25	0.32	32.43	0.03
K6B	57.23	152.39	72	82	78-141	137	1676	8.31	263.1	8.26	263.0	14.27	8.57	55.76	13.12	0.00	0.00	70.14	2.32	0.00	0.00
K7A	57.06	152.30	28	80	77-292	142	2245	10.52	336.7	10.59	337.1	25.27	13.96	133.08	72.35	5.20	1.01	22.97	0.68	32.40	0.05
K7B	57.09	152.22	29	84	78-141	135	2513	8.77	318.9	8.99	318.8	19.79	10.11	71.32	26.63	7.99	1.21	28.70	0.59	32.11	0.05
K7A	57.06	152.30	70	80	77-292	142	1984	7.65	325.5	7.66	325.8	16.58	9.25	46.92	26.84	5.20	0.75	70.14	0.66	33.00	0.05
K7B	Bad data		74				1675														
K8A	57.12	152.75	25	150	77-292	141	2500	25.04	201.6	25.08	201.8	29.64	26.47	176.69	156.64	5.14	1.53	22.52	0.77	32.36	0.07
K8B	57.11	152.72	30	155	78-141	135	3174	17.90	216.3	17.87	216.1	19.82	18.23	86.12	47.23	8.36	1.63	27.16	0.64	32.14	0.12
K8A	Incomplete		67				1829														
K8B	57.11	152.72	75	155	78-141	135	1827	10.52	220.7	10.66	220.5	13.87	11.36	35.21	16.72	0.00	0.00	0.00	0.00	0.00	0.00
K8A	57.12	152.75	140	150	77-292	65	1827	11.47	199.8	12.22	199.3	15.85	14.04	103.59	67.87	0.00	0.00	143.57	1.30	0.00	0.00
K9A	Incomplete		25				2505														
K9B	56.99	152.56	13	146	78-141	137	3172	4.82	218.1	5.04	221.5	19.47	9.81	77.42	35.93	9.53	1.99	11.04	0.76	31.77	0.56
K9A	57.01	152.62	67	86	77-292	141	1978	0.00	150.1	0.00	150.1	0.00	0.00	0.00	0.00	5.17	1.03	67.89	2.71	32.50	0.02
K9B	56.99	152.56	58	146	78-141	137	3185	4.38	260.3	4.35	260.4	17.97	9.09	60.70	30.33	6.37	0.37	56.78	0.44	32.49	0.01
K9A	57.01	152.62	148	86	77-292	141	1808	2.81	300.2	2.79	299.7	10.80	6.86	29.64	17.46	0.00	0.00	152.55	0.73	0.00	0.00
K9B	56.99	152.56	142	146	78-141	137	2498	3.77	292.8	3.84	293.0	8.49	4.72	20.09	7.54	4.93	0.02	142.30	0.56	32.89	0.02
K10A	Incomplete		25				1811														
K10B	56.83	152.39	24	153	78-141	136	2512	4.60	291.5	4.74	291.0	13.57	6.91	38.16	18.24	8.68	1.88	23.74	0.53	32.31	0.03
K10A	56.85	152.43	144	154	77-292	141	1987	5.62	332.0	5.57	332.1	11.64	7.75	45.80	31.55	5.21	0.07	143.87	0.18	33.02	0.09
K10B	56.83	152.39	69	153	78-141	136	2502	5.78	307.9	5.82	306.8	14.56	7.93	32.58	18.73	5.86	0.08	69.03	0.19	32.43	0.01
K10B	56.83	152.39	149	153	78-141	136	3287	6.21	338.3	6.30	338.6	9.89	6.69	27.41	12.82	4.82	0.03	149.50	0.42	0.00	0.00
K11A	Incomplete		31				598														
K11B	56.03	155.10	25	60	78-142	67	2355	10.02	224.6	10.12	223.9	54.85	10.70	370.86	33.60	6.38	0.39	23.97	0.55	32.46	0.01
K12A	55.99	156.30	18	213	77-297	135	1815	24.30	201.5	24.59	202.6	45.26	32.36	437.94	354.75	4.72	1.36	16.69	1.85	31.86	0.09
K12B	Bad data		24				3183														
K12A	55.99	156.30	203	213	77-297	135	1673	6.45	179.1	6.86	181.6	21.31	14.71	158.53	64.59	5.04	0.05	202.84	0.24	33.29	0.24
K12B	Bad data		208				1671														
K13A	Not deployed						1988														
K13B	56.40	156.82	28	115	78-142	138	3178	13.62	221.1	13.88	220.4	25.17	16.50	234.33	72.66	8.13	2.61	32.69	1.14	31.44	0.35
K13A	Incomplete		102				2356														
K13B	56.40	156.82	111	115	78-142	138	3289	2.65	200.7	2.68	201.5	12.67	5.82	42.50	8.65	5.79	0.78	114.94	0.18	32.02	0.02
MI-A	55.79	158.65	51	71	77-301	130	2504	15.87	219.0	16.07	219.0	21.82	17.88	123.58	89.41	4.67	2.34	55.25	0.73	31.61	0.10
MI-B	Incomplete		50				1833														
MI-D	55.76	157.52	50	118	77-301	16	1826	12.19	318.1	11.24	314.1	20.95	12.18	93.63	22.46	7.25	0.07	56.47	0.45	31.34	0.02
MI-B	55.42	157.98	90	110	77-301	129	2501	7.44	29.2	7.27	28.6	17.27	10.36	96.14	50.47	5.08	1.46	92.76	0.50	32.18	0.04
MI-D	55.76	157.52	90	118	77-301	33	2502	10.09	320.3	10.13	320.7	18.72	11.41	104.51	18.27	6.90	0.42	97.32	0.21	31.70	0.03
MI-D	55.76	157.52	70	118	77-301	129	603	10.65	323.5	10.64	323.6	21.05	12.91	109.45	39.88	4.81	1.71	73.39	0.00	32.10	0.06

Appendix A. Continued

			"In" Water OBS.					2.86 hr. Net Drift		35 hr. Net Drift		2.86 Mean	35 Mean	2.86	35	Temp.		Pressure		Salinity	
Mooring	Lat.	Long.	Meter Depth	Bott. Depth	Date	Per. 'Days'	Meter #	Speed	Direc.	Speed	Direc.	Speed	Speed	Var.	Var.	Mean	Var.	Mean	Var.	Mean	Var.
WGC-1A	54.03	163.0	20	188	75-248	57	1678	27.13	263.6	27.17	263.6	35.67	29.54	206.10	184.94	7.97	0.78	19.23	0.37	31.93	0.03
WGC-1B	54.02	163.0	20	194	75-306	131	1455	11.94	243.0	12.22	243.0	17.58	15.68	176.55	138.38	4.31	0.51	0.00	0.00	0.00	0.00
WGC-1A	54.03	163.0	103	188	75-248	57	1677	15.22	256.8	14.93	257.2	21.15	16.22	57.55	65.51	5.41	0.33	100.47	1.04	32.94	0.06
WGC-1B	54.02	163.0	100	194	75-306	58	645	20.99	262.8	21.47	262.8	28.07	23.95	330.86	348.98	5.10	0.84	112.50	2.21	32.13	3.83
WGC-1C	54.02	163.0	20	186	76-073	90	1982	25.33	253.8	25.13	253.5	32.48	26.73	162.34	123.85	2.68	0.99	11.55	0.42	32.23	0.07
WGC-1D	54.02	163.0	20	89	76-164	110	1973	11.15	253.2	11.17	252.9	22.20	12.97	88.94	59.20	8.02	1.61	17.41	0.30	32.04	0.04
WGC-1C	54.02	163.0	50	186	76-073	90	1978	24.36	254.7	24.42	254.1	30.77	25.38	102.88	110.13	2.73	0.51	42.03	0.43	32.38	0.11
WGC-1D	54.02	163.0	50	89	76-164	110	598	10.23	254.6	10.33	254.6	20.48	11.66	55.53	39.50	4.57	1.32	49.97	20.87	31.87	0.01
WGC-1C	54.02	163.0	100	186	76-073	90	1985	18.98	243.1	19.06	242.8	24.19	19.99	58.98	76.47	3.07	0.22	91.96	0.32	33.06	0.06
WGC-1C	54.02	163.0	175	186	76-073	90	1832	7.56	225.3	7.66	225.2	11.37	9.06	52.71	37.02	4.57	0.27	171.19	14.87	32.13	0.07
WGC-1E	54.05	163.1	18	88	76-275	209	2245	23.32	258.5	23.63	258.2	39.41	28.74	227.11	162.84	5.57	2.08	0.00	0.00	31.59	0.04
WGC-1F	54.06	163.1	20	88	77-120	131	1825	16.29	261.5	16.16	262.1	26.31	17.58	98.07	61.92	8.00	5.41	11.19	0.36	31.56	0.06
WGC-1E	54.05	163.1	78	88	76-275	78	2249	12.46	250.5	12.19	250.3	19.42	14.05	81.49	45.25	6.72	0.42	0.00	0.00	0.00	0.00
WGC-1F	54.06	163.10	76	88	77-119	131	1973	6.86	249.6	7.07	248.8	12.65	8.50	33.49	12.78	5.54	0.78	75.55	0.16	32.09	0.04
WGC-2A	57.45	150.49	20	185	75-265	56	1684	32.96	226.8	33.51	226.5	43.29	34.16	270.82	74.74	7.24	1.87	16.73	0.64	32.14	0.07
WGC-2B	Lost mooring																				
WGC-2A	57.45	150.49	100	185	75-265	56	1683	25.64	224.3	25.73	224.1	30.16	25.91	109.46	41.70	5.31	0.07	96.84	0.33	33.04	0.09
WGC-2B	Lost mooring																				
WGC-2C	57.45	150.49	24	185	76-070	90	1977	21.63	226.6	21.80	226.9	30.10	23.41	160.37	119.84	4.86	0.82	19.20	0.81	32.40	0.05
WGC-2D	57.56	150.82	20	92	76-160	132	1678	3.27	242.4	3.23	244.6	33.79	5.52	223.78	12.10	7.85	1.44	21.02	0.72	31.23	3.47
WGC-2C	57.45	150.49	54	185	76-070	90	1825	23.83	232.3	24.06	232.2	30.21	25.08	122.38	100.38	4.53	0.38	49.15	0.33	32.56	0.01
WGC-2D	57.56	150.82	50	92	76-160	132	1808	3.81	234.0	3.69	235.4	31.62	4.89	177.03	8.06	6.92	0.76	47.99	0.71	31.90	0.91
WGC-2C	57.45	150.49	104	185	76-070	61	1818	25.54	235.3	24.80	235.0	30.19	25.13	164.33	60.17	4.28	0.16	98.87	0.53	32.78	0.02
WGC-2D	57.56	150.82	80	92			1455	1.19	181.1	1.20	181.0	19.77	2.52	104.14	2.10	6.63	0.50	0.00	0.00	32.18	0.20
WGC-2C	57.45	150.49	179	185	76-070	90	1837	12.77	182.5	13.05	182.3	25.36	15.07	195.43	55.97	4.76	0.10	175.05	0.27	33.17	0.07
WGC-2E	57.56	150.82	20	90	76-293	155	1807	2.49	239.5	2.31	240.6	41.13	10.43	219.60	33.93	6.06	0.80	17.24	0.85	32.27	0.16
WGC-2F	57.57	150.83	20	90	77-084	167	1815	34.08	7.04	246.27	17.75	4.68	218.7	4.69	22.04	7.46	5.06	18.89	0.51	31.97	0.27
WGC-2E	57.56	150.82	80	90			1814	0.05	280.7	0.05	287.05	1.47	0.29	0.01	0.05	2.46	0.29	78.23	0.84	36.10	0.02
WGC-2F	57.57	150.83	80	90	77-084	167	1826	2.83	178.3	2.80	178.6	20.38	3.93	114.56	4.36	6.06	0.90	77.96	0.61	32.12	0.09
WGC 3A	Lost mooring																				
WGC-3B	55.19	156.97	20	111	76-162	129	1817	21.35	255.0	21.41	255.7	43.78	22.95	412.01	101.55	8.17	2.21	18.28	0.37	32.90	0.16
WGC-3C	55.20	156.95	28	112	76-292	138	1829	26.19	239.7	26.07	238.8	50.46	33.50	485.54	219.17	6.17	0.60	20.77	34.00	0.00	0.00
WGC-3B	Inst. failed						1834														
WGC-3C	55.20	156.95	90	112	76-292	153	2168	19.59	231.8	19.81	231.6	34.96	20.79	242.37	131.11	6.00	0.37	99.75	0.16	32.90	0.11
WGC-3B	Inst. failed						1831														
WGC-3D	55.20	156.96	20	112	77-191	131	1682	23.82	254.6	24.11	254.9	43.29	25.71	401.53	87.75	7.79	5.57	9.82	0.13	32.06	0.16
WGC-3D	Inst. failed						1803														

Appendix B. Release and recovery information for drift cards released in the Kodiak Island region during 1978.

RELEASED	RECOVERED				
	CARD	DATE	LATITUDE	LONGITUDE	COMMON NAME
101 - 200	107	05/20/78	57 24.0N	156 22.0W	SLAUGHTER ISL
03/06/78	123	07/24/78	59 0.0N	153 37.0W	KAMISHAK BAY
59 4.6N	155	07/24/78	59 0.0N	153 37.0W	KAMISHAK BAY
150 39.4W	171	05/30/79	59 4.0N	153 44.0W	CAPE DOUGLAS
201 - 300	219	04/10/78	58 37.8N	152 27.5W	CARSHAN PT
03/06/78	245	06/18/78	58 22.4N	152 6.9W	SEAL BAY
58 31.8N	250	07/08/78	58 23.3N	152 7.5W	TOLSTOI PT
150 45.0W	263	05/19/78	57 50.2N	152 21.0W	MILLER PT
	268	07/24/78	57 5.2N	153 11.7W	OCEAN BAY
	292	07/08/78	58 23.3N	152 7.5W	TOLSTOI PT
301 - 400	306	07/22/78	57 18.1N	153 0.0W	KILUDA BAY
03/06/78	319	04/09/78	57 27.8N	152 27.0W	PASAGSHAK BAY
58 16.2N	325	05/08/78	57 27.8N	152 27.0W	PASAGSHAK BAY
149 52.0W	342	04/22/78	57 5.3N	153 11.0W	OCEAN BEACH
	343	04/09/78	57 27.8N	152 27.0W	PASAGSHAK BAY
	352	07/22/78	57 10.0N	153 8.5W	PORT HOBRON
	365	07/01/78	56 29.3N	154 35.0W	TUGIDAK ISL
	366	04/05/79	57 31.0N	152 56.0W	HIDDEN BASIN
	371	06/04/78	57 18.0N	153 3.0W	KILUDA BAY
	372	10/10/78	57 9.0N	153 11.0W	PORT HOBRON
	380	07/22/78	57 1.0N	153 36.0W	KIAVAK BAY
	388	05/13/79	57 31.5N	152 16.6W	SACROMENTO RIVER
	392	03/27/79	57 12.0N	153 10.0W	MCCHORD RANCH
	395	04/26/78	57 17.9N	153 3.0W	KILUDA BAY
401 - 500	454	10/14/78	56 52.0N	158 54.0W	STROGNOFF PT
03/06/78	464	06/12/79	59 41.7N	140 17.5W	POINT MANBY
58 3.6N					
149 10.3W					
501 - 600					
03/10/78					
58 27.6N					
151 50.0W					
601 - 700	609	07/22/78	57 12.5N	153 16.0W	OLD HARBOR
03/10/78	625	08/03/78	57 26.0N	152 43.0W	EAGLE COVE
57 58.3N	628	02/22/79	57 12.0N	153 10.0W	MCCHORD RANCH
150 44.6W	630	04/09/78	57 27.8N	152 27.0W	PASAGSHAK BAY
	634	10/09/78	57 25.2N	152 43.0W	EAGLE HARBOR
	644	04/29/78	57 17.9N	153 3.0W	KILUDA BAY
	664	04/12/78	57 27.8N	152 27.0W	PASAGSHAK BAY
	671	09/12/78	57 9.0N	153 11.0W	MCCORD RANCH
	695	03/27/79	57 12.0N	153 10.0W	MCCHORD RANCH

Appendix B. Continued

RELEASED	RECOVERED				
	CARD	DATE	LATITUDE	LONGITUDE	COMMON NAME
701 - 800	743	07/24/78	56 24.0N	154 45.0W	TUGIDAK ISL
03/13/78	777	10/01/78	56 30.0N	160 0.0W	PORT HEIDEN
57 25.8N	798	05/05/79	59 21.0N	146 25.0W	MIDDLETON ISL
151 25.8W					
801 - 900					
03/14/78					
57 16.3N					
151 42.2W					
901 -1000	904	11/23/78	57 51.0N	152 38.0W	CANNONS BEACH
03/10/78	908	04/20/78	58 8.8N	153 16.8W	NORTH BEACH
58 21.4N	910	05/17/78	57 24.0N	156 22.0W	WIDE BAY
151 6.9W	920	11/06/78	57 52.0N	153 50.0W	CP UGAT
	958	07/11/78	57 44.0N	153 30.0W	PACKERS SPIT
	966	04/20/78	58 8.8N	153 16.8W	NORTH BEACH
	973	08/02/79	58 0.0N	153 17.0W	OUTLET CAPE
	985	06/19/78	57 39.0N	154 7.0W	7 MILE BEACH
	998	10/22/78	58 7.0N	153 2.0W	
1001-1100	1010	06/30/78	56 32.0N	154 8.0W	SITKINAK ISL
03/14/78	1022	07/22/78	56 53.0N	154 12.0W	LAZY BAY
57 3.1N	1046	07/01/78	56 29.3N	154 35.0W	TUGIDAK ISL
152 7.8W	1062	05/02/78	56 56.1N	154 10.0W	AKHIOK VILLAGE
1101-1200	1133	11/10/78	54 36.0N	164 52.0W	CAPE SARICHEF
03/14/78	1165	07/04/79	55 49.5N	155 32.0W	CHIRIKOF ISL
56 53.6N					
152 33.0W					
1201-1300	1242	10/01/78	56 30.0N	160 0.0W	PORT HEIDEN
03/14/78	1243	10/17/79	53 27.0N	166 55.0W	SW. UNALASKS ISL
56 53.6N					
152 33.0W					
1301-1400	1322	08/15/79	52 56.0N	168 54.0W	NIKOLSKI
03/16/78					
56 7.5N					
153 56.2W					
1401-1500	1413	05/05/79	56 0.0N	161 16.0W	NELSON LAGOON
03/10/78	1423	05/03/78	58 18.1N	153 2.0W	CP PARAMANOF
58 50.0N	1448	05/02/78	58 18.4N	153 2.7W	CP PARAMANOF
151 39.0W	1452	04/20/78	58 8.8N	153 16.8W	NORTH BEACH
	1464	05/14/78	58 18.4N	153 2.7W	CP PARAMANOF
	1486	06/26/78	57 39.1N	154 7.0W	7 MILE BEACH
	1495	07/26/78	58 17.0N	152 55.5W	CP PARAMANOF

Appendix B. Continued

RELEASED	RECOVERED				
	CARD	DATE	LATITUDE	LONGITUDE	COMMON NAME
3001-3100	3036	07/04/78	57 39.1N	154 7.0W	7 MILE BEACH
05/23/78	3058	07/30/78	57 40.0N	152 28.0W	MIDDLE BAY
58 48.3N					
149 36.1W					
3101-3200	3102	08/01/78	59 32.0N	153 46.2W	URSUS COVE
05/23/78	3107	07/03/78	60 21.0N	152 0.0W	KALGIN ISL
59 20.3N	3111	07/25/78	59 18.4N	154 6.0W	AMAKDORI BEACH
150 7.3W	3144	03/27/79	57 12.0N	153 10.0W	MCCHORD RANCH
	3156	07/01/78	59 20.0N	153 22.0W	ST AUGUSTINE
3201-3300	3203	12/31/78	58 12.0N	152 21.0W	KITOI BAY
05/23/78	3221	06/21/79	56 57.0N	153 41.0W	JAP BAY
58 51.3N	3221	06/21/79	56 57.0N	153 41.0W	UPPER JAP BAY
149 45.4W	3228	09/19/78	57 25.5N	152 20.0W	NARROW CAPE
	3242	11/01/78	58 16.0N	151 16.0W	MARMOT ISL.
	3267	07/25/78	59 18.4N	154 6.0W	AMAKDEDORI BEACH
	3276	10/29/78	58 9.0N	152 6.0W	PILLAR CAPE
	3278	07/25/78	59 18.4N	154 6.0W	AMAKDEDORI BEACH
	3294	07/31/78	57 40.0N	152 28.0W	MIDDLE BAY
	3297	09/22/78	58 29.3N	152 33.9W	DAYLIGHT HRB
	3297	09/22/78	58 29.3N	152 33.9W	DAYLIGHT HRB
3301-3400	3322	11/12/78	57 52.6N	152 41.2W	CRAG PT
05/23/78	3346	11/01/78	57 51.0N	153 51.0W	CAPE UGAT
58 59.9N	3351	08/22/78	57 57.0N	152 28.0W	SPRUCE ISLAND
149 56.7W	3366	09/09/78	59 17.0N	154 8.0W	KAMISHAK
3401-3500	3402	07/25/78	59 18.4N	154 6.0W	AMAKDEDORI B
05/23/78	3405	07/23/78	58 39.0N	152 26.0W	MIDDLE BAY
59 4.6N	3408	07/31/78	57 56.0N	152 25.0W	PINAPPLE COVE
149 59.4W	3409	08/11/78	57 55.0N	153 42.0W	MINERS PT
	3416	04/18/79	57 6.0N	156 30.0W	PORT WRANGLE
	3446	06/27/78	57 10.5N	154 32.5W	AGAKULIK RIVER
	3480	07/12/78	57 40.0N	152 26.5W	MIDDLE BAY
3501-3600	3507	08/18/78	57 54.8N	152 59.5W	DRY SPRUCE BAY
05/23/78	3508	07/25/78	59 18.4N	154 6.0W	AMAKDEDORI B
58 44.7N	3511	07/31/78	57 56.0N	152 25.0W	PINAPPLE COVE
149 27.5W	3520	08/13/78	59 32.0N	153 46.2W	UPSUS COVE
	3527	06/22/79	56 33.0N	157 9.0W	SUTWIK ISL
	3535	04/15/79	57 40.0N	152 28.0W	
	3546	09/21/78	56 57.5N	153 35.5W	KNOLL BAY
	3583	09/06/78	59 30.0N	153 44.0W	URSUS COVE
	3585	08/21/78	57 27.5N	152 27.0W	PASAGSHAK BAY

Appendix B. Continued

RELEASED	RECOVERED				
	CARD	DATE	LATITUDE	LONGITUDE	COMMON NAME
3601-3700	3610	07/19/78	59 12.5N	154 8.1W	CHENIK LAGOON
05/23/78	3657	09/09/79	57 46.9N	152 21.5W	WOODY ISL
58 37.8N	3673	10/11/78	57 56.5N	152 29.0W	W SIDE SPRUCE ISL
149 7.5W	3684	08/05/78	59 21.3N	153 57.5W	CONTACT PR
	3686	06/25/78	60 11.0N	151 26.0W	CLAM GULCH
	3689	07/25/78	59 18.4N	154 6.0W	AMAKDEDORI B
	3690	07/24/78	59 30.8N	154 45.3W	URSUS COVE
	3691	07/14/78	59 18.0N	154 6.7W	AMAKDEDORI B
	3698	08/11/78	59 23.0N	153 31.0W	W ST AUGUSTINE
	3700	07/25/78	59 18.8N	154 6.0W	AMAKDEDORI B
3701-3800	3710	08/02/78	57 5.3N	153 11.0W	OCEAN BAY
05/23/78	3792	09/09/79	56 32.5N	154 39.0W	TUGIDAK ISL
58 24.5N	3794	03/25/79	57 4.0N	153 34.0W	KAISIGNAK BAY
148 27.0W	3800	08/03/78	57 53.7N	153 48.0W	RINER CREEK
3801-3900	3812	07/01/78	56 57.0N	154 9.0W	MOSER BAY
05/23/78	3823	10/22/78	57 56.5N	152 29.0W	SPRUCE ISLAND
59 10.3N	3826	06/12/78	57 45.0N	155 36.5W	PAULE BAY
150 .7W	3841	10/28/78	57 17.5N	154 45.0W	GURNEY BAY
	3842	07/21/78	57 39.1N	154 7.0W	7 MILE BEACH
	3873	06/26/78	57 56.5N	153 16.0W	VIEKODA BAY
3901-4000	3902	10/14/78	57 36.0N	152 16.0W	LONG ISL
05/23/78	3904	08/10/78	59 32.0N	153 46.2W	URSUS COVE
58 32.0N	3906	08/01/78	59 32.0N	153 46.2W	URSUS COVE
148 48.2W	3913	08/09/78	58 11.2N	152 22.0W	KITIO BAY
	3914	08/29/78	58 31.0N	153 54.0W	CHINIAK BAY
	3915	07/13/78	59 29.0N	153 42.8W	ROCKY COVE
	3943	08/01/78	59 32.0N	153 46.2W	URSUS COVE
	3945	06/27/78	59 50.0N	151 48.0W	WHISKEY GULCH
	3960	07/08/78	57 47.8N	152 21.8W	MISSION BEACH
	3978	09/26/78	56 52.0N	154 14.0W	CAPE AKHIOK
	3982	06/09/79	57 12.0N	153 10.0W	PORT HOBRON
	3987	07/25/78	59 18.4N	154 6.0W	AMAKDEDORI B
4001-4100	4027	09/17/79	57 12.0N	153 10.0W	SITKALIDAK
10/03/78	4030	10/07/78	57 1.6N	153 23.8W	NATALIA PENN
57 5.6N	4031	10/07/78	57 1.6N	153 23.8W	NATALIA PENN
152 12.9W	4046	07/10/79	57 12.0N	153 10.0W	PORTHOBRON
	4051	10/07/78	57 1.6N	153 23.8W	NATALIA PENN
	4065	10/07/78	57 1.6N	153 23.8W	NATALIA PENN
	4077	10/07/78	57 1.6N	153 23.8W	NATALIA PENN
	4078	10/07/78	57 1.6N	153 23.8W	NATALIA PENN
	4087	10/07/78	57 1.6N	153 23.8W	NATALIA PENN
	4091	10/07/78	57 1.6N	153 23.8W	NATALIA PENN

Appendix B. Continued

RELEASED	RECOVERED				
	CARD	DATE	LATITUDE	LONGITUDE	COMMON NAME
4101-4200 10/04/78 56 49.4N 152 24.3W					
4201-4300 10/04/78 57 6.4N 152 43.9W	4239	11/05/78	57 .2N	153 33.0W	KIAVAK BAY
	4269	04/05/79	57 .3N	153 33.0W	KIAVAK BAY
	4276	11/03/78	57 .2N	153 33.0W	KIAVAK BAY
	4277	11/08/78	57 .2N	153 33.0W	KIAVAK B
	4288	11/04/78	57 .2N	153 33.0W	KIAVAK BAY
	4292	04/07/79	57 .3N	153 33.0W	KIAVAK BAY
4301-4400 10/05/78 56 59.6N 152 34.0W	4338	03/17/79	56 34.0N	169 38.0W	ST GEORGE ISL
	4340	08/26/79	55 44.0N	159 54.0W	DENT POINT
4401-4500 10/05/78 57 13.6N 152 23.1W					
4501-4600 10/07/78 56 13.2N 154 59.0W	4549	08/15/79	56 43.0N	154 4.0W	ATAKALIK ISL
4601-4700 10/07/78 56 8.5N 155 9.6W	4677	03/26/79	56 34.0N	169 38.0W	ST GEORGE ISL
4701-4800 10/08/78 56 3.9N 155 16.3W					
4801-4900 10/08/78 55 58.4N 155 25.8W					
4901-5000 10/07/78 56 .7N 155 5.1W	4960	07/07/79	55 49.5N	155 32.0W	CHIRICOF ISL

Appendix B. Continued

RELEASED	RECOVERED				
	CARD	DATE	LATITUDE	LONGITUDE	COMMON NAME
5001-5100	5011	01/14/79	57 35.5N	152 27.5W	KALSIN BECH
10/10/78	5013	11/01/78	57 51.0N	153 51.0W	UGAT CAPE
59 2.8N	5019	10/30/78	57 42.2N	153 50.2W	SPIRIDON BAY
150 57.2W	5053	10/30/78	57 42.2N	153 50.2W	SPIRIDON BAY
	5064	07/08/79	56 54.0N	154 18.0W	ALITAK LAGOON
	5088	10/30/78	57 42.2N	153 42.2W	SPIRIDON BAY
	5099	01/17/79	57 12.0N	153 10.0W	MCCHORD RANCH
5101-5200	5134	10/30/78	57 42.2N	153 50.2W	SPIRIDON BAY
10/10/78	5180	10/30/78	57 42.2N	153 50.2W	SPIRIDON BAY
58 58.1N	5188	10/30/78	57 42.2N	153 50.2W	SPIRIDON BAY
150 56.2W	5200	10/30/78	57 42.2N	153 50.2W	SPIRIDON BAY
5201-5300	5203	10/30/78	57 42.2N	153 50.2W	SPIRIDON BAY
10/10/78	5208	06/06/79	57 38.0N	154 21.0W	CAPE UYAT
58 51.6N	5235	12/14/78	57 42.2N	153 50.2W	SPIRIDON BAY
150 53.0W	5278	10/30/78	57 42.2N	153 50.2W	SPIRIDON BAY
5301-5400	5323	11/10/78	58 3.5N	153 14.0W	ONION BAY
10/10/78	5328	11/08/78	59 21.2N	151 55.3W	ENGLISH BAY
58 44.9N					
150 51.6W					
5401-5500	5467	03/18/79	57 25.5N	152 20.0W	
10/10/78					
58 38.6N					
150 48.0W					
5501-5600	5516	05/10/79	57 30.0N	152 44.0W	SALTERY COVE
10/10/78					
58 32.3N					
150 44.9W					
5601-5700	5606	06/27/79	55 47.0N	155 41.0W	S. CHIRIKOF ISL
10/10/78	5615	03/21/79	57 49.0N	152 26.0W	MONASHKA BAY
58 24.5N	5649	01/06/79	57 46.8N	152 26.5W	GIBSON COVE
150 49.0W	5675	05/01/79	58 55.8N	152 12.4W	USHAGAT ISL
	5683	01/20/79	57 38.5N	152 26.0W	BROAD PT
5701-5800	5732	12/27/78	57 28.2N	152 30.0W	CAPE CURRENT
10/10/78	5742	07/08/79	55 20.0N	160 26.0W	POPOFF ISL
58 18.8N	5748	03/27/79	57 12.0N	153 10.0W	MCCHORD RANCH
150 37.8W	5782	04/12/79	57 40.0N	152 29.0W	MIDDLE BAY
5801-5900	5807	05/27/79	57 12.0N	153 10.0W	PORT HOBORN
10/10/78	5819	01/15/79	58 56.0N	152 15.0W	USHAGAT ISL
58 11.3N	5851	03/18/79	57 25.5N	152 20.0W	
150 26.6W					

Appendix C. Release and recovery information for seabed drifters, including returns through February, 1980.

Cruise Number	Date Released	Release Location Latitude N	Longitude W	Recovery Date	Recovery Location Latitude N	Longitude W
4MF 77	5 Nov 77	58°02'	151°38'	Jan 79	Nataliu Bay	
	5 Nov 77	56°53'	153°04'	8 Jan 78	56°50'	153°18'
	2 Nov 77	57°37'	151°55'	-	57°03'	152°48'
4DI 78	9 Apr 78	57°07'	153°00'	Jan 79	Nataliu Bay	
	8 Apr 78	57°47'	151°41'	19 May 78	57°25'	152°30'
	9 Apr 78	57°28'	152°10'	30 Sep 78	57°32'	151°42'
	29 Mar 78	58°04'	151°45'	-	-	-
	29 Mar 78	58°04'	151°45'	23 Sep 79	Chiniak Gulley	
2MF 78	24 Jun 78	56°55'	153°22'	29 Jan 79	57°08'	153°25'
	24 Jun 78	57°04'	153°03'	11 Nov 78	Ocean Bay, Sitkalidak Isl.	
	26 Jun 78	57°16'	151°17'	18 Sep 78	57°34'	151°51'
	26 Jun 78	56°59'	152°55'	17 Sep 78	57°08'	152°44'
	24 Jun 78	56°55'	153°22'	17 Nov 78	57°05'	153°26'
	26 Jun 78	57°16'	151°17'	6 Dec 78	57°38'	151°52'
	26 Jun 78	57°16'	151°17'	28 Sep 78	57°32'	151°42'
	22 Jun 78	57°36'	151°48'	21 Sep 78	57°32'	151°40'
	22 Jun 78	57°36'	151°48'	24 Sep 78	57°25'	151°26'
	27 Jun 78	57°43'	150°54'	26 Sep 78	57°22'	151°22'
	24 Jun 78	57°12'	152°44'	27 Sep 78	56°52'	153°26'
	24 Jun 78	57°19'	152°24'	27 Oct 78	57°24'	152°24'
	24 Jun 78	56°55'	153°22'	15 Sep 78	57°03'	153°25'
	24 Jun 78	56°55'	152°22'	23 Sep 78	57°03'	153°25'
	26 Jun 78	57°00'	151°55'	29 Sep 78	57°03'	152°30'
	26 Jun 78	57°16'	151°17'	29 Sep 78	57°38'	151°58'
	21 Jun 78	58°03'	151°25'	20 Jan 79	57°40'	151°50'
	24 Jun 78	56°55'	153°22'	6 Dec 78	57°05'	153°26'
	24 Jun 78	56°55'	153°22'	23 Oct 78	57°05'	153°26'
	27 Jun 78	57°43'	150°54'	-	-	-
	24 Jun 78	57°04'	153°03'	18 Feb 79	Ocean Bay, Sitkalidak Isl.	
	22 Jun 78	57°37'	151°47'	18 Feb 79	57°21'	152°33'
	21 Jun 78	58°03'	151°25'	11 Feb 79	57°31'	152°17'
	24 Jun 78	56°55'	153°22'	28 Feb 79	57°10'	153°20'
	24 Jun 78	56°55'	153°22'	26 Feb 79	57°10'	153°19'
	24 Jun 78	56°55'	153°22'	24 Feb 79	57°09'	153°21'
	22 Jun 78	58°18'	150°12'	8 Jan 79	-	-
	30 Jun 78	56°26'	153°44'	11 Apr 79	-	154°32'
	24 Jun 78	57°04'	153°03'	3 Feb 80	56°37'	153°06'
	27 Jun 79	57°43'	150°55'	20 Nov 79	57°43'	152°20'
	27 Jun 78	57°43'	150°55'	27 Oct 79	Cape Chiniak on NE Side Kodiak	
	22 Jun 78	58°18'	150°12'	4 Jul 79	57°16'	150°46'
	22 Jun 78	58°18'	150°12'	19 Oct 79	Chiniak Gully	

Appendix C. Continued

1WE 78	28 Oct 78	56°55'	153°22'	17 Mar 79	57° -	153°25'
	28 Oct 78	57°16'	151°17'	2 Feb 79	Silver Bay,	Cape Chiniak
	1 Nov 78	57°36'	151°46'	5 Jan 79	57°25'	152°00'
	28 Oct 78	56°55'	153°22'	28 Jan 79	57°07'	153°25'
	27 Oct 78	57°29'	152°07'	19 Jan 80	56°53'	152°35'
	2 Nov 78	58°03'	151°27'	6 Jan 80	57°32'	151°44'
	1 Nov 78	57°45'	151°28'	3 Jan 80	Cap Chiniak	
	1 Nov 78	58°18'	150°12'	31 Dec 79	57°34'	151°49'
	1 Nov 78	57°37'	151°47'	29 Dec 79	57°33'	151°48'
	1 Nov 78	58°18'	150°12'	24 Nov 79	57°38'	152°20'
1MF 79	15 Feb 79	57°04'	153°04'	29 Mar 79	Ocean Bay,	Sitkalidak Isl.
	15 Feb 79	57°04'	153°04'	29 Mar 79	"	"
	18 Feb 79	57°45'	151°28'	25 Mar 79	57°56'	151°57'
	15 Feb 79	57°04'	153°04'	4 Apr 79	Ocean Bay,	Sitkalidak Isl.
	15 Feb 79	57°04'	153°04'	4 Apr 79	"	"
	15 Feb 79	57°04'	153°04'	4 Apr 79	"	"
	15 Feb 79	57°04'	153°04'	4 Apr 79	"	"
	18 Feb 79	57°45'	151°28'	23 Sep 79	"	"
	15 Feb 79	57°04'	153°02'	12 Jan 80	56°58'	153°29'
	22 Feb 79	58°04'	151°24'	19 Jan 80	57°08'	152°31'
	22 Feb 79	58°04'	151°24'	29 Dec 79	57°20'	152°30'
	18 Feb 79	57°29'	152°06'	31 Oct 79	57°14'	152°54'
	15 Feb 79	57°04'	151°02'	11 Nov 79	56°46'	153°29'
	7 Mar 79	58°18'	150°12'	2 Nov 79	Loran:31402-11697-7960	
					32070-43168-9990	
	15 Feb 79	57°04'	153°02'	12 Oct 79	Newman Bay	
					Loran-31228-32535	

Appendix D. CTD stations used in NWGOA program, listed by cruises.

Cruise ID	Vessel	Dates	No. Casts
RP4-DI77C2	Discoverer	4-12 Oct 77	186
RP4-DI77C3	Discoverer	13-21 Oct 77	97
RP4-DI77C4	Discoverer	27 Oct-5 Nov 77	127
RP4-SU77B5	Surveyor	6-15 Sep 77	130
RP4-SU77C2	Surveyor	4-17 Nov 77	46
RP4-DI77A2	Discoverer	2-10 Mar 77	58
Acona 245	Acona	30 June-16 Jul 77	109
RP4-DI76A	Discoverer	13 May-2 June 76	130
RP-DI76BL6	Discoverer	14-23 Oct 76	39
RP4-DI77A3	Discoverer	15 Mar-1 Apr 77	141
RP4-DI77A4	Discoverer	5-22 Apr 77	106
RP4-DI76A	Discoverer	7-13 Apr 76	27
DS5	Discoverer	9-16 Nov 77	94
Acona 205	Acona	13 Feb 75	3
814	Uncertain	30 Oct-13 Nov 75	116
MW3	Moana Wave	20 Apr-1 May 76	99
RP4-SU78A2	Surveyor	4-17 Mar 78	179
RP4-DI78A1	Discoverer	6-24 Mar 78	180
RP4-DI78A2	Discoverer	14-20 Apr 78	26
RP4-DI78A4	Discoverer	26 May-7 June 78	135
OP 343603	Silas Bent	1-26 Sep 75	127
MW4	Moana Wave	7-20 May 76	94
MW5	Moana Wave	22 Jul-1 Aug 76	69
RP4-DI78A2	Discoverer	28 Mar-14 Apr 78	91
RP4-DI78B4	Discoverer	6-22 Oct 78	171
RP4-MF77A4	Miller Freeman	3-7 April 77	25
RP4-MF78A4	Miller Freeman	20 Jun-5 Jul 78	106
RP4-SU78A3	Surveyor	24-27 Mar 78	21
RP4-DI78A3	Discoverer	25 Apr-5 May 78	42
RP4-MF78A1	Miller Freeman	9-12 May 78	20
RP4-MF78A5	Miller Freeman	13-18 Jul 78	53
RP4-SU78B1	Surveyor	14-18 Aug 78	36
RP4-MF78A3	Miller Freeman	7-11 June 78	49
Wekoma-78	Wekoma	27 Oct-13 Nov 78	94
RP4-MF78A	Miller Freeman	20-30 May	107
RP4-SU79B	Surveyor	5-14 Aug	79
RP4-SU79A	Surveyor	23 Mar-3 Apr 79	141
248IMS	Acona	10-16 Aug 77	20
SU41MS	Surveyor	21 Sep-2 Oct 76	79
IMS79A	Surveyor	9-21 Feb 79	133
241IMS	Acona	24 Apr 77	5
FN9IMS	Miller Freeman	29 Mar-2 Apr 77	32
254IMS	Acona	28 Nov-2 Dec 77	9
FN8IMS	Miller-Freeman	12-18 Nov 76	87
FN7IMS	Miller Freeman	10-19 Nov 76	24
IMS812	Discoverer	10-15 Oct 75	24
MW6	Moana Wave	13-19 Oct 76	22